DISTRIBUTIONS AND REACTIVITIES OF PHENOLIC ANTIOXIDANTS IN VARIOUS AGGREGATION SYSTEMS

By

QING GU

A dissertation submitted to the

Graduate School—New Brunswick

Rutgers, The State University of New Jersey

in partial fulfillment of the requirements

for the degree of

Doctor of Philosophy

Graduate Program in Department of Chemistry and Chemical Biology

written under the direction of

Professor Laurence S. Romsted

and approved by

_____

_____

_____

_____

_____

New Brunswick, New Jersey

October, 2015

ABSTRACT OF THE DISSERTATION

Distributions and reactivities of phenolic antioxidants in various aggregation systems

By QING GU

Dissertation Director:

Professor Laurence S. Romsted

Selecting the best antioxidant, AO, for a particular food application is still a major problem in food science because AO efficiencies are determined by a variety of factors. One major difficulty in establishing a scale of AO efficiencies has been the lack of reliable methods for determining AO distributions between the different regions of aggregated systems, which arises from the physical impossibility of separating the interfacial region from the aqueous or oil regions. We have developed a "non-invasive" approach to estimate AO distributions in various aggregated systems. The observed rate constant, k_{obs}, for the reaction of a chemical probe, 4-*n*-hexadecylbenzenediazonium ion (16-ArN_2^+), that is located in the interfacial region of an aggregation system with an AO is measured by a chemical derivatization method or directly by UV-Vis spectroscopy depending upon the system turbidity. The kinetic data is interpreted by using a well established pseudophase kinetic model that was originally developed for treating chemical reactivity in micelles and microemulsions, and in this thesis we demonstrate that the model can be applied to nonionic emulsions, ionic emulsions, and vesicles.

Chapter 1 is a general introduction on pertinent background information including dynamic equilibrium in surfactant aggregates, basic assumptions of the pseusophase kinetic model and logic of the chemical trapping method, and effect of AO distributions on AO efficiency. Chapter 2 describes the application of the pseudophase kinetic model to cationic and anionic emulsions in the absence and presence of added salt to obtain estimates of the partition constants of *t*-butylhydroquinone, TBHQ, between the oil and interfacial region, $P^{\mathrm{I}}_{\mathrm{O}}$, and the aqueous and interfacial region, $P^{\mathrm{I}}_{\mathrm{W}}$, and the second-order interfacial rate constant, k_{I}, that is independent of AO distributions. Chapter 3 reports measurements of k_{obs} for 16-ArN_2^+ reacting with TBHQ in $\mathrm{C}_{12}\mathrm{E}_6$ nonionic emulsions of constant composition but different droplet size distributions together with hydration number estimates for $\mathrm{C}_{12}\mathrm{E}_6$. The results support the pseudophase model assumptiont that rate constants for reactions in emulsions are insensitive to changes in droplet size and that the medium properties of the interfacial region are virtually constant. Chapter 4 demonstrates that the AO reactivity of a homologous series of gallate esters as characterized by the observed rate constant, k_{obs}, for their reactions with 16-ArN_2^+ plateaus in vesicular solutions once the AOs are fully associated with the vesicles. This plateau differs from the "cutoff effect" observed in oil-in-water emulsions, the AO activity increases with the alkyl chain length of AO and reaches a maximum at an intermediate chain length, after which further increase in AO chain length results in a decrease in activity.

Acknowledgments

I would like to give my special thanks to my advisor, Prof. Larry Romsted, who is a serious scientist, an enthusiastic democracy advocate, and a caring friend. His curiosity and dedication for chemistry has always been inspiring me. His sense of humor makes my six years' research experience enjoyable and invigorating. He is the best mentor I've ever had in my life.

I would like to thank all my committee members, Prof. Kai Hultzsch, Prof. Ralf Warmuth, Prof. Kathryn Uhrich, and Prof. Qingrong Huang. I also would like to thank our collaborator, Prof. Carlos Bravo-Diaz, for his guidance and input on my research work.

I am very grateful to Prof. Qingrong Huang, Prof. Kathryn Uhrich, Prof. Fernando Muzzio and Prof. Jing Li and their group members for giving me access to their instruments, especially Frank Romanski and Eric Jayjock from Prof. Fernando Muzzio's group for the laser diffraction. Without their assistance, I won't be able to finish my thesis work efficiently.

I woud like to thank everyone I spent time with in Romsted's group: Gunaseelan Krishnan, Yan Cai, Steven Bachofer, Sander de Jong, Yongliang Zhang, Xiang Gao, Changyao Liu, Aijaz Ahmad, Tarek Awad, and Yanqiu Zhu. Their help and accompanies is unforgettable.

Finally, I would like to thank my husband Yanan for teaching me to use Latex for thesis writing.

Dedication

To everyone who loved me and is loving me and will love me

Table of Contents

List of Tables

List of Figures

Chapter 1

Introduction

1.1 Surfactant aggregates

The word surfactant, short for surface active agent, is equivalent to amphiphile, a long hydrophobic tail attached to a relatively small hydrophilic head group, Figure 1.1.[1] The hydrophobic tail is usually a hydrocarbon chain containing 8-18 carbon atoms, which can be linear, branch, or aromatic.

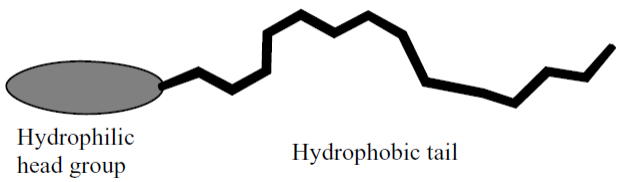

Figure 1.1: Schematic illustration of a surfactant

The differences in the head group structures are generally more varied than those in the tail. Head group charge is primarily divided into four categories: cationic, anionic, nonionic and zwitterionic. Figure 1.2 shows the structures of some representative surfactants.[1, 2]

Cationic: the head group bears a positive charge. The vast majority of cationic head groups are a tetrasubstituted nitrogen atom with alkyl or aryl groups or a hydrogen. Quaternary ammonium based molecules are the most common and protonated pH-sensitive long chain amines can also function as surfactants. The counterion of a cationic head group is negatively charged, including halide ions, nitrate, sulfate, etc.

Anionic: the head group bears a negative charge. Carboxylate, sulfate, sulfonate and phosphate are the common head groups found in anionic surfactants. The counterion of

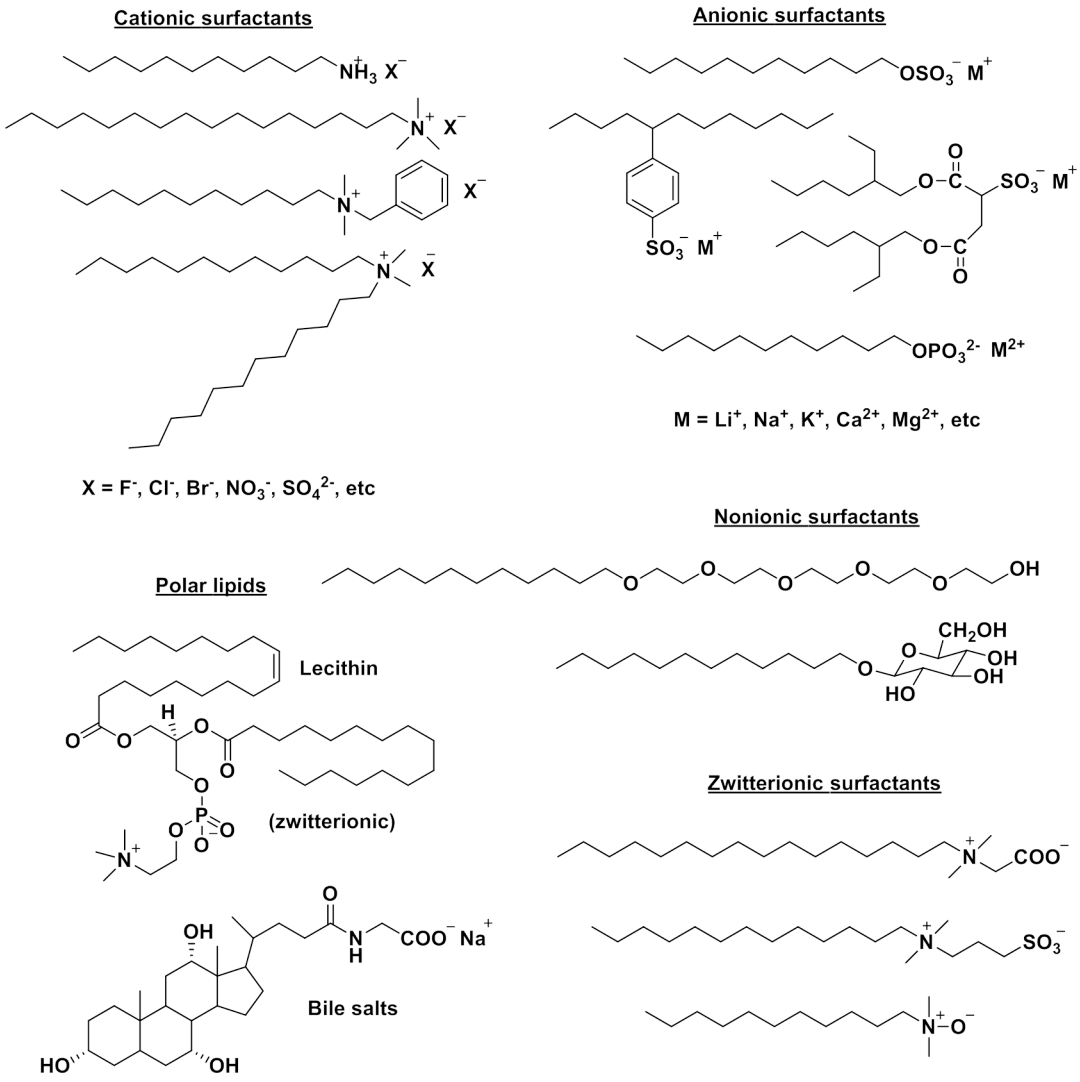

Figure 1.2: Structures of some representative surfactants

an anionic head group is positively charged, including alkali and alkaline earth metals and ammonium groups. Anionic surfactants are used in larger quantity than any other surfactant class.

Nonionic: the head group bears no charge. Polyether and polyhydroxyl units are the typical polar groups in nonionic surfactants, and polyether comprising ethylene oxide units constitutes the vast majority of nonionic surfactants. The single most important type of nonionic surfactant is fatty alcohol ethoxylates, which are referred to as C_mE_n, with m being the number of carbon atoms in the alkyl chain and n being the number of ethylene

oxide units.

Zwitterionic: the head group bears both a positive and negative charge. The positive charge is almost invariably based on amines or ammonium, whereas the negative charge is more variable and include a carboxylate group which is more common than a phosphate, sulfate and sulfonate group.

Surface active compounds are abundant in nature and are often referred to as polar lipids, Figure 1.2. In biological systems, surfactants are used in almost the same way as they are utilized in commercial systems: to overcome solubility problems as solubilizers or emulsifiers, to modify surfaces, etc. For example, biles salts solubilize hydrophobic components in the blood extremely efficiently, and mixtures of phospholipids constitute the membranes of cells.

Polar head groups like water while nonpolar tail groups dislike water. However, despite their mutual antipathy, the covalently bonded head and tail groups cannot leave one another. This dilemma faced by surfactant molecules is resolved in vivo and in vitro by the intriguing phenomenon called molecular self-assembly or self-aggregation, which was first suggested by McBain in 1913 based on his studies on the conductivity of soap solutions.[3] He found that soap solutions exhibited lower osmotic activity and higher conductivity than would be expected if one assumed that soap existed in solution as simple undissociated molecules. To account for the apparently abnormal results, McBain postulated that fatty acid salts spontaneously form stable aggregates in solutions. In general, the hydrophobic tails come close to each other to minimize their contact with water, while the hydrophilic head groups remain hydrated, forming three-dimensional structures with distinct and separate regions composed of the nonpolar parts and the polar parts, as illustrated in Figure 1.3. The increase in entropy from release of more ordered water surrounding the hydrocarbon chain is believed to be a major factor to spontaneous aggregation at ambient temperatures.[4] The sizes and shapes of these structures depend on the head group and counterion type, the solvent type, the structure of the hydrophilic tail, the additive type such as alcohol,

electrolyte, or another surfactant, and the experimental conditions such as temperature and surfactant concentration.[1, 5, 6, 7, 8, 9]

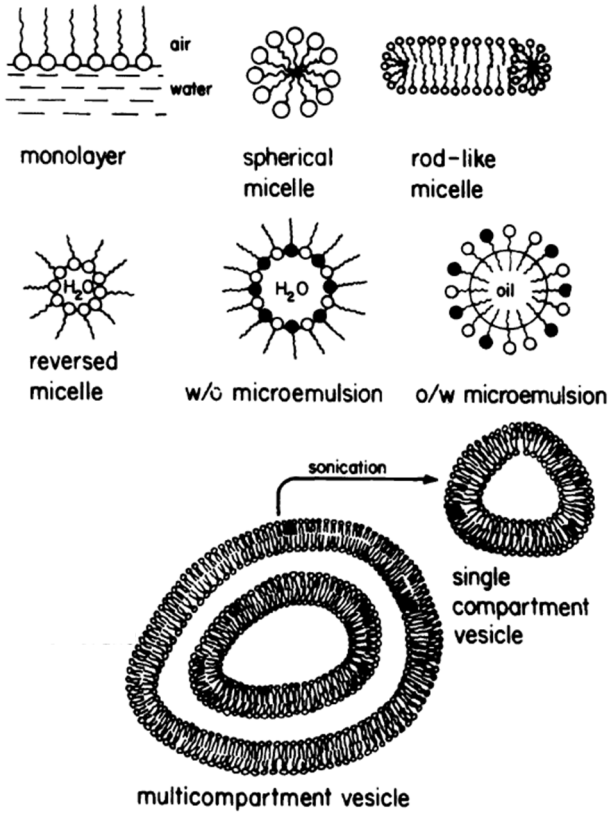

Figure 1.3: A simplified representation of self-assembled structures of surfactants[10]

Surfactant molecules adsorb at the air-water interface by sticking their hydrophobic tails into the air with the hydrophilic head groups immersed in the water forming a monolayer, Figure 1.3. Spherical micelles are generally formed by single-tailed surfactants in dilute aqueous solution and reversed micelles in nonpolar solvents such as cycohexane, *n*-heptane, isooctane, decane, toluene, etc. Sphere-to-rod transitions can occur with increasing surfactant concentrations. Both oil-in-water and water-in-oil microemulsions are composed of water, oil, surfactants, and additives such as a medium-chain alcohol. They contain considerably larger hydrocarbon regions than aqueous micelles and water pools than reversed micelles, respectively. Vesicles are closed bilayer structures and are characterized by two distinct water compartments, with one forming the interior and one the external medium.

Spontaneous formation of vesicles is achieved by dispersing twin-tailed surfactants or phospholipids in water or by mixing single-tailed cationic and anionic surfactants at specific ratios.[11, 12, 13, 14] Under certain conditions, micelles formed by single-tailed surfactants can transform into vesicles.[15, 16]

1.2 Dynamics of micelles

The formation of micelles starts at a certain concentration, the so-called critical micellization concentration (cmc). Below the cmc, surfactant molecules exist as free monomers in solution. Above the cmc, surfactants self-aggregate into micelles that are in equilibrium with free (nonmicellized) surfactants. Surfactant molecules are constantly exchanging between micelles, surrounding solution and the air/water interface. They can enter (associate with) micelles or exit (dissociate) from micelles. Due to these entry/exit processes, usually referred to as exchange processes, a surfactant monomer resides in a micelle for a finite time.[17]

The aggregation number of a micelle, i.e., the number of surfactant monomers per micelle, fluctuates as a result of the exchange processes. Some of the fluctuations can result in the complete dissociation of micelles into monodispersed surfactants. Conversely, free surfactants can self-aggregate and form micelles. Therefore, micelles are constantly forming/breaking down and they also have a finite lifetime.

In a nutshell, dynamics of micelles refers to the rate at which micelles form or break down, or the time a surfactant remains in a micelle. A schematic representation of dynamic equilibrium in micellar solution is shown in Figure 1.4. Values of the rate constants k^+ and k^- for the association and dissociation of one surfactant to/from a micelle have been estimated by using Aniansson and Wall theory of micellar kinetics.[18] Table 1.1 lists values of the aggregation number N, the rate constants k^+ and k^-, and the cmc of representative anionic, cationic, nonionic, and zwitterionic surfactants.[17] For all the listed surfactants, the values of k^+ fall between 1×10^8 and 9×10^9, regardless of the head group charge and

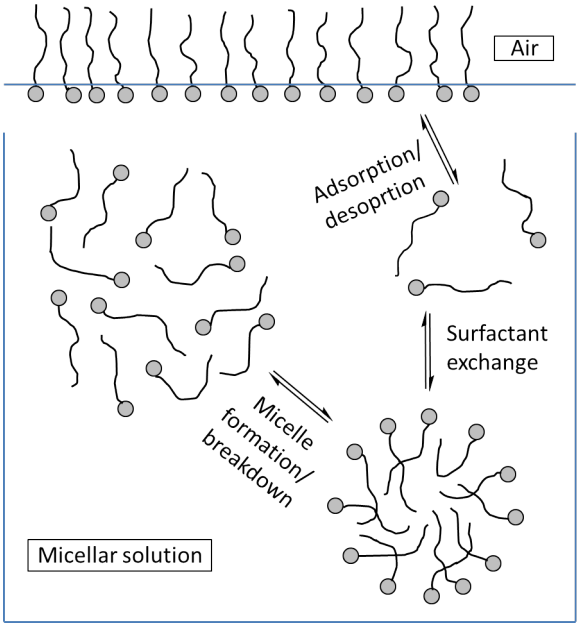

Figure 1.4: Dynamic equilibria in a micellar solution

chain length (from C_6 to C_{18}), which are close to the values of the rate constants calculated for diffusion-controlled processes. This means that the rate of association of a surfactant to a micelle is almost equal to the rate of collisions between free surfactants and micelles, i.e., there is little or no barrier to a monomer entering a micelle. The values of k^- decrease with the increase of the surfactant chain length, like the cmc of the surfactant, as can be seen from entries 1-8 and 10-13. Thus, surfactants with longer hydrophobic tails also have a longer residence time in micelles.

Micelles have the capacity to solubilize compounds (solubilizates) that are poorly soluble in water and the solubilizates are constantly exchanging (in dynamic equilibrium) between micelles and bulk solution like surfactant molecules. Some values of the exit (dissociation) rate constant k_s^- of a solubilizate from micelles and the entry (association) rate constant k_s^+ of the solubilizate into micelles for some solubilizates determined by experimental methods are listed in Table 1.2.[17] It shows that k_s^+ for all the solubilizates is in the range of 10^9-10^{10} $M^{-1}S^{-1}$, indicating the association of the solubilizates in micelles is very close to being diffusion-controlled. However, k_s^- varies with the hydrophobicity of the solubilizate to a

Table 1.1: Kinetic parameters of association and dissociation of anionic, cationic, nonionic, and zwitterionic surfactants from their micelles at 25 °C

Surfactant	N	$k^-(s^{-1})$	$k^+(M^{-1}S^{-1})$	cmc (mM)
1. $NaC_6H_{13}SO_4$	17	1.32×10^9	3.2×10^9	420
2. $NaC_7H_{15}SO_4$	22	7.3×10^8	3.2×10^9	220
3. $NaC_8H_{17}SO_4$	27	1.0×10^8	0.77×10^9	130
4. $NaC_9H_{19}SO_4$	41	1.4×10^8	2.3×10^9	60
5. $NaC_{10}H_{21}SO_4$	50	6.8×10^7	2.1×10^9	34
6. $NaC_{12}H_{25}SO_4$	64	1×10^7	1.2×10^9	8.2
7. $NaC_{14}H_{29}SO_4$	80	9.6×10^5	0.47×10^9	2.05
8. $NaC_{16}H_{33}SO_4$ (30°C)	100	6×10^4	0.13×10^9	0.45
9. $C_8H_{17}N(CH_3)_3Br$	25	1×10^9	3.6×10^9	280
10. $C_{10}H_{21}N(CH_3)_3Br$	38	1.7×10^8	2.6×10^9	66.3
11. $C_{12}H_{25}N(CH_3)_3Br$	49	3.2×10^7	2.2×10^9	14.6
12. $C_{14}H_{29}N(CH_3)_3Br$	66	3.2×10^6	0.86×10^9	14.6
13. $C_{18}H_{37}N(CH_3)_3Br$	125	6.4×10^5	0.96×10^9	0.245
14. $C_8H_{17}(OCH_2CH_2)_8OH$	72	8.7×10^7	8.3×10^9	10.4
15. $C_{12}H_{25}N(CH_3)_2SO_3$	44	1.7×10^8	4.5×10^9	38

great extent whether it is aromatic (see entries 1, 2, 3, 8, 9) or aliphatic (compare entries 4 and 5; entries 10 and 11) or is aromatic with an increasing aliphatic moiety (compare entries 6 and 7).

In principle, the above statement for micelles also holds for larger self-assembled systems: microemulsion and emulsion droplets, vesicles, and mesophases. In addition to providing a better knowledge of micellar system, a good understanding of the dynamics in micellar solutions is a requirement for interpreting the experimental results in other areas of surfactant science, such as surfactant adsorption on surfaces; the interaction between surfactant assemblies; rheology of surfactant solutions; solubilization in, and emulsification, wetting, and foaming by, micellar solutions; the use of micelles and other association colloids as microreactors in which chemical reactions are performed.[17]

Table 1.2: Values of k_s^+ and k_s^- for some compounds in micelles at 25 °C

Compound	Surfactant[a]	$k_s^-(s^{-1})$	$k_s^+(M^{-1}S^{-1})$
1. Naphthalene	SDS	1.3×10^6	1.9×10^{10}
2. 1-Bromonaphthalene	SDS	2.5×10^4	4×10^{10}
3. *m*-Dicyanobezene	SDS	6×10^6	1×10^{10}
4. Methylene iodide	CTAB	9.5×10^6	2.5×10^{10}
5. Ethyl iodide	SDS	5×10^6	2×10^{10}
6. Acetophenone	SDS	7.8×10^6	2.6×10^{10}
7. Propiophenone	SDS	3×10^6	1.4×10^{10}
8. Benzophenone	SDS	2×10^6	5.2×10^{10}
9. Xanthone	SDS	1.6×10^6	1.2×10^{10}
10. cis 1,3-Pentadiene	SDS	8.9×10^6	1.2×10^9
11. 1,3-Hexadiene	SDS	2.3×10^6	8.3×10^8
12. Acetone	SDS, CTAB	$1 - 4 \times 10^8$	$> 10^{10}$
13. Molecular oxygen	SDS, CTAB	$< 5 \times 10^7$	1.3×10^{10}

a. SDS: sodium dodecyl sulfate; CTAB: cetyl trimethylammonium bromide.

1.3 Reactivity in surfactant aggregates

1.3.1 Overview

Surfactant aggregates including aqueous and reversed micelles, microemulsions and emulsions, vesicles play an important role in reactivity control for thermal reactions. They all have interfacial regions containing hydrated head groups and water molecules that can solubilize, concentrate, and organize reactants and products, shift chemical equilibria, and alter chemical pathways and rates. Orders of magnitude rate enhancements[19, 20, 21, 22, 23, 24, 25, 26, 27, 28, 29, 30] as well as inhibitions[31, 32, 33, 34] have been extensively reported in these systems. Changes of the rate depend on the nature of the reaction, i.e., spontaneous unimolecular or bimolecular, the distribution of the reactants, and the charge of the reactants relative to that of the surfactants, i.e., co-ions or counter-ions of the surfactant head group. To interpret the aggregate effects on chemical reactivity, a number of models have been developed, for example, the enzyme model[35] and the coulombic model.[36] The most successful and widely used model is the pseudophase kinetic model[19, 20, 21, 25, 37, 38, 39], which will be discussed in detail in the next section.

1.3.2 Pseudophase kinetic model

The basic assumptions of the pseudophase kinetic model are:

1. The totality of the interfacial regions created by surfactant molecules is treated as a separate phase or region that is distinct from bulk solution and is called a "pseudophase". The overall, observed rate of a reaction is the sum of the rates in the aqueous phase and the surfactant pseudophase.

2. Component molecules and ions diffuse orders of magnitude faster than rates of most thermal reactions studied in association colloids and emulsions. Their diffusivities may be near their diffusion control limit within and between regions. Therefore, reactant distributions throughout the total volume of an aggregate system are in dynamic equilibrium i.e., their concentrations in each region are constant after initial mixing is complete. (See Section 1.2 Dynamics in micelles above.)

3. The concentrations of reactants in each region are proportional to their relative solubilities in each region, and their distributions are described by partition constants or association constants between regions.

4. The medium properties of the amphiphilic aggregates are not significantly perturbed by the reactants present in the system provided that the stoichiometric concentration of the reactants are kept significantly lower than that of the surfactant. Experimentally, the ratio of the concentration of surfactant over reactants is typically maintained as $> 100{:}1$.

Application of the pseudophase kinetic model to unimolecular and bimolecular reactions in micelles are demonstrated below.

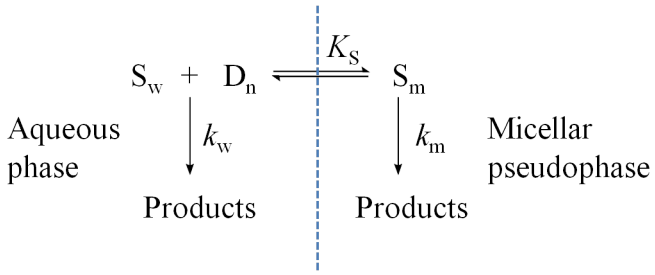

Figure 1.5: Pseudophase model applied to unimolecular reactions in micellar solutions

Figure 1.5 shows the representation of the pseudophase model of spontaneous, unimolecular reactions in aqueous micellar solutions. S_w and S_m represent free and micellar bound substrates, respectively and D_n stands for micellized surfactants (detergents). The distribution of the substrate between the two regions at equilibrium is generally described by an association constant, K_S.

$$K_S = \frac{[S_m]}{[S_w][D_n]} \tag{1.1}$$

$$[D_n] = [D_T] - \text{cmc} \tag{1.2}$$

Square brackets indicate the concentration in moles per liter of total solution volume and subscript T denotes the stoichiometric concentration. The size of K_S value is determined by the substrate hydrophobicity, i.e., the more hydrophobic the substrate is, the larger the value of K_S. Equation 1.2 shows that the micellized surfactant concentration is the difference between the stoichiometric surfactant concentration and the cmc under experimental reaction conditions. Often, reactions are carried out at surfactant concentrations well above the cmc, i.e., $[D_T] \gg \text{cmc}$, $[D_n] \approx [D_T]$. The pseudophase model is a two-site model, thus the substrate is either micellar bound or free in the bulk aqueous phase. The total substrate concentration, $[S_T]$, is given by the mass balance equation:

$$[S_T] = [S_w] + [S_m] \tag{1.3}$$

The observed rate is the sum of the rate of the reaction in the aqueous and micellar pseusophases:

$$\frac{-\mathrm{d}[S_T]}{\mathrm{dt}} = k_{obs}[S_T] = k_w[S_w] + k_m[S_m] \tag{1.4}$$

where k_{obs}, k_w, and k_m are first-order rate constants for the overall reaction and the reaction in the aqueous and micellar regions, respectively. Combining Equations 1.1, 1.2, 1.3, and 1.4 gives an expression for k_{obs}:

$$k_{obs} = \frac{k_w + k_m K_S([D_T] - \text{cmc})}{1 + K_S([D_T] - \text{cmc})} \tag{1.5}$$

Equation 1.5 predicts that reactivity in aggregates is determined by independent rate constants in each pseudophase and by the equilibrium constant for substrate distribution, and is independent of the size or shape of the aggregates. Comparison of micellar and aqueous rate constants reflect differences in medium properties of micelles and water. When $k_m/k_w > 1$, spontaneous reaction is catalyzed by micelles and rate increases initially at surfactant concentration greater than cmc then levels off after the substrate is fully associated with micelles; when $k_m/k_w < 1$, micellar inhibition occurs and rate-surfactant concentration profile is opposite to that of micellar catalysis.[37, 40, 41] Values of k_w and k_m can be estimated under limiting conditions: when surfactant concentration is below the cmc, i.e., $[D_T] \leq$ cmc, $[S_T] = [S_w]$ and $k_{obs} = k_w$; when the substrate is completely micellar bound at high surfactant concentration, i.e., $K_S[D_n] \gg 1$ and $[S_T] = [S_m]$, $k_{obs} = k_m$. In both cases, k_{obs} is independent of the surfactant concentration.

For bimolecular reactions, reaction rate within the micellar pseudophase depends on the *local concentration* of the second reactant, N, Figure 1.6, and not its stoichiometric concentration.[20]

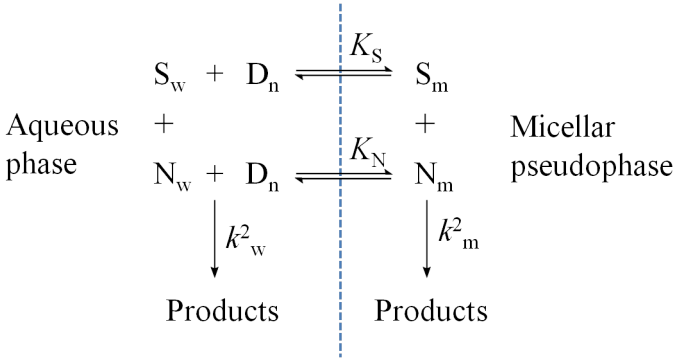

Figure 1.6: Pseudophase model applied to bimolecular reactions in micellar solutions

The observed rate is given by Equation 1.6:

$$\frac{-d[S_T]}{dt} = k_{obs}[S_T] = k_2[S_T][N_T] = k_2^w[S_w][N_w] + k_2^m[S_m](N_m) \tag{1.6}$$

where parenthesis indicates the reactant concentration in moles per liter of the volume of

micellar pseudophase. Bimolecular reactions are generally run under pseudo first-order conditions when the stoichiometric concentration of the second reactant is in large excess over the substrate, i.e., $[N_T] \gg [S_T]$. The observed first-order rate constant, k_{obs}, is expressed in terms of the overall second-order rate constant and the stoichiometric concentration of the second reactant.

The relationship between (N_m) and $[N_m]$ is shown in Equation 1.7:

$$(N_m) = \frac{[N_m]}{V_m[D_n]} \tag{1.7}$$

where V_m is the molar volume in liters per mole of reactive region in the micellar pseudophase and $V_m[D_n]$ denotes the micellar fractional volume in which the reaction occurs. The value of V_m is much smaller than that of the total solution, thus binding the reactant to the aggregates strongly enhances its local molarity, which accounts for most of the micellar "catalysis". Values of V_m cannot be measured independently and it is often set equal to the molar volume of the micelle or of the interfacial region.[38]

Combining Equations 1.1, 1.2 and 1.6 gives

$$k_{obs} = \frac{k_2^w[N_w] + k_2^m K_S(N_m)([D_T] - cmc)}{1 + K_S([D_T] - cmc)} \tag{1.8}$$

Equation 1.8 describes rate-surfactant concentration profile for bimolecular reactions under pseudo-first order conditions in aggregation systems as a function of the total aggregate concentration. Both the substrate binding constant and the second-order rate constant in each pseudophase do not depend on the size or shape of the aggregates. k_{obs} is also affected by the concentration of the second reactant in the bulk aqueous phase of the total solution volume, $[N_w]$, and the concentration of the second reactant associated with the aggregates of the reaction volume, (N_m).

However, the above treatments based on the pseudophase model fail to explain the effect of added salts on the reactivity of reactions involving ionic reactants at charged interfaces. Modification of the pseudophase model was made by Romsted and the pseusophase ion exchange (PIE) model was developed.[37]

Two assumptions in the PIE model are: (1) The micellar surface acts as a selective ion exchanger. Reactive counterions, N, and inert counterions, X, undergo one to one exchange between the aqueous and micellar pseudophases, Figure 1.7, and the competition between

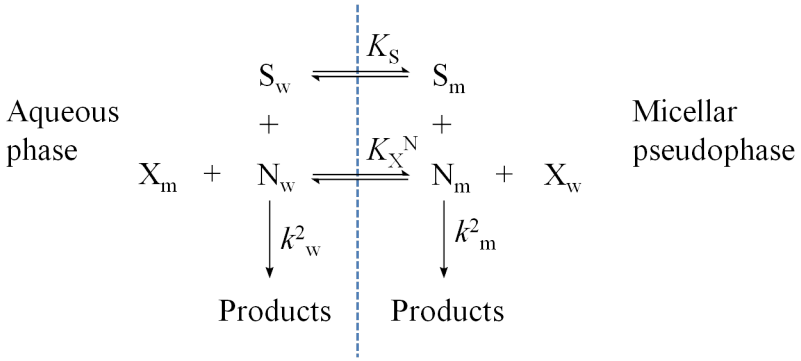

Figure 1.7: Pseudophase ion exchange model applied to bimolecular reactions in micellar solutions

them is described by an ion-exchange constant, K_X^N, indicative of the selectivity of the micellar interface towards the two counterions:

$$K_X^N = \frac{[N_m][X_w]}{[N_w][X_m]} \tag{1.9}$$

Values of K_X^N for a variety of counterions are similar to those of loosely cross-linked ion-exchange resins[42, 43] and depend on specific ion interactions, e.g., hydration and polarizability. A large, weakly hydrated polarizable anion, e.g., Br^-, binds strongly to the micelle and displaces a reactive counterion, e.g., OH^-, thus lowering the local concentration of one of the reactants within the micellar pseudophase.

(2) The fraction of the surface occupied by the two counterions is assumed to be constant:

$$\beta = \frac{[N_m] + [X_m]}{[D_n]} \tag{1.10}$$

where β is the degree of counterion association. Estimated values of β from the fractional micellar charge α ($\alpha = 1 - \beta$) for different counterions are numerically similar ($\beta = 0.6 - 0.9$) and are insensitive to surfactant and salt concentrations.[44, 45]

The PIE model has been successfully applied to bimolecular reactions between an organic substrate and an ionic reactant in micelles as well as in other aggregation systems such as

reverse micelles, microemulsions, and vesicles to interpret kinetic profiles.[27, 43, 46, 47, 48, 49, 50, 51, 52, 53, 54]

1.4 Investigating interfacial properties and determining component distributions and activities using arenediazonium probes

Long chain arenediazonium probes were developed in our group to estimate the interfacial compositions and determine the distributions and activities of phenolic compounds in a variety of aggregation systems.[55, 56, 57, 58, 59, 60, 61, 62, 63, 64, 65, 66, 67, 68, 69] The methodologies are based on two types of reactions of two analogue probe molecules: one called chemical trapping is between 4-*n*-hexadecyl-2,6-dimethylbenzenediazonium ion, 16-2,6-ArN_2^+, and weakly basic nucleophiles, such as water, alcohol, halides, sulfonate, carboxylate, etc. The other is called kinetic method between 4-*n*-hexadecylbenzenediazonium ion, 16-ArN_2^+, and phenolic compounds such as *tert*-butylhydroquinone. Both arenediazonium ions, themselves, are cationic surfactants that bind strongly to the surfactant aggregates, thus the reactions only take place at the interfaces. The mechanisms of the reactions and the logic of our approaches will be elaborated below.

1.4.1 Reactivity of arenediazonium ions

Arenediazonium ions react with a variety of nucleophiles via different reaction pathways depending upon the type of the substituent on the aromatic ring, the type of the nucleophile, the nature of the solvent, pH, the presence or absence of catalyst, light, etc. The reaction mechanisms of arenediazonium ions have been extensively explored but some pathways are still under debate.[70, 71, 72, 73] Two major pathways pertinent to the thesis work are summarized below:

1. Replacement of nitrogen by nucleophiles (Dediazoniation)

In the absence of UV light, base, reducing and electron transfer agents, arenediazonium ions generally undergo spontaneous dediazoniation reaction. Three ionic pathways for the

replacement of nitrogen from an arenediazonium ion by a nucleophile Y^- are presented in Fig 1.8. Pathway (a) has S_N1 character in which a phenyl cation intermediate is formed by

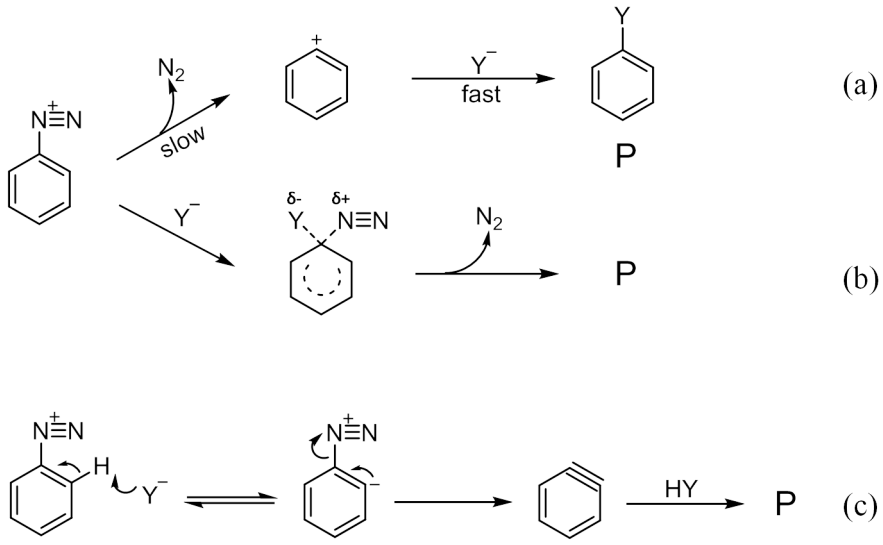

Figure 1.8: Reaction pathways for dediazoniation

rate-determining loss of N_2. Although the phenyl cation has never been detected in solution, its lifetime is estimated to be in the picosecond time scale.[73, 74, 75] Pathway (b) is a bimolecular nucleophilic aromatic substitution in which a transition state or an intermediate is produced by synchronous loss of N_2 with attack by Y^-, and either the formation or breakdown of the intermediate can be rate determining. Pathway (c) is an elimination-addition reaction which involves the formation of an aryne followed by the addition of HY. The rate determining step in this pathway can be any of the steps on the reaction sequence. These three pathways apply to reactions under different conditions. The aryne route (c) has not been observed in aqueous solutions for simple arenediazonium salts. This is simply demonstrated by the absence of rearranged products. For example, dediazoniation of *o*-toluenediazonium chloride in water yields only *o*-cresol but no *m*-cresol.[72] The distinction between mechanisms (a) and (b) remains controversial.[71]

The unimolecular, phenyl cation pathway (a) has been supported by several pieces of evidence from kinetic studies on dediazoniation reaction of benzenediazonium tetrafluoroborate ($C_6H_5N_2BF_4$) in solutions.[72] The observed first-order rate constant is remarkably

insensitive to solvent polarity and solvent composition, Table 1.3.[55, 72] In terms of transition state theory, this means that solvents affect the ground and transition state to similar extents, i.e., the free energy of activation is approximately constant.

Table 1.3: First-order rate constants for dediazoniation of benzenediazonium tetrafluoroborate in various solvents at 25 °C

Solvent	$10^5 k_{obs}$ (s^{-1})	Dielectric constant
0.1% (0.01 M) H_2SO_4	4.55	80.1
105% (21 M) H_2SO_4	2.15	110.0
100% CH_3COOH	2.26	6.2
100% CH_3COOH + 1.0 M LiCl	4.51	
CH_2Cl_2	2.20	8.9
CH_3CN	3.3	37.5
CH_3OH	9.1	32.7
CH_3CH_2OH	8.2	24.3
DMSO	4.16	48.9
3-Methylsulfolane	1.36	43.3
Dioxane	1.15	2.2

The entropy of activation for the hydrolysis of $C_6H_5N_2^+$ (+10.5 cal mol^{-1} deg^{-1}) is similar to that for the solvolysis of *t*-butyl chloride but significantly different from the large negative entropies of activation for reactions in which water participates in the rate determining step. Also, the hydrolysis shows no solvent isotope effect ($k_{H_2O}/k_{D_2O} = 0.98 \pm 0.01$) ruling out any mechanism involving the charge buid-up on oxygen of water in the transition state.[72]

Linear dependences of the rates of dediazoniation on the concentration of anion, i.e., nucleophiles, were found for several anions including bromide and thiocyanate ion.[76, 77] This suggests participation of the nucleophile in the rate-determining step. However, the increase in rate is quite small which makes it inherently difficult to unambiguously distinguish between the phenyl cation and bimolecular pathways. By contrast, straightforward second-order kinetics were observed for arylations of a series of aromatic substrates by benzenediazonium tetrafluoroborate in trifluoroethanol.[78] Calculations have shown that free phenyl cation is not an obligatory intermediate in aqueous solutions.[73]

Generally, pathway (a) is followed in water with most nucleophiles, e.g., H_2O, Cl^-, F^-, Br^-, whereas pathway (b) may occur when stronger nucleophiles, e.g., NCS^-, are

present in solvents of lower ionizing power and when there are strongly electron-withdrawing substituents on the arenediazonium ion.

2. Reaction of nucleophiles at the terminal nitrogen

Strong nucleophiles, e.g., OH^-, CH_3O^-, PhO^-, $ArNR_2$, CN^-, RNH_2, generally attack the terminal nitrogen of arenediazonium ions to give azo adducts, Figure 1.9. If the nucleophile can form a relatively stable radical via electron transfer, then homolytic cleavage leading to phenyl radical and ultimately arylation products may predominate.

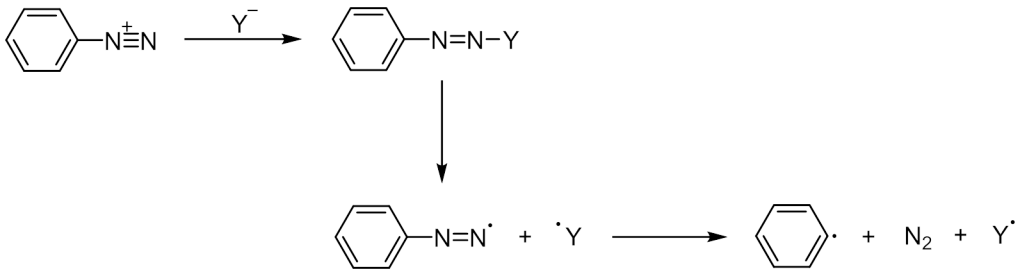

Figure 1.9: Nucleophilic attack on the terminal nitrogen

1.4.2 The chemical trapping method

Understanding relationships between solution composition, component distributions, and aggregate structure and stability in surfactant aggregates requires determination of their interfacial compositions. A variety of techniques, e.g., conductometry, potentiometry, and spectrophotometry (NMR, ESR, UV-visible, fluoresence, IR, and circular dichroism) have been used to examine the compositions of multicomponent aggregation systems.[79] Some methods measure only one component at a time, some have limits on composition ranges, and others report on physical properties such as surface polarity rather than composition. Our chemical trapping method is a probe technique that provides simultaneous measurements of concentrations of more than one component in the interfacial regions of surfactant aggregates.

The method is based on the dediazoniation reaction of 4-alkyl-2,6-dimethylbenzenediazonium ions (prepared as their tetrafluoroborate salts), z-2,6-ArN_2BF_4 (z = 16 or 1), with

weakly basic nucleophiles, e.g., H_2O, ROH, Br^-, Cl^-, RSO_3^-. As discussed in section 1.4.1, the rate of the reaction is insensitive to solvent polarities, and also insensitive to nucleophile concentrations and types.[79, 80, 81] This means that the distribution of nucleophiles in the immediate vicinity of the ensemble of the ground state arenediazonium ions remain constant through product formation. Therefore, product yields reflect concentrations of nucleophiles within the immediate vicinity of the ground sate arenediazonium ions. Products formed from the dediazoniation reaction of competitive nucleophiles, H_2O and X^-, with z-2,6-ArN_2^+ are shown in Figure 1.10.

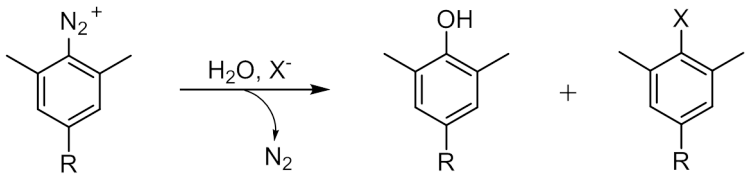

R = $C_{16}H_{33}$ or CH_3, X^- = Br^-, Cl^-, RSO_3^-, etc

Figure 1.10: Dediazoniation reaction of z-2,6-ArN_2^+ with H_2O and X^- nucleophiles

The long chain derivative, 4-*n*-hexadecyl-2,6-dimethylbenzenediazonium ion, 16-2,6-ArN_2^+, is added to surfactant solutions to probe the interfacial regions. Because 16-2,6-ArN_2^+ is insoluble both in water and oil and it has a long hydrophobic tail attached to a cationic headgroup, it binds strongly to surfactant aggregates and reacts with nucleophiles only within the interface. Recent molecular dynamics simulation results from our collaborators in France show that the diazonio group of 16-2,6-ArN_2^+ is in the same average location in the interfacial region as the ammonium headgroup of CTAB.[82] The stoichiometric probe concentration in the total solution is kept very low, typically on the order of 10^{-4} M, to minimize perturbation of the structure and medium properties of surfactant aggregates. The water-soluble short chain analogue, 2,4,6-trimethylbenzenediazonium ion, 1-2,6-ArN_2^+, is used to determine the selectivity of the dediazoniation reaction toward different nucleophiles, usually relative to water, in the absence of surfactants.

Figure 1.11 illustrates the dediazoniation reaction of 16-2,6-ArN_2^+ and 1-2,6-ArN_2^+ in

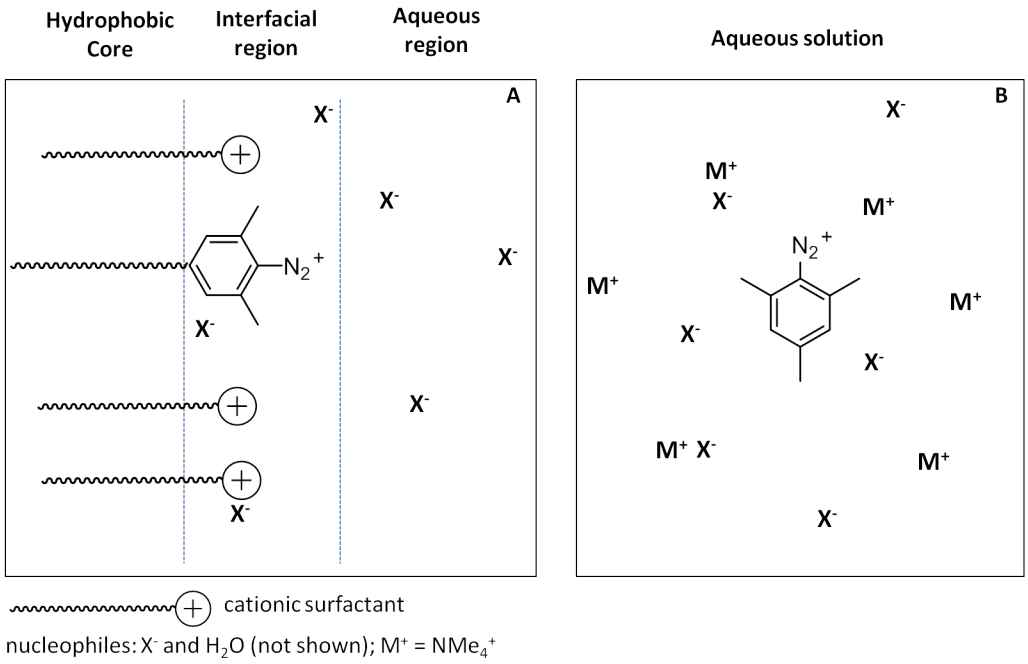

Figure 1.11: A: a small section of the interfacial region of a cationic micelle illustrating the location of the reactive group of 16-2,6-ArN_2^+ when it reacts with X^- and H_2O in the interfacial region. B: an aqueous reference solution containing the same nucleophiles

micellar and in aqueous reference solutions, respectively. Figure 1.11A is a cartoon not a real picture of the interfacial region because surfactant and probe molecules and all other components are constantly moving rapidly throughout the micellar solution, the locations of the head groups of the surfactant and probe molecules shown in Figure 1.11A are time averaged estimates.

The components in the aqueous solution (Figure 1.11B) are comparable to that of interfacial region in the micelle (Figure 1.11A): cationic headgroup models, counterions, water, and arenediazonium ions. Both in surfactant aggregate and bulk solutions, all the components are assumed to be in dynamic equilibrium such that product yields are proportional to their concentrations in solution. The fundamental assumption of estimating interfacial concentrations of weakly basic nucleophiles is that the selectivity of the dediazoniation reaction of 16-2,6-ArN_2^+ toward two different nucleophiles within the interfacial region of a surfactant aggregate is the same as that of 1-2,6-ArN_2^+ toward the same nucleophiles in a

reference bulk solution of the same composition. The selectivity is defined as:

$$S_{\mathrm{W}}^{\mathrm{X}} = \frac{\frac{(\%1-\mathrm{ArX})}{[\mathrm{X}]}}{\frac{(\%1-\mathrm{ArOH})}{[\mathrm{H_2O}]}} = \frac{\frac{(\%16-\mathrm{ArX})}{\mathrm{X_m}}}{\frac{(\%16-\mathrm{ArOH})}{\mathrm{H_2O_m}}} \tag{1.11}$$

where $S_{\mathrm{W}}^{\mathrm{X}}$ is the selectivity of the dediazoniation reaction toward nucleophile X compared to water; square brackets indicate the concentration in moles per liter of total solution volume; subscript m indictes the interfacial molarity in moles per liter of interfacial volume; % denotes the percent yield of a product; and parentheses are symbols for product yields. The assumption is logical because rate constants of dediazoniation reactions are extremely insensitive to solvent effects and nucleophile concentrations and because the selectivities are small. For neutral nucleophiles, e.g., alcohols, urea, acetamides, values of their selectivities in water are between 0.1 to 1[57, 83] and for anionic nucleophiles, the values range from about 2.3 to 22.[61, 79, 84] Based on these characteristics, we assume that when the product yield from reaction of a particular nucleophile with 16-2,6-$\mathrm{ArN_2^+}$ in the interfacial region of a surfactant aggregate is the same as the product yield from reaction of the same nucleophile with 1-2,6-$\mathrm{ArN_2^+}$ in bulk aqueous solution, i.e., when (%16-ArX) = (%1-ArX) and (%16-ArOH) = (%1-ArOH), then the concentration of a nucleophile in the interfacial region and in aqueous solution are the same, i.e., $\mathrm{X_m} = [\mathrm{X}]$ or $\mathrm{H_2O_m} = [\mathrm{H_2O}]$. In short, *when the yields are the same, the concentrations are the same.*

For example, to estimate interfacial concentration of $\mathrm{Br^-}$ in CTAB micelles, dediazoniations of 16-2,6-$\mathrm{ArN_2^+}$ and 1-2,6-$\mathrm{ArN_2^+}$ were carried out in CTAB micelles and in aqueous solution of tetramethylammonium bromide, TMABr, over a wide range of TMABr concentrations, respectively. The product yields of %16-ArBr and %1-ArBr are measured by HPLC. The relationship between %1-ArBr and [TMABr] defines a standard curve, Figure 1.12.[4] The dashed line in Figure 1.12 indicates that %16-ArBr = %1-ArBr = 36%. At this yield, the interfacial concentration of $\mathrm{Br^-}$ in 0.01 M CTAB is assumed to be equal to the stoichiometric concentration of $\mathrm{Br^-}$ in bulk TMABr solution, 2.25 M. The interfacial water molarity, $\mathrm{H_2O_m}$, can be estimated in the same way or calculated by using equation (1.11)

and the corresponding values of %16-ArOH, %16-ArBr, and Br_m.

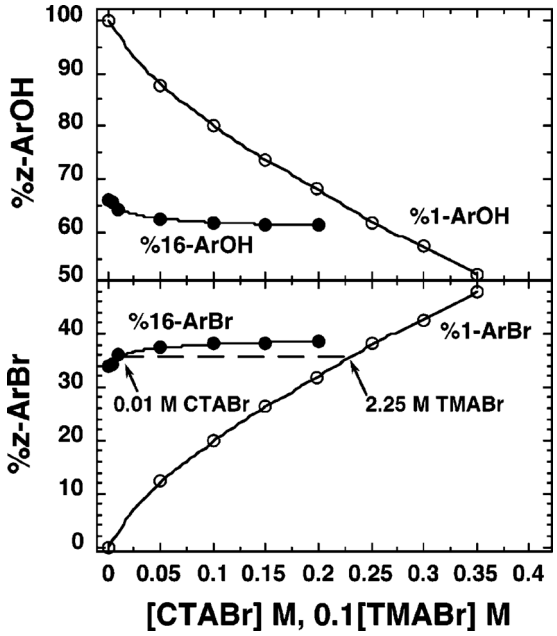

Figure 1.12: Product yields from dediazoniation reaction of 16-2,6-ArN_2^+ in CTAB micelles (•) and 1-2,6-ArN_2^+ in aqueous TMABr solutions (∘) with H_2O (top) and Br^- (bottom) at 40 °C

.

The chemical trapping method has been applied to a variety of surfactant aggregates to probe their interfacial compositions. Results include: hydration numbers of and terminal OH distributions in nonionic micelles,[57, 58, 59] interfacial water and anion concentrations in and degree of ionization of CTACl and CTABr cationic micelles,[55, 85] interfacial counterion, water and alcohol concentrations in reverse microemulsions,[86] interfacial halide ion concentrations in zwitterionic micelles and vesicles.[87, 88] Trapping and cleavage of the amide bonds of polypeptides at aggregate interfaces provides insight into the topology of protein.[62, 69] Dediazoniation reactions of z-2,6-ArN_2^+ with various nucleophiles that are commonly found in both commercial surfactant solutions and in biomembranes and proteins is shown in Figure 1.13.

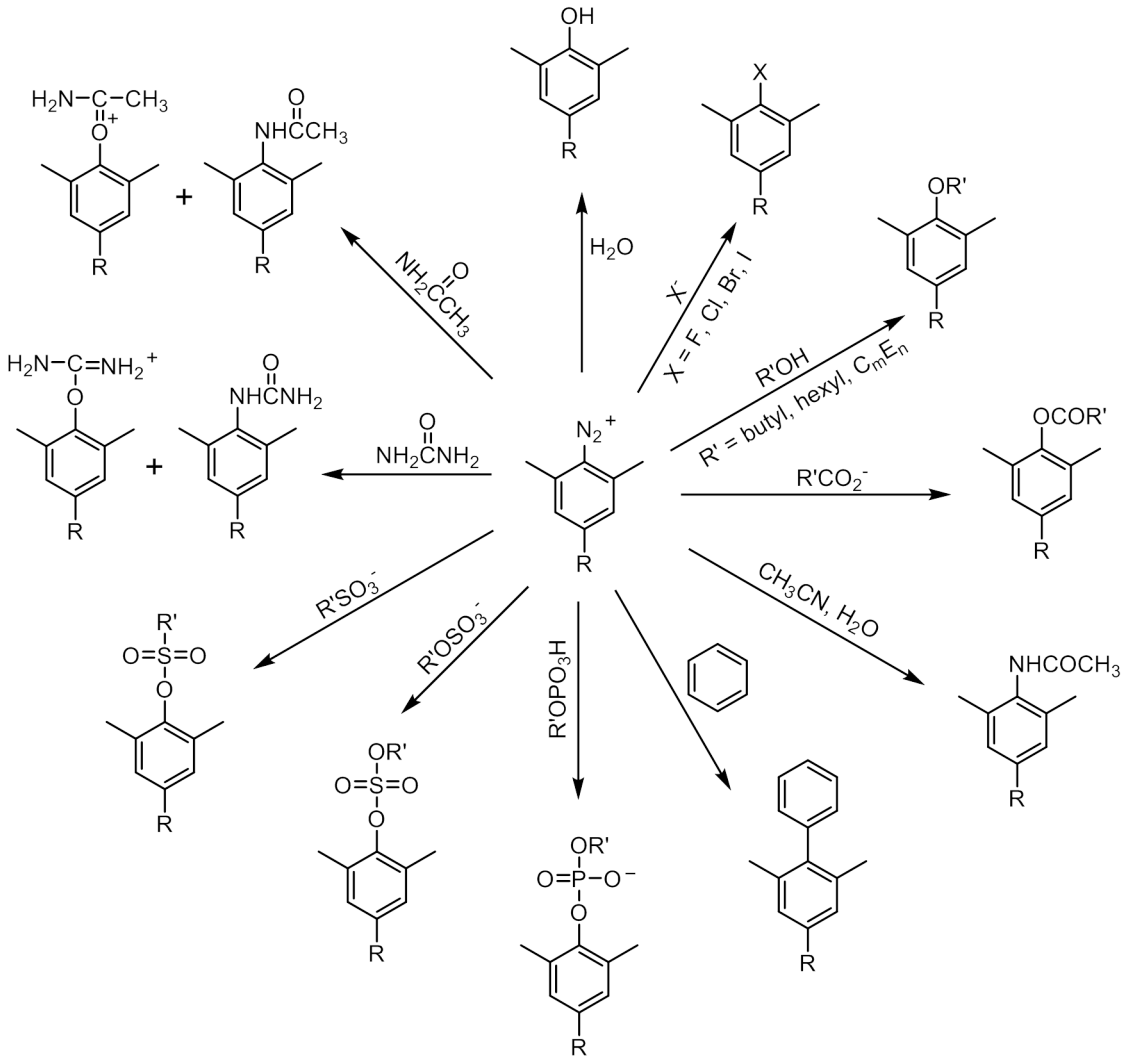

Figure 1.13: Dediazoniation reactions with different reactants[79]

1.4.3 The chemical kinetic method

Rates of reactions in surfactant aggregates are primarily affected by the distributions of the solubilized species within the aggregates. Based on the pseudophase model, substantial progress has been achieved in understanding the factors that control the partition behavior and chemical reactivity of polar organic molecules in homogeneous solutions of association colloids such as micelles, microemulsions, and vesicles.[38, 89] However, the study in opaque, biphasic emulsions is more challenging because they contain large droplets and low concentrations of solutes and they are more difficult to observe by conventional methods used

in homogeneous solutions such as UV-visible, fluorescence, or NMR spectroscopies. Our group has developed a new approach for estimating distributions of polar additives such as antioxidants in emulsions by combining a conceptual kinetic model with novel experimental methods.

Reaction of hydroquinone with arenediazonium ion

Arenediazonium ions are highly susceptible to reduction via one-electron transfer processes. Two particular mechanisms for the reaction are recognized. One is a "nonbounded" outer-sphere mechanism (path *a* in Figure 1.14) involving direct electron transfer from a reducing agent ($Red:^-$) to the diazonium ion. The second is a "bonded" inner-sphere mechanism (path *b* in Figure 1.14, the same mechanism discussed in section 1.4.1 called nucleophilic attack on the terminal nitrogen) involving the formation of an intermediate complex (Ar-N=N-Red) which subsequently decomposes into radicals.[90]

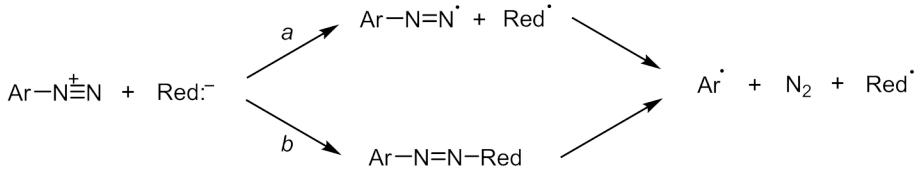

Figure 1.14: Reaction mechanisms for the reduction of arenediazonium ions via electron transfer processes

Some reductive transformations of arenediazonium ions undergo inner-sphere pathways,[71] for example, the reaction with $H_2PO_2^-$ or $PhSO_2^-$. Outer-sphere pathways were reported for reduction of arenediazonium ions by potassium ferrocyanide and decamethylferrocene.[91] Both the inner-sphere[70] and outer-sphere[92] pathways have been proposed for reactions of arenediazonium ions with phenolic compounds. Brown and Doyle[93] performed a detailed study on the kinetics and mechanism for the reaction between arenediazonium ions and hydroquinone(H_2Q). They found that the reaction occurs with the stoichiometry ArN_2^+/H_2Q of 2:1. The absence of evidence for a diazo ether intermediate suggested that electron transfer occurs by an outer-sphere mechanism. Further evidence supporting this

mechanism was provided by showing that the values of the rate constants obtained by experiments are in agreement with a predicted outer-sphere electron transfer process. Figure 1.15 shows the reaction mechanism proposed by Brown and Doyle.

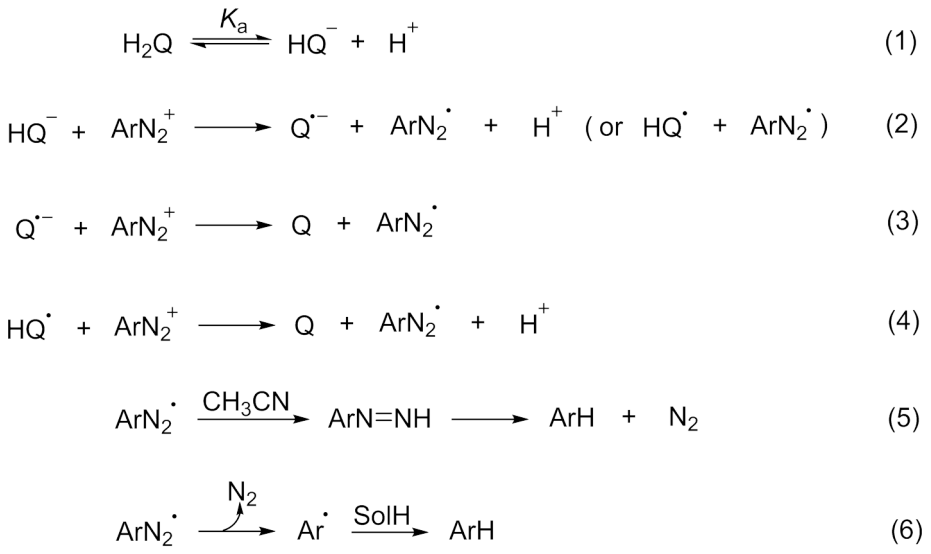

Figure 1.15: Mechanism for reaction between hydroquinone and arenediazonium ion

The reaction is a multi-step free radical reaction that is first order in both hydroquinone and arenediazonium ion and is pH-dependent. H_2Q (the first pKa of H_2Q is about 10) is in equilibrium with its monobasic anion, HQ^-, Equation (1). Single electron transfer occurs from HQ^- to arenediazonium ion, ArN_2^+, and aryldiazenyl radical, $ArN_2^\bullet$, and semiquinone radical anion, $Q^{\bullet -}$ (or its protonated analogue, the semiquinone radical, $HQ^\bullet$), are formed, Equation (2). $Q^{\bullet -}$ and $HQ^\bullet$ are themselves susceptible to further oxidation by ArN_2^+ through fast single electron transfer to produce quinone, Q, and a new $ArN_2^\bullet$, Equation (3) and (4). $ArN_2^\bullet$ can undergo hydrogen abstraction from the hydrogen-donor solvent such as acetonitrile with subsequent nitrogen extrusion, Equation (5), or loss of nitrogen and subsequent hydrogen abstraction from the solvent, Equation (6). Hydrogen transfer from water or hydroquinone does not occur as evidenced by the absence of isotope incorporation by deuterium abstraction from deuterium oxide or acetonitrile-d_3. Jirkovsky et al.[94] have found out that the rate constant for the reduction of ArN_2^+ by $Q^{\bullet -}$ is three orders of

magnitude higher than the rate constant for the reduction of ArN_2^+ by HQ^-. This indicates that the rate-limiting step is the reduction of ArN_2^+ by HQ^-.

Oil-in-water microemulsions and emulsions

Both single phase microemulsions and two phase emulsions are composed of oil, water and surfactant. Microemulsions become emulsions by adding excess oil or emulsions become microemulsions by adding excess surfactant. From the perspective of aggregate structure, microemulsions contain droplets of nanometer size that are optically transparent, but emulsions contain droplets of micrometer size that scatter visible light and appear opaque. In terms of stability, microemulsions are thermodynamically stable, but emulsions are only kinetically stable.

At the molecular level, however, microemulsion and emulsion properties are essentially the same in terms of treating chemical reactions within them. In surfactant aggregates, component molecules and ions exchange rapidly (orders of magnitude faster than rates of most thermal reactions studied) between regions because intermolecular interactions such as hydration, hydrogen bonding, dipole, and polarization are noncovalent and weak. Figure 1.16 is a hypothetical ternary phase diagram for a three-component system of water, oil and surfactant.[95] Steady addition of oil to a homogeneous microemulsion composition(the lower left of Figure 1.16) near a two phase region will reduce the composition that cross a phase boundary and the homogeneous microemulsion will become a two phase emulsion. At the molecular level, the primary difference between the initial microemulsion and the emulsion is caused by relatively small changes in the stoichiometric concentrations of the three components. When the bulk composition is changed in a three-component system, the types of intermolecular interactions remain the same, only the number of them changes, and the changes are small enough not to produce a dramatic difference in the rates of diffusion of the molecules on either side of a two phase boundary, e.g., from near the diffusion control limit in the homogeneous region to orders of magnitude slower in the

two phase region. Therefore, after bulk mixing of both homogenous microemulsions and hetergeneous emulsions, the overall distributions of reactants are in dynamic equilibrium and are determined by their relative solubility in each region, oil, interfacial and aqueous, i.e., their concentrations in each region remain constant.

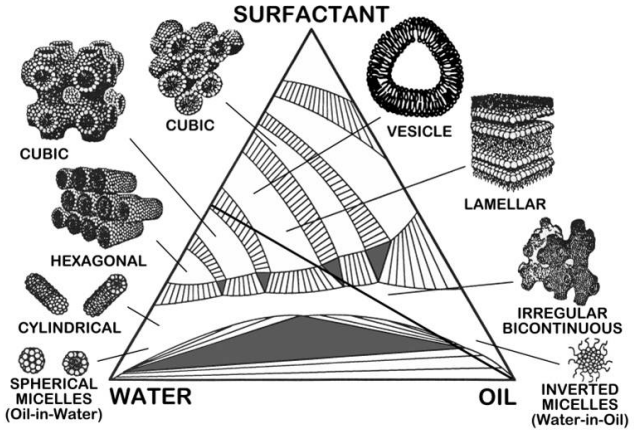

Figure 1.16: A hypothetical ternary phase diagram for a three-component system of water, oil and surfactant showing the images of various aggregate structures of different compositions. The open regions are homogeneous mesophases. Lined regions are bi-phasic and grey regions are tri-phasic.

Application of the pseudophase kinetic model to emulsions

Pseudophase kinetic models originally developed for modeling chemical reactivity in microemulsions[52, 89, 96] were recently shown to work equally well in kinetically stable or stirred emulsions because their component distributions are also in dynamic equilibrium. Conceptually, microemulsions or emulsions are divided into three distinct regions: the oil droplet interior, the continuous aqueous phase, and the interfacial region created by surfactant molecules. Although droplets are separated from each other by the interfacial layer, the totality of the three regions are continuous from the perspective of reactants. A concept called *Discrete Structures-Separate Continuous Regions Duality* was recently proposed by Romsted et al.[97], Figure 1.17. Microscopy and scattering methods detect mesophasic structures, e.g., droplet size and shape. Chemical reaction methods report on different

properties of separate continuous regions. Region continuity is determined by component transfer rates that are near the diffusion-controlled limit such that their distributions are in dynamic equilibrium. Values for partition constants between regions and rate constants for reactions within the interface are obtained by reaction kinetics, NMR, fluorescent and UV probes, etc. The dual approaches provide independent complementary information about the properties of surfactant aggregates.

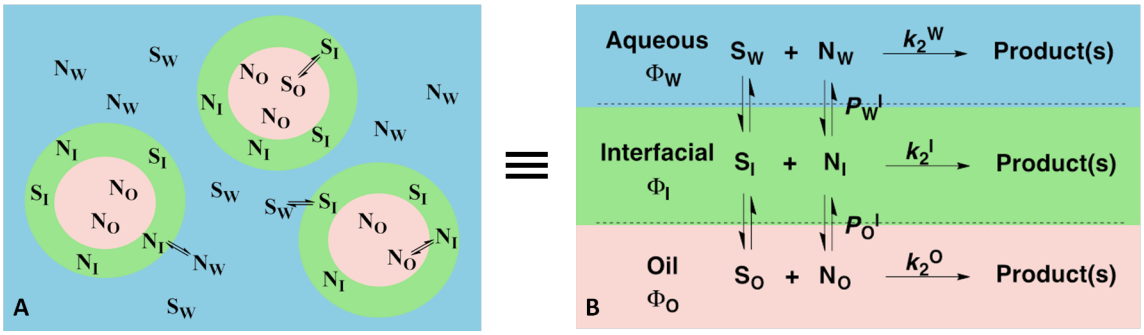

Figure 1.17: A: a cartoon of oil-in-water droplets observed by microscopy and scattering methods. Reactants S and N are exchanging between them. B: treatment of a chemical reaction between S and N in a microemulson or emulsion based on the pseudophase kinetic model.

In Figure 1.17, subscripts O, I, and W represent oil, interfacial, and water regions, respectively. The volume of the interfacial region, V_I, is the totality of all the interfacial regions in all the aggregates and is set equal to the total volume of added surfactant. The total volume of the oil within the droplets and the total volume of water are set equal to the volume of added oil and water. The volume fraction of a region, Φ, is defined as

$$\Phi = V_{region}/(V_O + V_I + V_W) \tag{1.12}$$

and the sum of the volume fractions of all three regions is unity:

$$\Phi_O + \Phi_I + \Phi_W = 1. \tag{1.13}$$

Both reactants, S and N, are rapidly exchanging between the three regions. Figure 1.17A emphasizes the exchange between droplets. Figure 1.17B emphasizes the exchange between

the totalities of the three regions. At dynamic equilibrium, their concentrations in each region become constant and are dependent on their relative solubilities in each region and the volumes of each region (the volumes of reactants are kept significantly smaller than the volumes of oil, interfacial, and water regions) and not droplet size or shape. The distributions of S and N are described by two extra thermodynamic partition constants, one between the oil and interfacial region, $P_{\mathrm{O}}^{\mathrm{I}}$, and one between the aqueous and interfacial region, $P_{\mathrm{W}}^{\mathrm{I}}$. k_2^{O}, k_2^{I} and k_2^{W} are second order rate constants in each region. k_2^{O} and k_2^{W} are assumed to be the same as in bulk oil and water, respectively, and can be measured independently in bulk solvent. However, the interfacial regions cannot be isolated and the rate constants within them cannot be determined independently, but only by the fitting of kinetic models to measured rate constants for the reactions of our long chain arenediazonium probe, 16-ArN_2^+.

Chemical kinetic method for determining AO reactivity and distributions in emulsions

The chemical kinetic method is based on the reduction of a chemical probe, 4-*n*-hexadecylbenzenediazonium ion, 16-ArN_2^+, by phenolic antioxidants (AOs) via electron transfer processes as discussed above (Figure 1.15). Figure 1.18 illustrates the crucial elements of the pseudophase kinetic model as applied to the reactions of AOs with 16-ArN_2^+ in microemulsions or kinetically stable emulsions. It is equivalent to Figure 1.17B, 16-ArN_2^+ = S, AO = N, except that the reaction takes place only in the interfacial region because 16-ArN_2^+ is insoluble both in water and oil and it has a long hydrophobic tail attached to a charged headgroup. One important reason that we select 16-ArN_2^+ as the probe molecule is that the oxidation/reduction reaction of 16-ArN_2^+ with AOs is significantly faster than its spontaneous dediazoniation reaction in various solvents and surfactant aggregates.[98, 99, 100]

Generally, in pseudophase kinetic models, the overall, observed rate of a reaction in emulsions is the sum of the rates in the oil, interfacial and aqueous regions. For a bimolecular

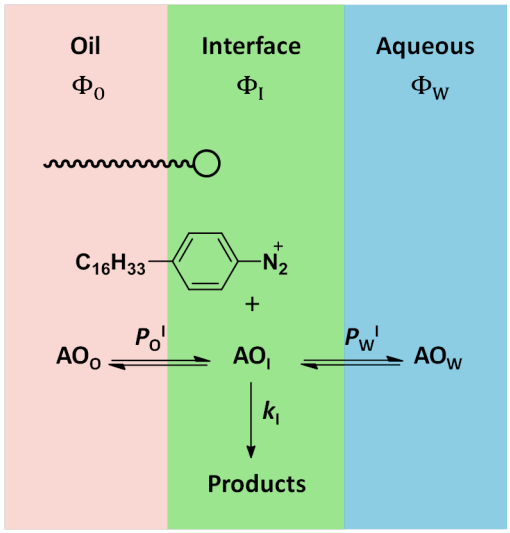

Figure 1.18: Reaction of 16-ArN_2^+ with an AO in the interfacial region of microemulsions or emulsions.

reaction between S an N, Figure 1.17B, the rate of reaction in each region is the product of the rate constant and concentration of each reactant in that region, Equation 1.14.

$$\frac{-\mathrm{d}[\mathrm{S_T}]}{\mathrm{dt}} = k_2[\mathrm{S_T}][\mathrm{N_T}] = k_\mathrm{O}(\mathrm{S_O})(\mathrm{N_O})\Phi_\mathrm{O} + k_\mathrm{I}(\mathrm{S_I})(\mathrm{N_I})\Phi_\mathrm{I} + k_\mathrm{W}(\mathrm{S_W})(\mathrm{N_W})\Phi_\mathrm{W} \tag{1.14}$$

where k_2, k_O, k_I and k_W are second-order rate constants for the overall reaction and the reaction in the oil, interfacial and aqueous regions, respectively; subscript T stands for the stoichiometric concentration; square brackets indicate the concentration in moles per liter of total emulsion volume and parentheses indicate the concentration in moles per liter of the volume of a particular region. The rate of reaction within a region is dependent on the totality of that particular region's volume and not on the total solution volume. When $[\mathrm{N_T}] \gg [\mathrm{S_T}]$, the reaction is assumed to be pseudo first-order. The observed first-order rate constant, k_obs is given by Equation 1.15.

$$k_\mathrm{obs} = k_2[\mathrm{N_T}] \tag{1.15}$$

Because 16-ArN_2^+ is located only in the interfacial region, Figure 1.18, i.e., (16-Ar$N_{2\,\mathrm{O}}^+$)

and (16-$ArN_{2\,W}^{+}$) = 0, Equation 1.14 simplifies to Equation 1.16 after setting S_I = (16-$ArN_{2\,I}^{+}$) and N_I = (AO_I).

$$\frac{-d[16 - ArN_{2\,T}^{+}]}{dt} = k_{obs}[16 - ArN_{2\,T}^{+}] = k_2[16 - ArN_{2\,T}^{+}][AO_T] = k_I(16 - ArN_{2\,I}^{+})(AO_I)\Phi_I \tag{1.16}$$

To apply Equation 1.16 to reactions in emulsions, the parameters in the last equality for reaction in the interfacial region must be converted into measurable stoichiometric concentrations and several definitions are needed. The partition constants describing the AO's distributions between the oil and interfacial, P_O^I, and aqueous and interfacial, P_W^I, regions are defined by Equation 1.17 and 1.18.

$$P_O^I = \frac{(AO_I)}{(AO_O)} \tag{1.17}$$

$$P_W^I = \frac{(AO_I)}{(AO_W)} \tag{1.18}$$

Combining Equations 1.16, 1.17, and 1.18 with a mass balance equation for the AO (not shown) gives an expression for k_{obs} in terms of partition constants, volume fractions, $[AO_T]$ and k_I.

$$k_{obs} = k_2[AO_T] = k_I(AO_I) = \frac{[AO_T]k_I P_O^I P_W^I}{\Phi_O P_W^I + \Phi_I P_O^I P_W^I + \Phi_W P_O^I} \tag{1.19}$$

In experiments, the variation in Φ_I is small, up to 5% of the total solution volume, and in general, $\Phi_I \ll \Phi_O$ and Φ_W. Thus, changing the surfactant concentration has a minor effect on the volume fractions of oil and water. At constant temperature, acidity, and $[AO_T]$, and at a constant Φ_O/Φ_W ratio, Equation 1.19 shows that the value of k_{obs} must decrease with increasing Φ_I. The two partition constants P_O^I and P_W^I appear as a product in Equation 1.19, therefore, their values cannot be obtained directly from the change in k_{obs} with Φ_I in a single set of kinetics experiments. A second independent relation of P_O^I and P_W^I is needed to estimate these two parameters. One approach is to obtain a second set of kinetic data at a different Φ_O/Φ_W ratio. However, a second and simpler approach is to measure the partition constant between the oil and water phases, P_W^O, in the absence of added

surfactant by some analytical method, e.g., spectrometrically because phenolic compounds have reasonably strong UV absorbances. In binary oil-water systems, Figure 1.19, the distribution of an AO or any other polar organic compound is described by a partition constant between the oil and water phases, $P^{\mathrm{O}}_{\mathrm{W}}$, and it is defined as the concentration ratio of AO in the two phases, Equation 1.20, first equality. The second and third equalities show the partition constants, $P^{\mathrm{I}}_{\mathrm{O}}$, and $P^{\mathrm{I}}_{\mathrm{W}}$, for the AO within emulsions. Equation 1.20 demonstrates that $P^{\mathrm{O}}_{\mathrm{W}}$ equals the ratio of $P^{\mathrm{I}}_{\mathrm{W}}$ and $P^{\mathrm{I}}_{\mathrm{O}}$ based on the extra-thermodynamic assumption that partition constants within a three-region system are equivalent to partition constants in a true two-phase system. Note that the binary system is the limiting condition of the emulsion or microemulsion when the surfactant concentration is zero, i.e., $\Phi_{\mathrm{I}} = 0$, Figure 1.19.

$$P^{\mathrm{O}}_{\mathrm{W}} = \frac{(\mathrm{AO_O})}{(\mathrm{AO_W})} = \frac{(\mathrm{AO_I})/(\mathrm{AO_W})}{(\mathrm{AO_I})/(\mathrm{AO_O})} = \frac{P^{\mathrm{I}}_{\mathrm{W}}}{P^{\mathrm{I}}_{\mathrm{O}}} \tag{1.20}$$

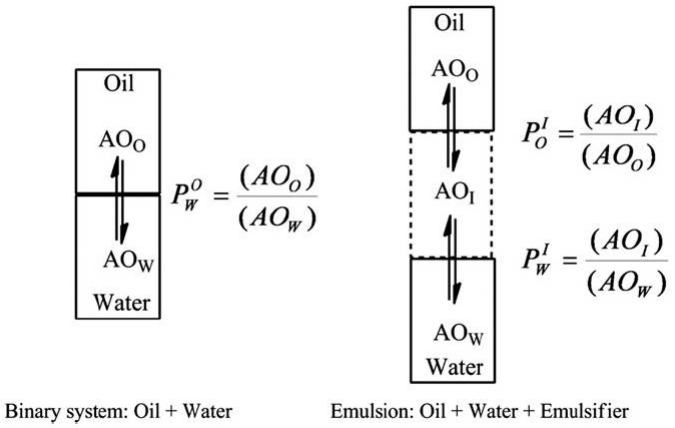

Figure 1.19: The distribution of an AO and the partition constants describing its distribution in a binary system and an emulsion or a microemulsion. Parenthesis indicates the concentration in moles per liter of the volume of a particular region.[101]

Values for $P^{\mathrm{I}}_{\mathrm{W}}$ and $P^{\mathrm{I}}_{\mathrm{O}}$ can be obtained by combining fits of k_{obs} versus Φ_{I} with the value for $P^{\mathrm{W}}_{\mathrm{O}}$ and solving two equations in two unknowns.

Experimental approaches for monitoring the reaction between 16-ArN_2^+ and AOs

1. Linear Sweep Voltammetry (LSV) method

At the surface of an electrode, arenediazonium ions, ArN_2^+, undergo homolytic fragmentation to produce aryl radicals upon electron transfer [102], Figure 1.20. Thus k_{obs} can

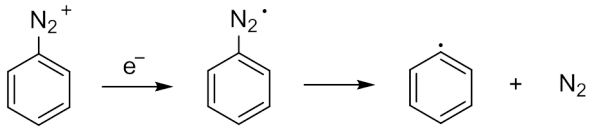

Figure 1.20: Reduction of arenediazonium ion at the surface of electrode

be obtained by monitoring the depletion of 16-ArN_2^+ with time in emulsions using LSV. Current-voltage (*i*-*E*) curves are collected at specific time intervals. The maximum in the peak current, i_p, which is directly proportional to the concentration of 16-ArN_2^+, decreases with time and becomes constant at the end of the reaction, Figure 1.21A. Figure 1.21B is a typical kinetic plot used to obtain the value for k_{obs} for the reaction between 16-ArN_2^+ and *tert*-butylhydroquinone, TBHQ, by fitting $\ln(i_p\text{-}i_\infty)$ versus time data to the integrated first-order equation.

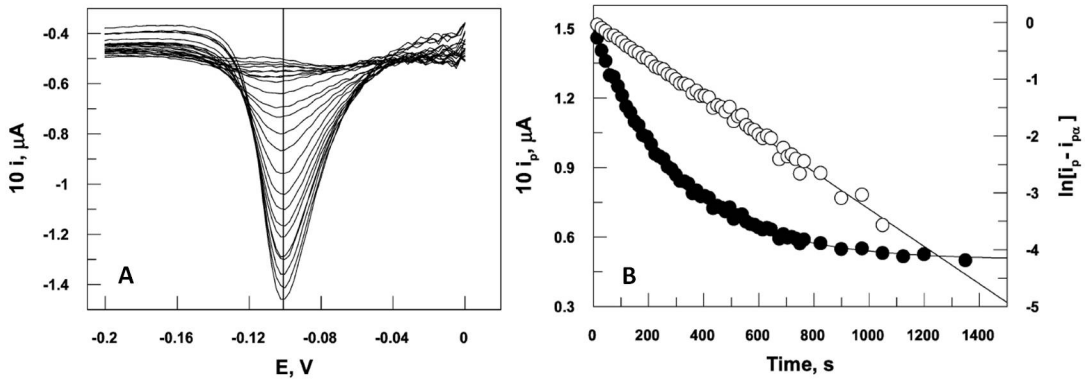

Figure 1.21: A: Voltammograms for the reduction peak of 16-ArN_2^+ in the presence of TBHQ at a series of time intervals in $C_{12}E_6$ emulsion of 1:1 (v:v) octane/water(HCl, pH = 2.5). $\Phi_I = 0.0349$, [16-ArN_2^+] $= 1.6 \times 10^{-4}$ M, [TBHQ] $= 1.93 \times 10^{-3}$ M, T = 25°C. B: The maximum of peak current, i_p, versus time plot and $\ln(i_p\text{-}i_\infty)$ versus time plot for reaction of 16-ArN_2^+ with TBHQ. $k_{obs} = 0.00327$ s^{-1} and $R^2 = 0.997$ for about 5 half-lives.[65]

2. Azo dye derivatization method

This method is based on the azo coupling reaction consisting of an electrophilic substitution of an arenediazonium ion with a nucleophile. The reaction mechanism has been discussed in Section 1.4.1. Typical components are aromatic systems with strong electron donating groups attached to aromatic rings, such as amines, naphthols or enolizable compounds with reactive methylene groups.[71] We chose *N*-(1-naphthyl)ethylenediamine, NED, as the coupling agent, Figure 1.22. k_{obs} for reaction of 16-ArN_2^+ with an AO was

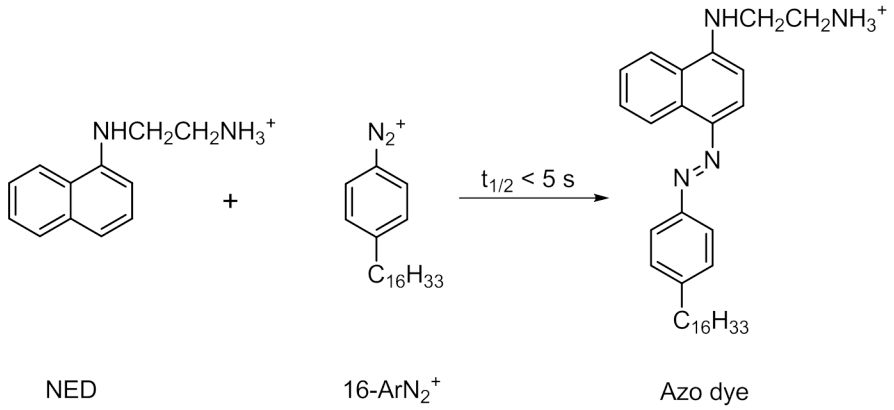

Figure 1.22: Reaction of the arenediazonium ion with NED to yield a stable azo dye.[66]

determined by trapping unreacted 16-ArN_2^+ with NED. The half-life, $t_{1/2}$, is less than 5 seconds. Kinetic plots for the reaction between 16-ArN_2^+ and gallic acid in nonionic emulsions using the azo dye derivatization method are shown in Figure 1.23.

1.5 Lipid oxidation and antioxidant

1.5.1 Lipid oxidation

Lipids are important nutrients and major structural and functional constituents of cells in biological systems. There is no precise definition available for the term "lipid". Generally, it refers to a variety of compounds that have common properties and compositional similarities and these relate to their solubilities to a greater extent than their structural characteristics.[103] Figure 1.24 shows the structures of some typical lipids. Glycerols and

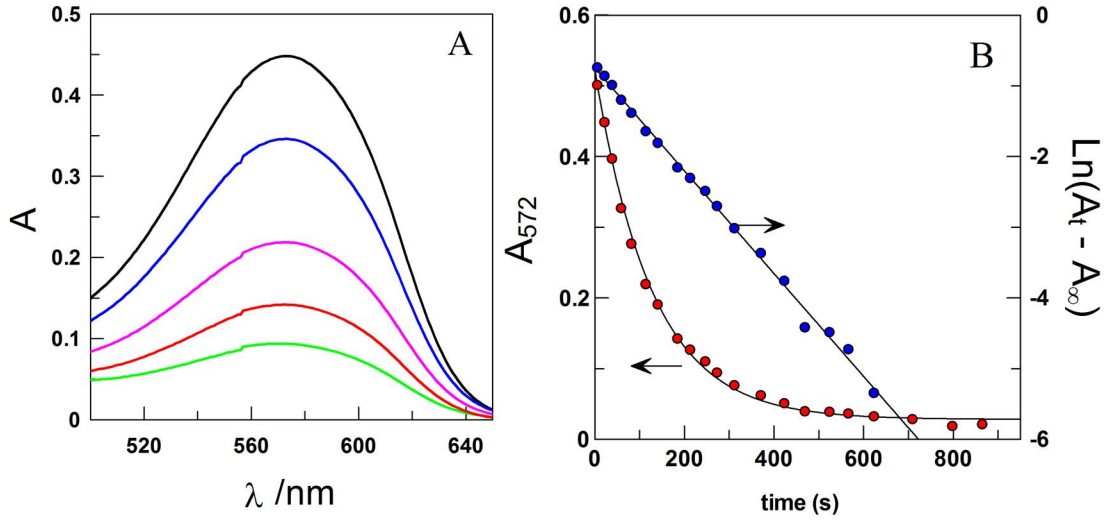

Figure 1.23: A: Spectra of the azo dye product obtained at selected times for the reaction between unreacted 16-ArN_2^+ and NED in Tween 20 emulsions of 1:9 (v:v) corn oil/water(acetate buffer, pH 3.65). $\Phi_I = 0.0204$, [16-ArN_2^+] $= 2.83 \times 10^{-4}$ M, [gallic acid] $= 4.21 \times 10^{-3}$ M, T = 25°C. B: Azo dye absorbance at $\lambda = 572$ nm versus time plot and ln(A_t-A_∞) plot.[97]

fatty acid constitute most of the lipids. Nearly 98% of lipids in plants and animals consist of acyglycerols. Lipid molecules are susceptible to oxidation by atmospheric oxygen. It is undesirable in lipid based foods because it leads to the loss of nutrients, development of unpleasant off-flavors, and formation of potentially toxic reaction products.

The commonly accepted pathway for lipid autoxidation occurs via a multistepped free radical chain mechanism.[103] Figure 1.25 illustrates the major parts of this mechanism including: (1) initiation: lipid molecules lose a hydrogen and lipid free radicals ($L^\bullet$) are formed in the presence of initiators such as heat, light/ionizing radiation, or metal ions. (2) propagation: lipid radicals ($L^\bullet$) react with oxygen to produce peroxyl radicals ($LOO^\bullet$), which attack a new lipid molecule to generate a new lipid radical. This process is repeated thousands of times until there is no hydrogen source or the chain is interrupted. Meanwhile, alkoxyl ($LO^\bullet$), hydroxyl ($OH^\bullet$) and new lipid radicals ($L^\bullet$) are produced from decomposition of hydroperoxides (LOOH), and further participate in the chain reaction. (3) termination: non-radical products are formed through radical-radical coupling or radical-radical disproportionation.

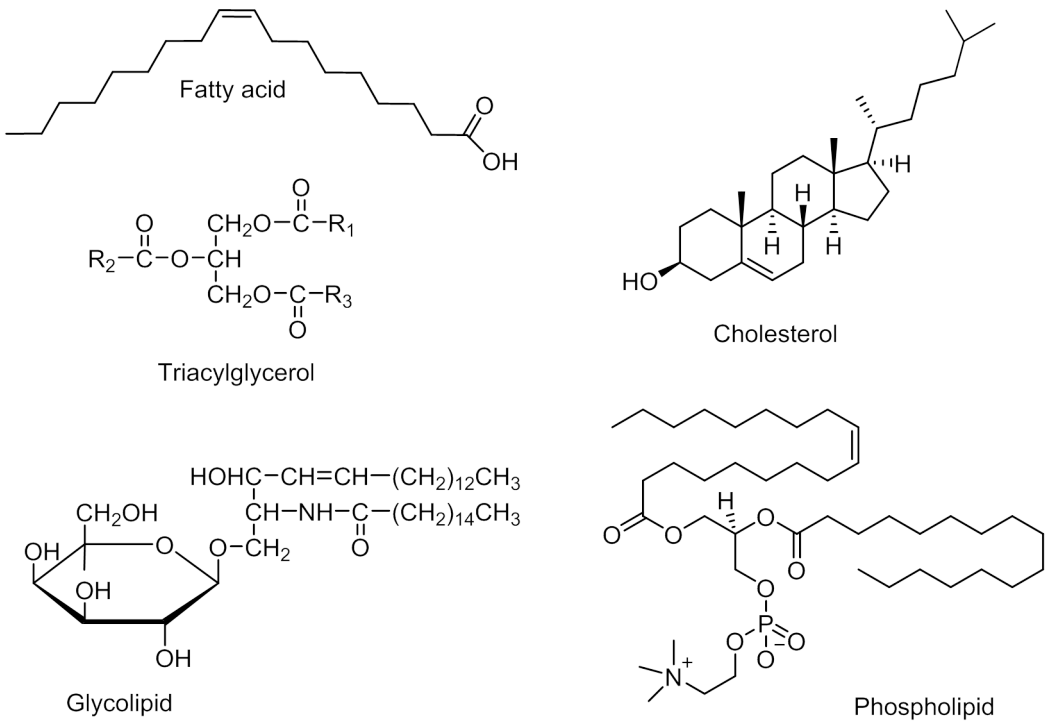

Figure 1.24: Examples of lipid molecules

1.5.2 Classification and function of antioxidants

The most effective way to retard lipid oxidation is to incorporate antioxidants into the lipid based foods. Antioxidants are classified into two main categories according to the mechanism of their action: primary antioxidants and secondary antioxidants. Primary antioxidants, also known as "chain-breaking" antioxidants, are usually phenol or polyphenol compounds, Figure 1.26, that are capable of donating hydrogen atoms to free radicals so that they can interrupt the propagation step of the free radical chain reaction in lipid autoxidation, as shown below.

$$L^{\bullet} + AH \rightarrow LH + A^{\bullet} \tag{1.21}$$

$$LOO^{\bullet} + AH \rightarrow LOOH + A^{\bullet} \tag{1.22}$$

$$LO^{\bullet} + AH \rightarrow LOH + A^{\bullet} \tag{1.23}$$

The resultant antioxidant radicals are stabilized by delocalization of the unpaired electron around the phenol ring, thus they do not initiate formation of new lipid radicals. In addition,

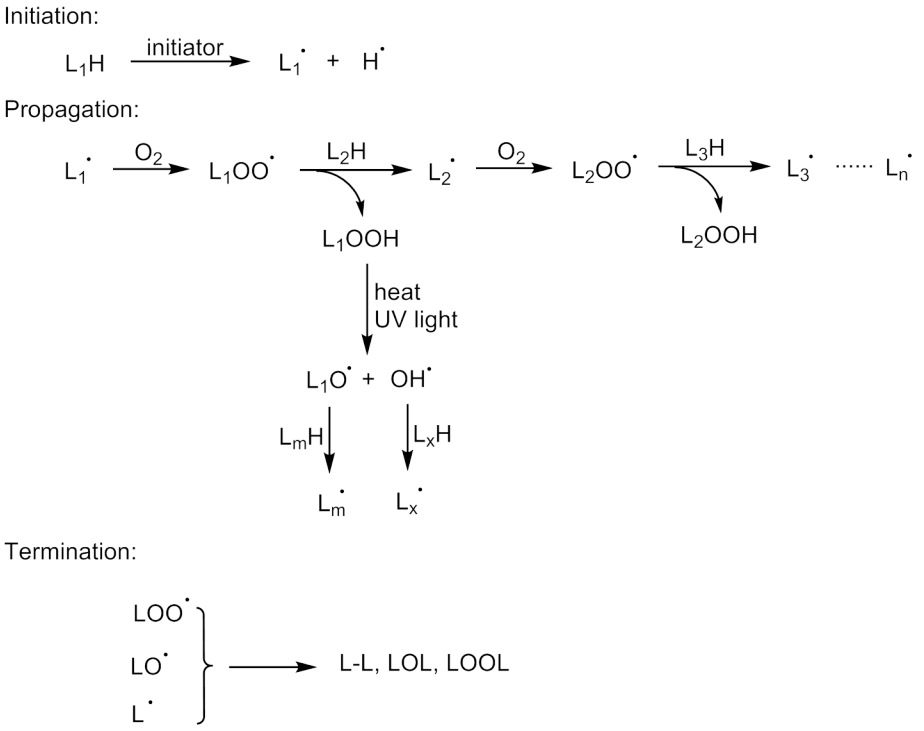

Figure 1.25: Lipid autoxidation mechanism[103]

the antioxidant radicals can further participate in the termination step.

$$\mathrm{LOO^{\bullet} + A^{\bullet} \rightarrow LOOA} \tag{1.24}$$

$$\mathrm{LO^{\bullet} + A^{\bullet} \rightarrow LOA} \tag{1.25}$$

Secondary antioxidants retard the lipid oxidation through various mechanisms, including chelation of transition metals, oxygen scavenging, replenishing hydrogen to primary antioxidants, etc, none of which involves conversion of free radicals to more stable products. EDTA, amino acids and ascorbic acid are examples of secondary antioxidants.

1.5.3 Effect of antioxidant distributions on antioxidant efficiency

Selecting the most efficient antioxidant for a particular food application remains a major unsolved problem in food science because antioxidant activities are affected by a number of factors, e.g., the type of the system, oil or emulsion, the types of the lipid and surfactant, the environmental conditions (acidity, temperature, salt concentration, etc), the nature of

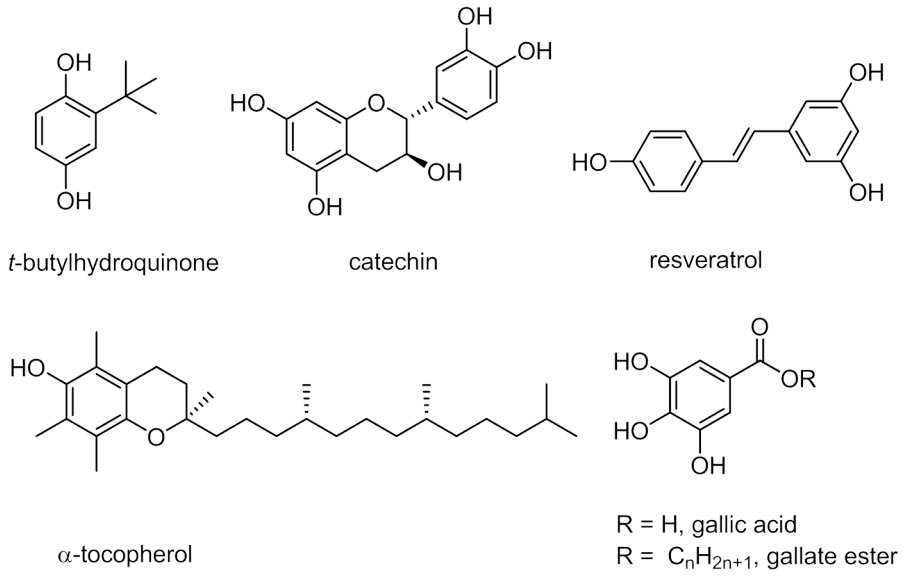

Figure 1.26: Examples of primary antioxidants

the antioxidant, and the partitioning of the antioxidant within the emulsion.[104, 105, 106, 107, 108, 109]

In 1986 Castle et al.[110] related, for the first time, antioxidant partitioning with antioxidant activity quantitatively. They demonstrated that 20% of Trolox partitions into SDS-micelles at pH 7.0. By contrast, 94%-100% of some ester derivatives of Trolox and tocopherols partition into the SDS-micelles. The small percentage of Trolox in the micelles accounts for its ineffectiveness as a chain-breaking inhibitor of lipid oxidation. Often studies indicated that antioxidant activity varies in systems that differ in the distribution of the lipid phase. It was reported in the 1970-1980s that trolox, ascorbic, gallic, caffeic, and ferulic acids exhibited higher antioxidant efficacies in bulk oil and lower efficacies in emulsions than their correspondent nonpolar alkyl esters.[111, 112, 113, 114] In addition, opposite trends in efficacy were observed for a series of gallates, among which gallates with longer alkyl chains were more effective in emulsions, while gallates with shorter alkyl chains were more effective in dry oils.[115] These apparent contradictory phenomena were summarized by Porter in his "polar paradox" hypothesis, i.e., polar antioxidants tend to

be more active in bulk oils whereas nonpolar antioxidants tend to be more active in relatively more polar lipid emulsions.[116] Recent studies also supported the polar paradox hypothesis.[117, 118, 119, 120, 121, 122, 123]

Frankel et al. postulated a mechanism based on the different affinities of hydrophilic and lipophilic antioxidants towards the air, oil and water phases as well as the air-oil and water-oil interface to explain this polar paradox.[117] In bulk oils, hydrophilic antioxidants are oriented at the air-oil interface, where surface oxidation occurs, to give better protection against lipid oxidation than lipophilic antioxidants which are dissolved in the oil phase, Figure 1.27A. However, the distribution of hydrophilic antioxidants at the air-oil interface was untenable because air is even less polar than oil (dielectric constant of air is 1.0 compared to approximately 3.0 for food oils[124]). Later, it was recognized that association colloids, e.g., lamellar structure and reverse micelles, may be formed in edible oils from self-assembly of amphilic compounds including naturally occuring lipid components (e.g., phospholipids) and oxidation products (e.g., hydroperoxides) in the presence of trace amounts of water from the atmosphere.[124] These mesostructures are the site of lipid oxidation in bulk oils and alter the physical locations of lipid and antioxidants. As shown in Figure 1.27B, hydrophilic antioxidants are actually located at the water-oil interface of the association colloids rather than at the air-oil interface. While in oil-in-water emulsions, hydrophobic antioxidants are more effective by being oriented at the water-oil interface than hydrophilic antioxidants which are predominantly partitioned into the aqueous phase, Figure 1.27C.

1.5.4 Current research status on determining antioxidant distributions

Aware of the significant effect of the location of an antioxidant on antioxidant efficiency, researchers made great efforts to determine the distributions of antioxidants in emulsions. To date, the general approach has been to prepare emulsions containing an antioxidant, separate the oil and water phases by some physical methods such as centrifugation or ultrafiltration and analyze the antioxidant concentration in each phase.[125, 126, 127, 128, 129]

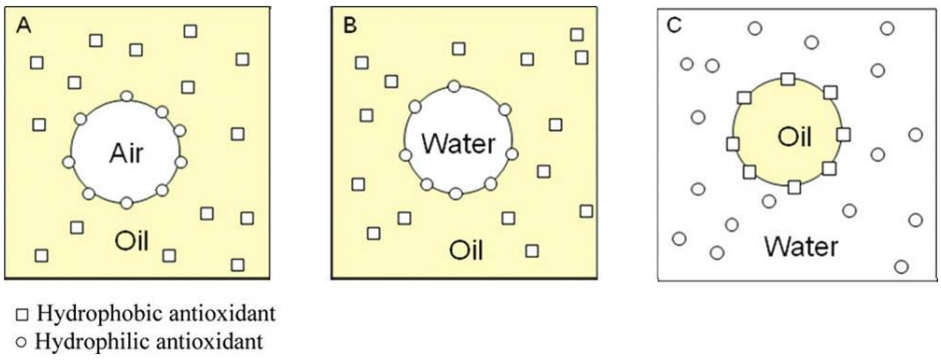

Figure 1.27: Distributions of antioxidants in bulk oils (A and B) and oil-in-water emulsions (C) based on interfacial phenomena and polar paradox.[107]

However, this approach does not provide the information on the antioxidant concentration in the interfacial region. When the system reaches the dynamic equilibrium, surfactants are associated with the oil, interfacial, and aqueous regions and the interfacial region cannot be physically isolated. The distributions of the antioxidant within the three regions are also in dynamic equilibrium with each other, and physical separation of phases destroy this equilibrium, thus changing the original antioxidant distributions in emulsions. Stockmann and Schwarz improved on this phase separation approach by combining experimental techniques with a mathematical model to estimate the amount of phenolic compounds in the interfacial region.[130] The results showed that a substantial fraction of the compounds partition into the interfacial region at low surfactant concentrations. However, their method involves empirical equations and is difficult to apply.

We have taken a very different approach for estimating antioxidant distributions in model food emulsions by combining a new conceptual kinetic model with novel experimental methods that do not require separation of phases.

Chapter 2

Using the pseudophase kinetic model to interpret chemical reactivity in ionic emulsions: Determining antioxidant partition constants and interfacial rate constants

Our kinetic results show for the first time that the pseudophase kinetic model works in both cationic and anionic emulsions. It also provides reasonable estimates of the partition constants of antioxidants, here *t*-butylhydroquinone (TBHQ) between the oil and interfacial region, $P^{\mathrm{I}}_{\mathrm{O}}$, and the water and interfacial region, $P^{\mathrm{I}}_{\mathrm{W}}$, and of the interfacial rate constant, k_{I}, for the reaction with 16-ArN_2^+ in emulsions containing a 1:1 volume ratio of medium-chain triglyceride (MCT), and aqueous acid or buffer. The results also provide: (a) an explanation for the large difference in pH, > 4 pH units, required to run the reaction in CTAB (pH 1.54, HBr) and SDS (pH 5.71, acetate buffer) at a reasonable speed; (b) a sensible interpretation of added counterion effects based on ion exchagne in SDS emulsions (Na^+/H_3O^+ ion exchange in the interfacial region) and Donnan equilibrium in CTAB emulsions (Br^- increasing the interfacial H_3O^+); and (c) the significance of the effect of the much greater solubility of TBHQ in MCT versus octane, 1000/1, as the oil. These results should aid in interpreting the effects of ionic surfactants on chemical reactivity in emulsions in general and in selecting the most efficient antioxidant for particular food applications.

2.1 Hypothesis

Because the pseudophase kinetic model provides kinetically stable nonionic emulsions reasonable estimates of antioxidant distributions and interpretations of their chemical reactivities, it should work equally well in ionic emulsions when the effects of surfactant head

group charge on ion distributions are taken into account. Cationic interfaces lower H^+ concentration and increase the pH in the interfacial region. Anionic interfaces do the opposite. Thus, cationic and anionic emulsions will have opposite effects on the rate of pH-sensitive reaction between the arenediazonium ion probe and an antioxidant. Added inert salt will further alter the ion distributions near charged interfaces, and their effects can be explained by using the pseudophase ion exchange model originally developed for treating chemical reactivity in ionic micelles.

2.2 Introduction

2.2.1 Background

The pseudophase model introduced in Chapter 1 (See p. 9) was developed for antioxidant distributions for nonionic emulsions. It is also important to investigate how antioxidants partition and act in the emulsions with charged surfaces because many food emulsifiers are either ionic or capable of being ionized.[131] Several papers have shown that antioxidant activity is related to the surface charge.[132, 133, 134] Pryor et al. observed that the protection of Trolox C on the oxidation of linoleic acid in hexadecyltrimethylammonium bromide micelles (CTAB, positively charged) was four times higher than in sodium lauryl sulfate micelles (SDS, negatively charged).[132] Similarly, Barclay and Vinqvist found out that Trolox C inhibited the oxidation of positively charged liposomes significantly, had low efficiency in neutral liposomes, and had no effect on negatively charged liposomes.[133] However, no explanation correlating the activity with the partition of antioxidant between oil, water regions and charged interface was provided. Schwarz and Frankel studied the partition of antioxidative phenolic compounds in emulsions containing 20% corn oil emulsified with either cationic DTAB, anionic SDS, or nonionic Tween 20.[134] They calculated the amount of the antioxidants associated with surfactant enriched environments based on the assumption that the partition between the oil and aqueous phase in biphasic systems and

emulsions are the same, and their results showed that the charge of the surfactants affected partitioning of phenolic antioxidants. Nevertheless, their approach was on the basis of centrifugal ultrafiltration technique, which is "invasive" in a sense that the distributions of all the components in the emulsions are probably disrupted during the separation process.

2.2.2 Surface charge effects on kinetics

Unlike nonionic surfactants, ionic surfactants create charged surfaces at droplet interfaces for micelles, microemulsions and emulsions because a fraction of the headgroup counterions, ca. 20-30% diffuse into the surrounding aqueous phase[135], Figure 2.1. As a result, counter anions condense onto cationic surfaces producing high local concentrations of anions, e.g., 1-3 mol/L of interfacial volume, even when stoichiometric concentrations of surfactants are low, 1-10 mM (above the cmc). The opposite is true for anionic surfaces.[136] Two opposing tendencies govern the organization of ions near a charged surface: one is electrostatic attractions favoring accumulation of counterions near a surface, and the other is thermal energy favoring a random distribution of the ions.[131] The resulting distribution of ions close to a charged surface is called the electrical double layer, Figure 2.2. The first layer is called the Stern layer, having a width about the size of the surfactant headgroup, contains the headgroups, a fraction of the counterions and water. The polarity of the Stern layer is between that of water and hydrocarbon, or alcohol like.[10, 20] The second layer is called the Gouy-Chapman layer, which extends out into the aqueous phase and contains the remaining counterions. This organization of ions changes the medium properties of the interfacial region at charged surface compared to that at neutral surface.

The pseusophase ion exchange (PIE) model introduced in Chapter 1 (See p. 12) was developed to describe ionic distributions at charged aqueous interfaces. In the PIE model, micellar surfaces are treateds as selective ion exchangers saturated with counterions. Ionic competition between inert counterions, X, and reactive counterions, N, at the interface is governed by differences in the specific interactions of two counterions, and is described by

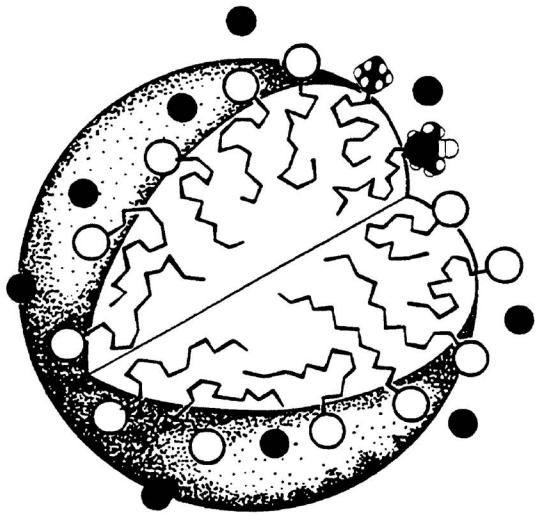

Figure 2.1: Cartoon of an aqueous cationic micelle showing the cationic headgroups (○) attached to hydrocarbon tails and a fraction of the anionic counterions (●). Interfacial and bulk water molecules are not shown.[4]

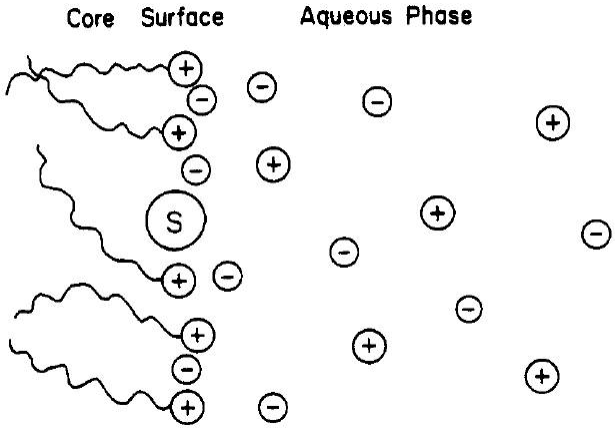

Figure 2.2: Cartoon illustrating ion distributions at a positively charged surface[20]

an ion-exchange constant, $K_{\mathrm{X}}^{\mathrm{N}}$. Reactions of substrates with co-ions are generally inhibited by surfactant aggregates because the substrate is associated with the aggregates and the co-ion is repelled. However, micellar rate enhancements were observed for reactions of co-ions including OH^-, SCN^-, and SO_3^{2-} in anionic micelles with added salt at high surfactant concentration[137] and for H_3O^+-catalyzed hydrolysis of a hydrophobic ketal in cationic micelles with added salt[138]. A Donnan equilibrium, instead of ion exchange, is used to describe the effect of added counterion on co-ion distributions between the micellar and aqueous pseudophase.[138] A Donna equilibrium constant between reactive co-ions, M, and

inert counterions X, $K_{\mathrm{M}}^{\mathrm{X}}$, is given by:

$$K_{\mathrm{M}}^{\mathrm{X}} = \frac{(\mathrm{M_m})(\mathrm{X_m})}{[\mathrm{M_w}][\mathrm{X_w}]} \tag{2.1}$$

where parentheses indicate the concentration within the micellar pseudophase and square brackets indicate the concentration within the total solution.

Charged interfaces alter the interfacial concentrations of H^+ or OH^- by 1-2 orders of magnitude.[20] A cationic interface repels H^+ and attracts OH^-, thus it has a lower local concentration of H^+ in the interfacial region than that in the bulk solution, but higher interfacial OH^- concentration than the bulk OH^-. Anionic interfaces do the opposite. These orders of magnitude differences in interfacial acidities versus bulk adicities can have a significant effect on the rate of reaction of 16-ArN_2^+ with phenolic AO because the reaction is pH sensitive. In water, reactions of AOs with arenediazonium ions are catalysed by base because it is the deprotonated form of the phenol that reacts with an arenediazonium ion in an overall bimolecular reaction, Figure 1.15. In basic solution the reaction is extraordinarily fast and approaches the diffusion controlled limit with increasing pH.[93] Consequently, about 3 mM HCl is required to slow the reaction between 16-ArN_2^+ and *tert*-butylhydroquinone (TBHQ) in $C_{12}E_6$ emulsions to a rate that can be measured by LSV or the dye derivatization methods. The optimal solution acidity for running the reactions in cationic and anionic emulsions were determined by trial and error because the interfacial acidity is controlled by micellar charge and counterion and co-ion concentrations. (See Discussion) At 3 mM H^+ the reaction would be speeded in cationic and slowed in anionic emulsions.

2.2.3 Kinetic model for determining antioxidant partition constants and interfacial rate constants in nonionic and ionic emulsions

We have successfully applied the pseudophase kinetic model to kinetically stable or continuously stirred nonionic emulsions and obtained antioxidant (AO) distributions from the

relationship between the measured rate constant, k_{obs}, for the reaction of 16-ArN_2^+ with an AO, and the surfactant volume fraction, Φ_I.[63, 65, 66, 139]

Figure 2.3 shows the application of the pseusophase model to premixed hexaethyleneglycol monododecyl ether ($C_{12}E_6$) nonionic emulsions at dynamic equilibrium. As discussed in Section 1.4.3, the reaction between 16-ArN_2^+ and AOs occurs only in the interfacial region, thus the rate of the reaction in emulsions under pseudo first-order condition, i.e., $[AO_T] \gg [16\text{-}ArN_{2\,T}^+]$, is given by Equation 2.2, and the molarity of 16-ArN_2^+ in the interfacial region can be converted to its stoichiometric molarity by Equation 2.3.

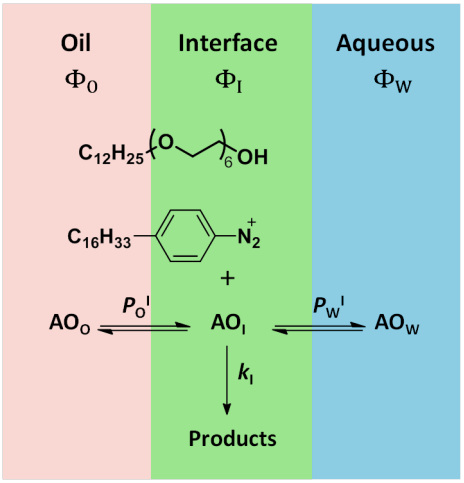

Figure 2.3: Cartoon of the pseudophase model as applied to uncharged emulsions illustrating the average location of the nonionic surfactant, $C_{12}E_6$, and the probe, 16-ArN_2^+, the partition of the AO between the oil, interfacial and aqueous regions, and the reaction between AO and 16-ArN_2^+ in the interfacial region and its second-order rate constant, k_I.

$$\frac{-d[16 - ArN_{2\,T}^+]}{dt} = k_{obs}[16 - ArN_{2\,T}^+] = k_2[16 - ArN_{2\,T}^+][AO_T] = k_I(16 - ArN_{2\,I}^+)(AO_I)\Phi_I \tag{2.2}$$

$$[16 - ArN_{2\,T}^+] = (16 - ArN_{2\,I}^+)\Phi_I \tag{2.3}$$

The distribution of the AO between the three regions of the emulsion is given by Equation 2.4, which states that the total or stoichiometric AO concentration in the entire emulsion is the sum of the AO concentrations in each region times the volume fraction of that region

after bulk mixing is complete and dynamic equalibrium has been reached.

$$[\mathrm{AO_T}] = \Phi_\mathrm{O}(\mathrm{AO_O}) + \Phi_\mathrm{I}(\mathrm{AO_I}) + \Phi_\mathrm{W}(\mathrm{AO_W}) \tag{2.4}$$

Two partition constants of the AO, one between the oil and interfacial regions, P^I_O, and one between the aqueous and interfacial regions, P^I_W, are expressed in Equation 2.5 and 2.6, respectively.

$$P^\mathrm{I}_\mathrm{O} = \frac{(\mathrm{AO_I})}{(\mathrm{AO_O})} \tag{2.5}$$

$$P^\mathrm{I}_\mathrm{W} = \frac{(\mathrm{AO_I})}{(\mathrm{AO_W})} \tag{2.6}$$

Combining Equations 2.4, 2.5 and 2.6 and solving for $(\mathrm{AO_I})$ in terms of $[\mathrm{AO_T}]$ gives:

$$(\mathrm{AO_I}) = \frac{[\mathrm{AO_T}]P^\mathrm{I}_\mathrm{O}P^\mathrm{I}_\mathrm{W}}{\Phi_\mathrm{O}P^\mathrm{I}_\mathrm{W} + \Phi_\mathrm{I}P^\mathrm{I}_\mathrm{O}P^\mathrm{I}_\mathrm{W} + \Phi_\mathrm{W}P^\mathrm{I}_\mathrm{O}} \tag{2.7}$$

which defines the concentration of any AO in the interfacial region of emulsions as a function of the stoichiometric concentration of the AO, its two partition constants and the volume fraction of each region.

Equation 2.8 is obtained by substituting Equations 2.3 and 2.7 into Equation 2.2 and canceling the $[16\text{-}\mathrm{ArN}^+_{2\,\mathrm{T}}]$ term.

$$k_\mathrm{obs} = k_2[\mathrm{AO_T}] = k_\mathrm{I}(\mathrm{AO_I}) = \frac{[\mathrm{AO_T}]k_\mathrm{I}P^\mathrm{I}_\mathrm{O}P^\mathrm{I}_\mathrm{W}}{\Phi_\mathrm{O}P^\mathrm{I}_\mathrm{W} + \Phi_\mathrm{I}P^\mathrm{I}_\mathrm{O}P^\mathrm{I}_\mathrm{W} + \Phi_\mathrm{W}P^\mathrm{I}_\mathrm{O}} \tag{2.8}$$

Equation 2.9 can be transformed to:

$$k_\mathrm{obs} = \frac{[\mathrm{AO_T}]k_\mathrm{I}P^\mathrm{I}_\mathrm{O}P^\mathrm{I}_\mathrm{W}(1 + \frac{\Phi_\mathrm{W}}{\Phi_\mathrm{O}})}{(P^\mathrm{I}_\mathrm{W} + \frac{\Phi_\mathrm{W}}{\Phi_\mathrm{O}}P^\mathrm{I}_\mathrm{O}) + ((1 + \frac{\Phi_\mathrm{W}}{\Phi_\mathrm{O}})P^\mathrm{I}_\mathrm{O}P^\mathrm{I}_\mathrm{W} - (P^\mathrm{I}_\mathrm{W} + \frac{\Phi_\mathrm{W}}{\Phi_\mathrm{O}}P^\mathrm{I}_\mathrm{O}))\Phi_\mathrm{I}} \tag{2.9}$$

Equation 2.9 shows that when $[\mathrm{AO_T}]$ and the ratio $\Phi_\mathrm{W}/\Phi_\mathrm{O}$ are constant, k_obs decreases with increasing Φ_I. Under this condition, Equation 2.9 can simplify to:

$$k_\mathrm{obs} = \frac{\mathbf{a}}{1 + \mathbf{b}\Phi_\mathrm{I}} \tag{2.10}$$

or

$$\frac{1}{k_\mathrm{obs}} = \frac{\mathbf{b}}{\mathbf{a}}\Phi_\mathrm{I} + \frac{1}{\mathbf{a}} \tag{2.11}$$

where **a** and **b** are constants and the expressions for them are given as follows:

$$\mathbf{a} = \frac{[\mathrm{AO_T}]k_\mathrm{I}P^\mathrm{I}_\mathrm{O}P^\mathrm{I}_\mathrm{W}(1+\frac{\Phi_\mathrm{W}}{\Phi_\mathrm{O}})}{P^\mathrm{I}_\mathrm{W}+\frac{\Phi_\mathrm{W}}{\Phi_\mathrm{O}}P^\mathrm{I}_\mathrm{O}} \tag{2.12}$$

$$\mathbf{b} = \frac{P^\mathrm{I}_\mathrm{O}P^\mathrm{I}_\mathrm{W}(1+\frac{\Phi_\mathrm{W}}{\Phi_\mathrm{O}})}{P^\mathrm{I}_\mathrm{W}+\frac{\Phi_\mathrm{W}}{\Phi_\mathrm{O}}P^\mathrm{I}_\mathrm{O}} - 1 \tag{2.13}$$

Fitting the data of k_obs versus Φ_I gives the values of **a** and **b**. Values for both partition constants P^I_O and P^I_W cannot be obtained directly from a single set of k_obs versus Φ_I data plots because they appear as product terms in Equations 2.12 and 2.13. However, a second independent relation of P^I_O and P^I_W can be obtained by carrying out kinetics experiments at a different $\Phi_\mathrm{W}/\Phi_\mathrm{O}$ ratio or by determining values of P^W_O in the absence of surfactant (the logic of this approach was elaborated in Section 1.4.3), Equation 2.14.

$$P^\mathrm{O}_\mathrm{W} = \frac{(\mathrm{AO_O})}{(\mathrm{AO_W})} = \frac{(\mathrm{AO_I})/(\mathrm{AO_W})}{(\mathrm{AO_I})/(\mathrm{AO_O})} = \frac{P^\mathrm{I}_\mathrm{W}}{P^\mathrm{I}_\mathrm{O}} \tag{2.14}$$

Once the partiton constants are known, k_I, the interfacial rate constant of the reaction between 16-ArN^+_2 and AO can be calculated from Equation 2.12. Comparison of k_I values for a series of AOs could lead to a scale of AO efficiency that is independent of the AO distributions in food emulsions.

In this chapter, we show that both cationic and anionic emulsions in the presence and absence of added salt have large, approximately two orders of magnitude, effects on the observed rate constant for the reaction of 16-ArN^+_2 with an AO and in opposite directions. Then we describe how the pseudophase model can be modified by using treatments for counterion and co-ion distributions already developed for reactivity in ionic association colloids to interpret the observed rate changes and conclude that this approach greatly expands the range of applicability of the kinetic method for determining AO partition constants and interfacial rate constants.

2.3 Results

2.3.1 Reactions of 16-ArN_2^+ with TBHQ ionic emulsions: effect of added surfactant on k_{obs}

Values of k_{obs} for the reaction of 16-ArN_2^+ and TBHQ (Figure 2.4) in hexadecyltrimethylammonium bromide (CTAB) and sodium dodecyl sulfate (SDS) emulsions of 1:1 (v:v) aqueous solution to medium-chain triglyceride (MCT) were determined by the azo dye derivatization method. Trial experiments showed that the reaction of TBHQ with 16-ArN_2^+ could

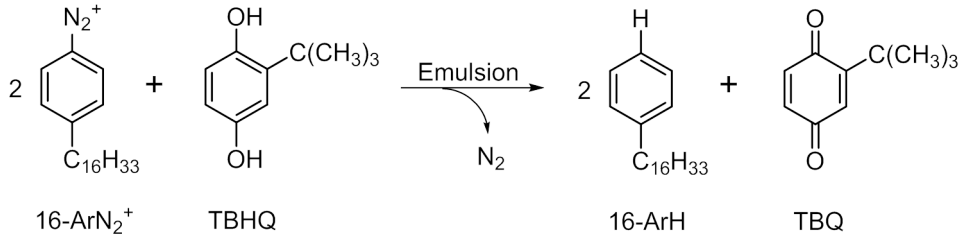

Figure 2.4: Reaction of 16-ArN_2^+ with TBHQ

be followed at a reasonable rate, at pH = 1.54 (HBr) in CTAB emulsions and at pH = 5.71 (acetate buffer) for SDS emulsions. Figure 2.5 show examples of the good first-order kinetics that were obtained in all kinetics experiments.

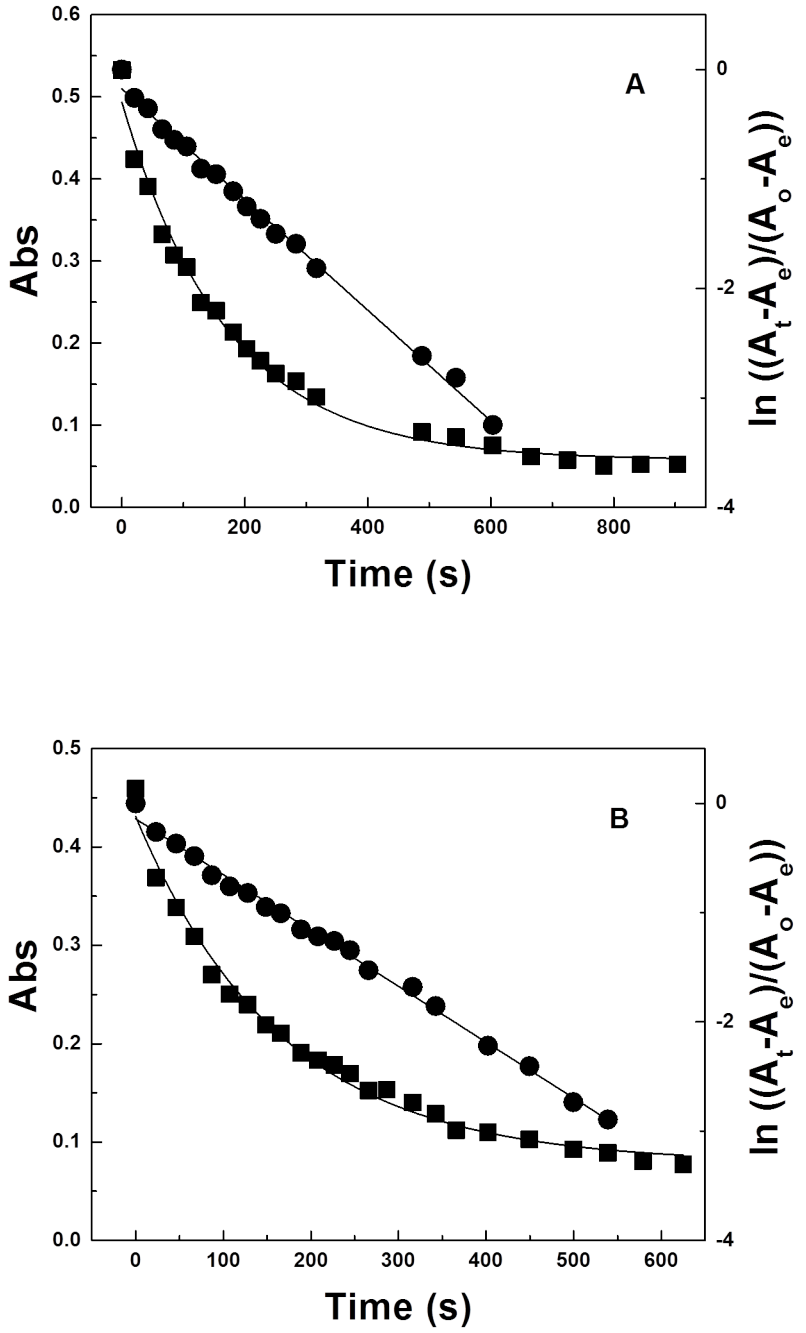

Figure 2.5: Typical azo dye absorbance versus time plot (■) and $\ln((A_t - A_e)/(A_o - A_e))$ versus time plot (●) for the reaction of 16-ArN_2^+ with TBHQ in CTAB (A, $\Phi_I = 0.01961$, pH = 1.54, 0.0316 M HBr) and SDS (B, $\Phi_I = 0.01965$, pH = 5.71, 0.01 M acetate buffer) emulsions of 1:1 MCT to water volume ratio in the absence of salt. [16-ArN_2^+] $= 3.24 \times 10^{-4}$ M, [TBHQ] $= 3.24 \times 10^{-3}$ M, T = 27 °C. In all runs, R^2 is at least 0.996 for 4-5 half-lives.

Plots of the k_{obs} versus Φ_I data in CTAB and SDS emulsions are shown in Figure 2.6.

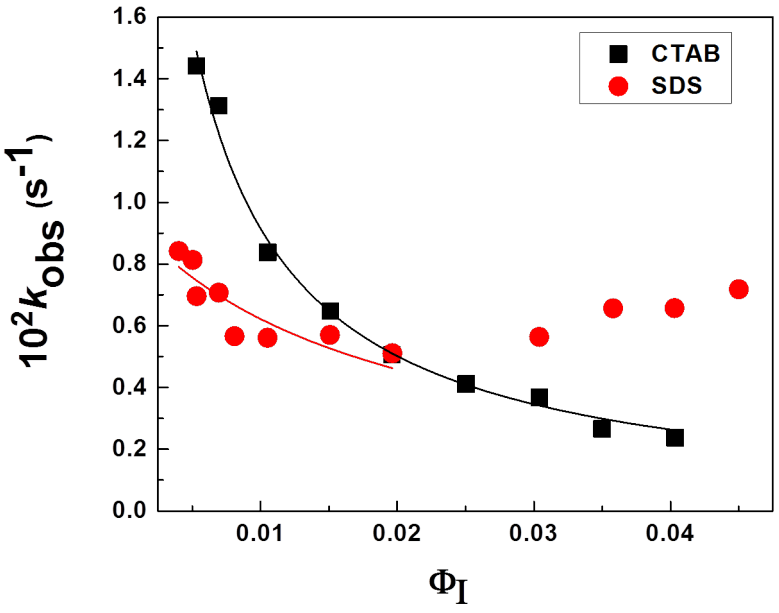

Figure 2.6: Plots of k_{obs} for the reaction of 16-ArN_2^+ with TBHQ in CTAB (pH = 1.54, 0.0316 M HBr) and SDS (pH = 5.71, 0.01 M acetate buffer) emulsions of 1:1 MCT to water volume ratio as a function of surfactant volume fraction, Φ_I, in the absence of added salt, T = 27 °C. Solid lines are fits of the data based on Equation 2.9. $R^2 = 0.989$ and 0.727 for CTAB and SDS, respectively.

In CTAB emulsions, k_{obs} decreases steadily with increasing Φ_I from about 0.005 to 0.04, consistent with Equation 2.8 based on the pseudophase model originally applied to nonionic emulsions. However, in SDS emulsions the change in k_{obs} with Φ_I is not monotonic : it initially decreases as Φ_I increases from 0.004 to 0.02, then increases steadily with Φ_I. The solid lines are the theoretical curves obtained by fitting the experimental data to Equation 2.10. Equation 2.11 predicts that a plot of $1/k_{obs}$ versus Φ_I should be linear with a positive intercept, Figure 2.7. Values for the partition constants P_O^I and P_W^I and the second order rate constant k_I are obtained in part from these plots.

2.3.2 Estimating values of P_O^W, P_O^I, P_W^I, and k_I for TBHQ

The partition constant, P_O^W, of TBHQ between MCT and water in the absence of surfactant was determined by UV-Vis method. Absorbance values of TBHQ in each phase, Table 2.1,

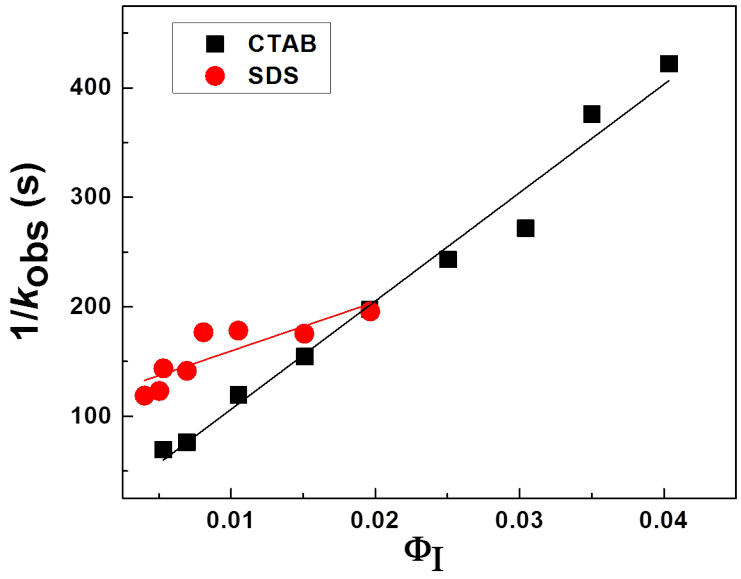

Figure 2.7: Plots of $1/k_{obs}$ versus Φ_I in CTAB and SDS emulsions in the absence of added salt, T = 27 °C. Straight lines are the linear fits based on Equation 2.10. $R^2 = 0.978$ and 0.700 for CTAB and SDS respectively.

were converted to concentrations by using calibration curves determined in MCT and water (See Experimental). The average value of P_O^W calculated using Equation 2.14, $P_O^W = 0.018$

Table 2.1: UV-Vis absorbance data for TBHQ from MCT/water partitioning experiments. P_O^W was calculated using Equation 2.14.

In MCT		In H_2O		P_O^W
Abs	Conc. ($\times 10^{-4}$ M)	Abs	Conc. ($\times 10^{-4}$ M)	
1.245	3.271	0.2207	0.685	0.0209
1.09	2.865	0.1614	0.488	0.0170
1.243	3.266	0.1665	0.505	0.0155
			average value =	0.018 ± 0.0028

± 0.0028, is much smaller than the partition constant of TBHQ between water and octane, $P_O^W = 27.5$[65], and slightly larger than the one between water and tributyrin, $P_O^W = 0.016$ (unpublished), Table 2.2. These values are consistent with the oil polarity order of: octane < MCT ≈ tributyrin, i.e., the more polar the oil, the higher the solubility of TBHQ in the

oil and the smaller $P_{\mathrm{O}}^{\mathrm{W}}$.

Table 2.2: TBHQ partition constants, $P_{\mathrm{W}}^{\mathrm{I}}$, $P_{\mathrm{O}}^{\mathrm{I}}$ and $P_{\mathrm{O}}^{\mathrm{W}}$, and the second-order interfacial rate constant, k_{I}, values obtained from the linear fit of $1/k_{\mathrm{obs}}$ versus Φ_{I} in CTAB and SDS emulsions of 1:1 MCT:water volume ratio, Figure 2.7 and in $C_{12}E_6$ emulsions of 1:1 octane:water volume ratio for comparison.

	CTAB	SDS	$C_{12}E_6$[65]
	MCT	MCT	Octane
$P_{\mathrm{W}}^{\mathrm{I}}$	3.79×10^4	1.13×10^3	6.73×10^2
$P_{\mathrm{O}}^{\mathrm{I}}$	6.83×10^2	20.4	1.84×10^4
$P_{\mathrm{O}}^{\mathrm{W}}$ (avg.)	0.018 ± 0.0028 (stdev) (n = 3)		27.5 ± 0.7 (stdev) (n = 21)
k_{I} ($\mathrm{M^{-1}s^{-1}}$)	3.12×10^{-2}		5.51×10^{-2}

Values of the partition constants for TBHQ between the oil and interfacial regions, $P_{\mathrm{O}}^{\mathrm{I}}$, and between the aqueous and interfacial regions, $P_{\mathrm{W}}^{\mathrm{I}}$, are listed in Table 2.2. The partition constants were calculated from the linear fits by solving, simultaneously, Equations 2.13 and 2.14.

The percentage of TBHQ in the interfacial region can ben estimated from the values of $P_{\mathrm{O}}^{\mathrm{I}}$ and $P_{\mathrm{W}}^{\mathrm{I}}$ at any surfactant volume fraction by using Equation 2.16 derived by combining Equation 2.7 and Equation 2.15.

$$\%\mathrm{AO_I} = \frac{100[\mathrm{AO_I}]}{[\mathrm{AO_T}]} = \frac{100(\mathrm{AO_I})\Phi_{\mathrm{I}}}{[\mathrm{AO_T}]} \tag{2.15}$$

$$\%\mathrm{AO_I} = \frac{\frac{100[\mathrm{AO_T}]P_{\mathrm{O}}^{\mathrm{I}}P_{\mathrm{W}}^{\mathrm{I}}\Phi_{\mathrm{I}}}{\Phi_{\mathrm{O}}P_{\mathrm{W}}^{\mathrm{I}}+\Phi_{\mathrm{I}}P_{\mathrm{O}}^{\mathrm{I}}P_{\mathrm{W}}^{\mathrm{I}}+\Phi_{\mathrm{W}}P_{\mathrm{O}}^{\mathrm{I}}}}{[\mathrm{AO_T}]} = \frac{100\Phi_{\mathrm{I}}P_{\mathrm{O}}^{\mathrm{I}}P_{\mathrm{W}}^{\mathrm{I}}}{\Phi_{\mathrm{O}}P_{\mathrm{W}}^{\mathrm{I}} + \Phi_{\mathrm{I}}P_{\mathrm{O}}^{\mathrm{I}}P_{\mathrm{W}}^{\mathrm{I}} + \Phi_{\mathrm{W}}P_{\mathrm{O}}^{\mathrm{I}}} \tag{2.16}$$

Table 2.3 lists the values of $\%\mathrm{TBHQ_I}$ at the lowest, intermediate, and highest volume fractions of CTAB and SDS, respectively. The results show that from about 0.005 to 0.04 Φ_{I} of CTAB, $\gg$ 90% of TBHQ is in the interfacial region. However, less than 50% of the TBHQ partitions into the interfacial regions of the SDS emulsions up to 0.0196 Φ_{I}.

Note that the value of $P_{\mathrm{W}}^{\mathrm{I}}$ in CTAB emulsions is on the order of 10^4, Table 2.2, which means the concentration of TBHQ in the interfacial region is about 10,000 times higher than in the aqueous region and therefore the concentration of TBHQ in aqueous region is

Table 2.3: Values of $\%TBHQ_I$ at different surfactant volume fractions in CTAB and SDS emulsions and in $C_{12}E_6$ emulsions for comparison.

Φ_I (CTAB)	$\%TBHQ_I$	Φ_I (SDS)	$\%TBHQ_I$	Φ_I ($C_{12}E_6$)[65]	$\%TBHQ_I$
0.00531	87.8	0.0040	13.9	0.0053	87
0.0196	96.4	0.0105	29.8	0.020	96
0.0403	98.3	0.0197	44.6	0.040	98

negligible, i.e., $(AO_W) \approx 0$, and only P^I_O is needed to describe its distribution in CTAB emulsions. Thus, the mass balance equation for TBHQ, Equations 2.4, was simplified to:

$$[AO_T] = \Phi_O(AO_O) + \Phi_I(AO_I) \tag{2.17}$$

Combining Equations 2.6 and 2.17 and solving for (AO_I) in terms of $[AO_T]$ gives:

$$(AO_I) = \frac{[AO_T]P^I_O}{\Phi_O + \Phi_I P^I_O} \tag{2.18}$$

And expressions for k_{obs}, $1/k_{obs}$, and $\%AO_I$ were simplified to:

$$k_{obs} = k_I(AO_I) = \frac{[AO_T]k_I P^I_O}{\Phi_O + \Phi_I P^I_O} \tag{2.19}$$

$$\frac{1}{k_{obs}} = \frac{1}{[AO_T]k_I}\Phi_I + \frac{\Phi_O}{[AO_T]k_I P^I_O} \tag{2.20}$$

$$\%AO_I = \frac{100\Phi_I P^I_O}{\Phi_O + \Phi_I P^I_O} \tag{2.21}$$

The value of P^I_O obtained from the slope and intercept of Equation 2.20 is 6.71×10^2, which is quite close to the value of P^I_O, 6.83×10^2, in Table 2.2 and supports using the simplified Equation 2.19. The value of k_I and the values of $\%TBHQ_I$ in CTAB emulsions at different surfactant volume fractions obtained from simplified equations are virtually identical to the values listed in Tables 2.2 and 2.3. These results confirmed the conclusion that TBHQ is far more soluble in the interfacial region of CTAB emulsions than in the aqueous region, and the percentage of TBHQ in the aqueous region is negligible. Therefore, the percentage of TBHQ in the oil region can be determined as $\%TBHQ_O = 100 - \%TBHQ_I$. In general, large partition constants such as $P^I_W = 3.79 \times 10^4$, Table 2.2, are imprecise because of the

small fraction of AO in the aqueous region. Excluding $P_{\mathrm{W}}^{\mathrm{I}}$ from the calculation of $P_{\mathrm{O}}^{\mathrm{I}}$ did not affect the values of other parameters.

2.3.3 Kinetics in CTAB and SDS emulsions in the presence of added NaBr

The effect of added NaBr on k_{obs} for the reaction of 16-ArN_2^+ with TBHQ in CTAB and SDS emulsions at constant surfactant concentration are shown in Figure 2.8. The values of k_{obs} decrease as a function of NaBr concentration in CTAB emulsions, but increase with added NaBr in SDS emulsions.

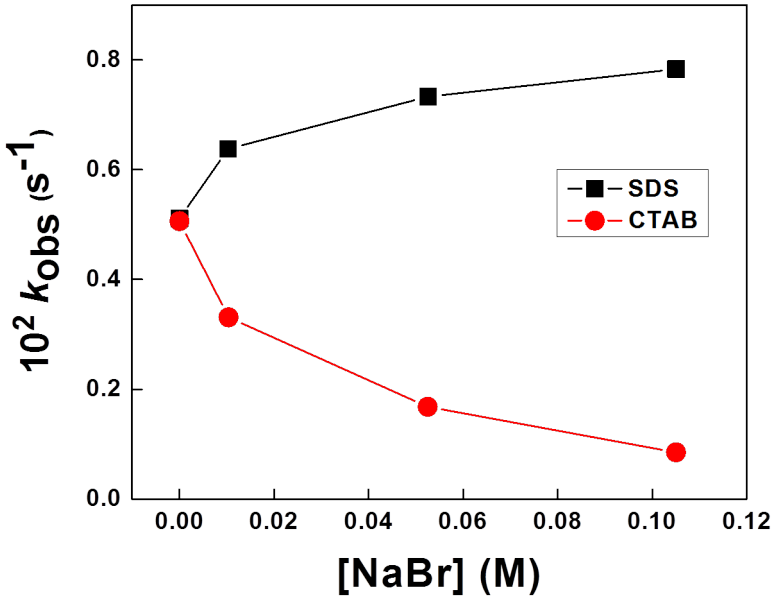

Figure 2.8: Variation of k_{obs} for the reaction between 16-ArN_2^+ and TBHQ at T = 27 °C as a function of added NaBr concentration in CTAB (pH = 1.54) and SDS (pH = 5.71) emulsions of 1:1 MCT to water volume ratio at constant volume fraction of surfactant, $\Phi_{\mathrm{I}} \approx 0.0196$. Lines are drawn to aid the eye.

2.4 Discussion

2.4.1 Application of the pseudophase model to H^+ distributions in ionic emulsions

The interpretation below on the effect of surfactant charge and concentration and NaBr concentration on k_{obs} is based on successful applications of the pseudophase kinetic models to ionic micelles and microemulsions, i.e., treating ionic interfaces as selective ion exchangers.[20, 38, 140] In ionic emulsions, as in ionic micellar solutions and microemulsions, the high local concentrations of cationic headgroups in CTAB emulsions and anionic headgroups in SDS emulsions significantly alter the interfacial H^+ concentration relative to the bulk H^+ concentration.[141]

Figure 2.9A illustrates the interfacial region created by a cationic emulsion that contains a high local Br^- concentration, on the order of 1 M and higher, whereas the Br^- concentration in the aqueous phase is on the order of 1-10 mM in the absece of added salt.[84] Conversely, the concentration of co-ions, e.g., H^+, may be 1-2 orders of magnituge lower than that in the aqueous region. The reverse is true for the anionic SDS interface, Figure 2.9B, i.e., high local concentrations of Na^+ and H^+ in the interfacial region and low concentrations of anions. Thus, charged interfaces alter the interfacial acidity significantly-cationic surfactants reduce it and anionic surfactants increase it.

Figure 2.9 also illustrates the effect of added salt, NaBr. In anionic emulsions, Figure 2.9B, added Na^+ displaces H^+ and reduces its concentration via the ion exchange equilibrium, which has been applied to association colloids and also to ion exchange resins for decades[20, 37, 142]:

$$H_I^+ + Na_W^+ \overset{K_H^{Na}}{\rightleftharpoons} H_W^+ + Na_I^+ \tag{2.22}$$

$$K_H^{Na} = \frac{[H_W^+][Na_I^+]}{[H_I^+][Na_W^+]} \tag{2.23}$$

K_H^{Na} is an empirical ion exchange constant, the value of which in SDS micelles is about 1.[38] In cationic emulsions, Figure 2.9A, the effect of added counterion Br^- on the H^+

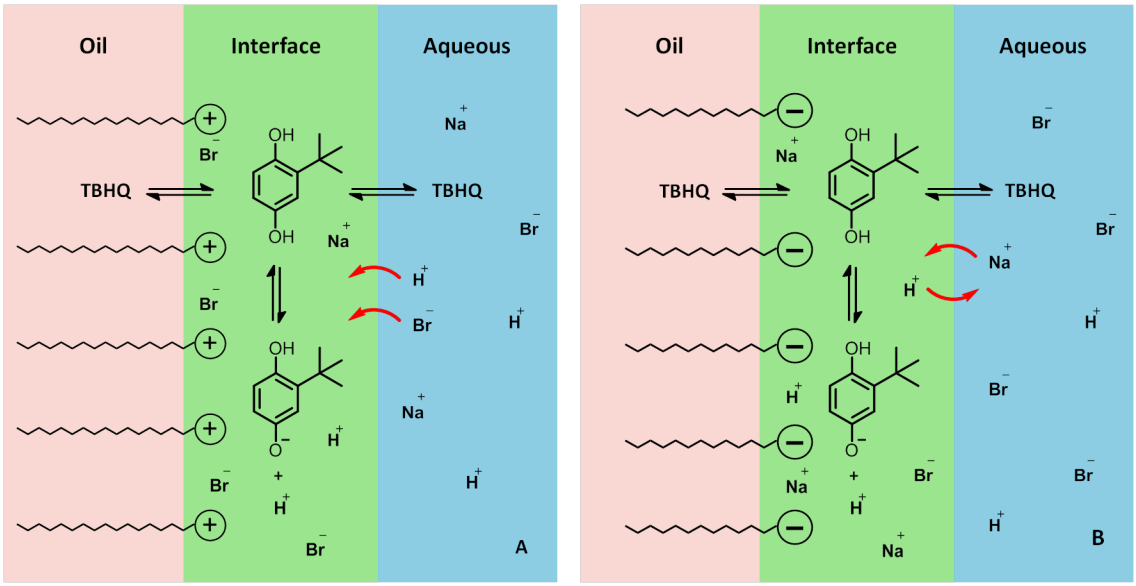

Figure 2.9: Cartoons of the pseudophase model applied to ionic emulsions in the presence of added salt, NaBr: (A) Donnan equilibrium in CTAB emulsions and (B) ion exchange in SDS emulsions. Also shown is the ionization equilibrium of TBHQ in the interfacial region.

distribution between the interfacial and aqueous regions can be described by a Donnan equilibrium constant, $K_{\mathrm{H}}^{\mathrm{Br}}$:

$$\mathrm{H_I^+} + \mathrm{Br_I^-} \overset{K_{\mathrm{H}}^{\mathrm{Br}}}{\rightleftharpoons} \mathrm{H_W^+} + \mathrm{Br_W^-} \tag{2.24}$$

$$K_{\mathrm{H}}^{\mathrm{Br}} = \frac{(\mathrm{H_I^+})(\mathrm{Br_I^-})}{[\mathrm{H_W^+}][\mathrm{Br_W^+}]} \tag{2.25}$$

Equation 2.25 states that at constant bulk $\mathrm{H^+}$, increasing the $\mathrm{Br^-}$ concentration in the aqueous region by adding NaBr, increases the $\mathrm{Br^-}$ and $\mathrm{H^+}$ concentration in the interfacial region, such that the ratio of the numerator and denominator remains constant.

Changing the $\mathrm{H^+}$ concentration in the interfacial region shifts the acid-base equilibra of TBHQ within the interfacial region. The position of equilibrium depends on both the interfacial $\mathrm{H^+}$ concentration and the $\mathrm{p}K_{\mathrm{a}}$ of the acid in the interfacial region as a reaction medium.[44, 45, 47] Together they determine the TBHQ anion concentration, $\mathrm{TBHQ^-}$, and the rate of reaction because it is $\mathrm{TBHQ^-}$ that reacts with 16-$\mathrm{ArN_2^+}$. As noted earlier, at 3 mM HCl (measured pH 2.52) in nonionic emulsions, the reduction of 16-$\mathrm{ArN_2^+}$ by TBHQ is slow enough to be monitored by conventional spectrometry or by linear sweep voltammetry,

i.e., the half-life is on the order of minutes. At pH 2.5 in aqueous solution, the H^+ concentration is more than eight orders of magnitude below the first pK_a of TBHQ of 10.8.[143] The interfacial H^+ in CTAB emulsions is lower than the aqueous H^+ concentration, which increases the interfacial $TBHQ^-$ concentration, Figure 2.9A, and may speed the reaction considerably, 1-2 orders of magnitude. Thus, a higher aqueous H^+ concentration (0.0316 M HBr, pH 1.54) was used to keep the rate of reaction in the measurable range. Conversely, in SDS emulsions, the interfacial H^+ concentration is higher than the aqueous H^+ concentration which shifts the position of equilibrium in the interfacial region in favor of neutral TBHQ, Figure 2.9B. Thus, the aqueous solution H^+ concentration must be reduced (0.01 M acetate buffer, pH 5.71) to keep the rate of reaction from being too slow to measure.

2.4.2 Effect of increasing Φ_I on k_{obs}

CTAB emulsions In the absence of added salt, the decrease in k_{obs} with increasing Φ_I, Figure 2.6, is caused by dilution of the TBHQ within the increasing total volume of the interfacial regions of the emulsions droplets, Equation 2.7. At constant Φ_O:Φ_W and constant $[AO_T]$, added CTAB dilutes interfacial TBHQ, $TBHQ^-$ and H^+ to approximately the same extent and should not change the position of TBHQ equilibrium in the interfacial region. However, dilution of $TBHQ^-$ slows the reaction with 16-ArN_2^+ and reduces k_{obs}. The fits of the k_{obs} versus Φ_I profile, Figure 2.6, and the $1/k_{obs}$ versus Φ_I profile, Figure 2.7, are excellent. The values of P_O^I and P_W^I are numerically large, Table 2.2, and the percentage of TBHQ in the interfacial region is high, Table 2.3. These results are similar to those obtained earlier in nonionic $C_{12}E_6$ emulsions with octane as the oil.[65] Note the large values of P_O^I and P_W^I for $C_{12}E_6$ emulsions, Table 2.2, and the high percentage TBHQ in the interfacial region, Table 2.3. Once the partition constants were obtained, the value of k_I (Table 2.2) was calculated from Equation 2.12. The value of k_I in the CTAB emulsions is similar to that for TBHQ, Table 2.2, in nonionic emulsions suggesting that the medium properties of emulsions interfaces are similar.

SDS emulsions These results are significantly different. The k_{obs} versus Φ_I profile decreases initially, but passes through a shallow minimun at about $\Phi_I = 0.025$ and then increases. Also, the %TBHQ in the interfacial region os SDS emulsions is less than half of that of in CTAB or nonionic emulsions, Table 2.3. We attribute the minimum to two opposing factors. As in CTAB and nonionic emulsions, dilution of TBHQ in the interfacial region of SDS emulsions with increasing Φ_I at low SDS concentrations is accompanied by a dilution of $TBHQ^-$ and a decrease in k_{obs}. At constant buffer concentration, the ratio of H^+ to Na^+, or the bulk pH should be constant. However, previous work has demonstrated that buffers do not hold the interfacial H^+ constant with increasing surfactant concentration in aqueous micellar solutions.[47] As Φ_I of SDS continues to increase, the interfacial H^+ concentration decreases because the interfacial Na^+ concentration increases. A decrease in interfacial H^+ shifts the acid-base equilibrium of TBHQ, and increases $TBHQ^-$. Therefore, k_{obs} increases. Thus, the two opposing effects are the simultaneous dilution of $TBHQ^-$ and the decrease in H^+ concentration in the interfacial region, which leads to an eventual increase in $TBHQ^-$ concentration and an increase in k_{obs}.

2.4.3 Effect of added NaBr on k_{obs}

At constant Φ_I, up to 0.1 M added NaBr increases k_{obs} in SDS emulsions and decreases k_{obs} in CTAB emulsions, Figure 2.8. Addition of moderate amounts of salt containing non-reactive counterions or co-ions at constant surfactant, oil and aqueous region volume fractions are assumed to not change the volume of the interfacial region significantly.[67] Thus, added NaBr effects on the interfacial H^+ concentration are responsible for the changes in k_{obs}, Figure 2.8. In terms of the Donnan equilibrium, Figure 2.9A, Equation 2.24, addition of NaBr to CTAB emulsions increases the interfacial acidity because added Br^- increases interfacial H^+ concentration, and shifts the acid-base equilibrium of TBHQ in favor of protonated TBHQ and reduces $TBHQ^-$, which decreases k_{obs} as observed in Figure 2.8.

In SDS emulsions, Na^+ and H^+ are competing counterions and emulsions interface acts

as an ion selective exchanger, Figure 2.9B, Equation 2.22. When NaBr is added to SDS emulsions, protons in the interfacial region are displaced by sodium ions from the aqueous region at constant bulk pH. As a result, the H^+ concentration within the interfacial region decreases and k_{obs} increases as the NaBr concentration increases, Figure 2.8. These results are consistent with aqueous buffer not controlling interfacial pH.

2.4.4 Partition constant values

Partition constants for TBHQ obtained from pseudophase models depend on intermolecular interactions within two environments, the interface and water and the interface and oil. Differences in partition constants values may depend on the interactions between the AO, headgroups, counterions and water in the interfacial region, but also on interactions in the oil or aqueous regions. The differences in P_{O}^{I} and P_{W}^{I} values in CTAB emulsions compared to SDS emulsions may reflect possible π-cation interactions between the aromatic ring of TBHQ and the quaternary ammonium headgroup of CTAB that may enhance the binding of TBHQ to the interfacial region.[144, 145] Indeed, Heins and coworkers probe the locations of propyl gallate in CTAB, SDS, and Brij 58 micelles by using T_1 relaxation times and concluded that the positive charge on CTAB enhanced the activity of the hydrophilic antioxidant.[146] Similarly, they used an ESR approach to determine the stoichiometric factor of hydrophobic galvinoxyl reacting with propyl gallate in the same surfactant micelles and concluded the depth of intercalation was in the order of SDS < Brij 58 < CTAB.[106]

One suprising result to us is the value of P_{O}^{W} in octane compared to MCT. P_{O}^{W} is about 1500 times greater when octane is the oil than when MCT is the oil, Table 2.2. Because the reference solvent is water for both oils, this $> 10^3$ difference in P_{O}^{W} values shows that TBHQ is about 1500 times more soluble in MCT than octane relative to water. Several interactions may contribute to this solubility difference. MCT is more polar than octane, it can accept hydrogen bonds from TBHQ, and unlike octane, may contain significant amounts of dissolved water. Note that this difference leads to an inversion of the P_{O}^{I} and P_{W}^{I} values

for TBHQ in ionic emulsions where MCT is the oil compared to nonionic emulsions where octane was used as oil, Table 2.2, as it must, because the values of $P_{\mathrm{O}}^{\mathrm{W}}$ are used to calculate $P_{\mathrm{O}}^{\mathrm{I}}$ and $P_{\mathrm{W}}^{\mathrm{I}}$.

2.5 Conclusions

The pseudophase kinetic model combined with chemical kinetic method provide quantitative estimates of AO partition constants and distributions between water and interfacial and oil and interfacial regions and an estimate of the second-order rate constant in the interfacial region in ionic emulsions just as they do in nonionic emulsions. Several factors contribute to the observed changes in k_{obs} that are part of pseudophase models including: the dilution of TBHQ in the interfacial region with added surfactant; the effect of added NaBr on the interfacial H^+ concentrations in CTAB and SDS emulsions by Donnan equilibrium and ion exchange, respectively. The basic requirements for measuring partition constants are three: (a) A probe molecule that is oriented in the interfacial region and that reacts with a second component whose distribution in the emulsions is of interest. (b) An experimental method that permits monitoring reaction progress in opaque mixtures such as electrochemistry or a trapping method such as we used here. (c) The emulsions must be fluid enough that simple mixing ensures that the reactive components are in dynamic equilibrium throughout the time course of the reaction. The application of this approach to a variety of different AOs and many different anionic or cationic surfactants as well as nonionic surfactants will broaden current understanding of AO distributions in emulsions over a wide range of experimental conditions.

2.6 Future work

The shallow minimum in the rate-surfactant concentration profile of SDS emulsions is apparently inconsistent with the pseudophase model. Experiments have been proposed to test our explanations and re-examine the surface charge effects on kinetics in anionic emulsion

system including: 1. changing the counterion of surfactant head group from Na^+ to Li^+ or Cs^+. This changes the capacity of head group counterion displacing H^+, with Li^+ being the weakest and Cs^+ being the strongest. We expect to see a more dramatic increase in k_{obs} at higher surfactant volume fraction with Cs^+ and a lesser one with Li^+ compared to Na^+. 2. selecting a more hydrophobic AO such as α-tocopherol. The initial decrease of k_{obs} with increasing surfactant volume fraction is much smaller in SDS emulsion compared to CTAB emulsion, and the percentage of TBHQ in the interfacial region is less than 50%, indicating that TBHQ is not fully associated with the interfacial region of SDS emulsion. As a result, the dilution effect of increasing surfactant volume fraction is not significant in SDS emulsion. α-tocopherol has a long hydrophobic tail and would completely partition into the interfacial region of SDS emulsion.

In principle, our chemical kinetic method combined with the pseudophase models modified with treatments for ion distributions should be applicable to any AO that reacts with the arenediazonium ion probe in ionic emulsions composed of virtually any type of oil and surfactant. We propose to investigate AOs with carboxylic acid functional groups whose distributions will depend on the charge of the surfactant and solution pH, e.g., Trolox and caffeic acid, at charged interfaces. Food grade surfactants, e.g., sodium stearoyl lactylate (dough strengthener), lauric arginate (N^{α}-lauroyl-L-arginine ethyl ester monohydrochloride) that is a highly potent antimicrobial against a wide range of food pathogens and spoilage organisms[147], and food proteins will be used for emulsion preparations.

2.7 Experimental

2.7.1 Materials

Cetyltrimethyl ammonium bromide (CTAB, ≥98%), sodium dodecyl sulfate (SDS, ≥99%), glyceryl trioctanoate (MCT, ≥99%), HPLC-grade methanol and acetonitrile, *tert*-butylhydroquinone (TBHQ, 97%), and inorganic reagents were purchased from Sigma Aldrich. N-(1-Naphthyl)ethylenediamine dihydrochloride (NED, 96%) was purchased from Alfa Aesar and acetic acid, glacial (≥99.7%) was purchased from Fisher Scientific. CTAB and TBHQ were recrystallized from methanol before use. All other reagents were used without further purification. 4-*n*-Hexadecylbenzenediazonium tetrafluoroborate (16-ArN_2BF_4) was prepared earlier in our lab. All water used in preparation of solutions was distilled, passed over activated carbon and deionizing resin, and redistilled.

2.7.2 Emulsion preparation

Both CTAB and SDS emulsions of 1:1 aqueous solution:oil, volume:volume ratio were prepared in an erlenmeyer flask by dissolving a weighed amount of surfactant in 7.5 mL of aqueous HBr or acetate buffer followed by addition of 7.5 mL of MCT to the micellar solution. Concentr ated HBr was diluted to give a single aqueous phase stock solution of 0.0316 M HBr (pH 1.54) that was used in all CTAB emulsions. In all SDS emulsions, a single acetate buffer solution (pH 5.71) was prepared by mixing 9:1 volume ratio of 0.01 M CH_3COONa and 0.01 M CH_3COOH stock solutions. The volume fraction of surfactant, Φ_I, was varied from 0.004 to 0.045. The emulsions were stirred continuously by using a magnetic stirrer and appeared uniformly opaque. pH measurements were made with an Accumet AR50 pH-meter, calibrated with standard pH 1.68 (Thermo Scientific), 4.00, 7.00 and 10.00 buffers (Fisher Scientific). The final pH values were in the ranges of 1.47-1.55 and 5.72-5.75 for CTAB and SDS emulsions, respectively.

2.7.3 Determining k_{obs} by the azo dye derivatization method

Values of k_{obs} s^{-1}, for the reaction of 16-ArN_2^+ and TBHQ in the emulsions were determined by trapping unreacted 16-ArN_2^+ with the coupling reagent NED as a function of time. The half-life for the coupling reaction when [NED] = 0.01 M, is less than 5 s, much shorter than the half-lives of the reaction of TBHQ with 16-ArN_2^+, which had half-lives of 50 s or longer. In a typical experiment, a freshly prepared emulsion was transferred from the erlenmeyer flask to a continuously stirred (magnetic stir bar), water-jacketed cell (T = 27 ^oC), and the temperature was equilibrated throughout the experiment. An aliquot (75 μL) of a 0.661 M TBHQ stock solution in methanol (final concentration, 3.24×10^{-3} M) was added. The reaction was initiated by adding an aliquot (43 μL) of a 0.115 M 16-ArN_2BF_4 stock solution in acetonitrile to the emulsion (final concentration, 3.24×10^{-4} M). During the reaction, aliquots (160 μL) of the reaction mixture were withdrawn at specific time intervals and added immediately to test tubes containing 2 mL of 0.01 M ethanol NED solution to initiate the azo dye formation. The resulting solution is homogeneous and transparent permitting direct spectrometric measurement of the azo dyes absorbance at 572 nm, which is proportional to the concentration of unreacted 16-ArN_2^+. Rate constants were obtained by the standard procedure of fitting absorbance-time data to the integrated first-order equation to calculate k_{obs} from least-square fits, where A_t, A_o, and A_e are the measured absorbance at any time, at $t = 0$, and at infinite time, respectively.

2.7.4 Salt effect on kinetics

NaBr was added to CTAB and SDS emulsions to study the effect of salt concentration, i.e., counterions, Na^+ in SDS and Br^- in CTAB emulsions, on k_{obs} for the reaction between 16-ArN_2^+ and TBHQ, at constant volume fraction of surfactant, $\Phi_I = 0.0196$. The stoichiometric concentrations of added NaBr in the whole emulsion ranged from 0.01 M to 0.1 M. Note, added NaBr did not change the appearance of the CTAB or SDS emulsions, i.e., the emulsions were as uniformly opaque under constant magnetic stirring with and without

added NaBr. The azo dye method, as described above, was used to obtain k_{obs} values.

2.7.5 Determining the partition constant, P_O^W, of TBHQ between MCT and water in the absence of surfactant by the UV-Vis method

A 5 mL aliquot of MCT was layered onto 15 mL of water containing a small magnetic stirrer in an erlenmeyer flask. The flask was sealed by a rubber septum and N_2 was gently bubbled into the water layer through a needle for 15 min (an exit needle was used as air outlet) to minimize the air oxidation of TBHQ. An aliquot (50 μL) of freshly prepared 0.396 M TBHQ stock solution in methanol was added into the MCT layer. The mixture was stirred gently to minimize emulsification of the two layers for 2 h to ensure that the distribution of TBHQ between the oil and water phases reached equilibrium. Aliquots, 2 mL, were withdrawn from each layer by pipet. A 500 μL aliquot of the MCT layer was diluted 10 times in ethanol in volumetric flask and the absorbance was measured by UV-Vis spectrometry. The absorbance of the water layer was measured directly without dilution. The UV-Vis spectra were recorded between 200 and 400 nm for both MCT and water layers in five separate runs. The spectra showed that in three runs the bubbling of N_2 completely suppressed the oxidation of TBHQ to TBQ. In the MCT layer, λ_{max} (TBHQ) = 293.8 nm and no peak was observed at 260 nm (λ_{max} for TBQ in oil); and in the water layer, λ_{max} (TBHQ) = 287.8 nm and no peak was observed at 252 nm (λ_{max} for TBQ in water). In other two runs, the bubbling of N_2 into water failed to suppress the oxidation of TBHQ in water and a peak at 252 nm appeared. The probable cause is leakage around or through the rubber septum. Therefore, the measured absorbances in these two runs were not included in calculation of P_O^W.

Calibration curves for TBHQ in MCT and in water were determined at the λ_{max} in MCT and water by adding incremental amounts of a freshly prepared TBHQ in methanol stock solution. The absorbance measurements in MCT and water were within the ranges of the absorbances of the calibration curves so that all estimates of concentrations used in

calculating the partition constants were obtained by interpolation.

2.8 Appendix

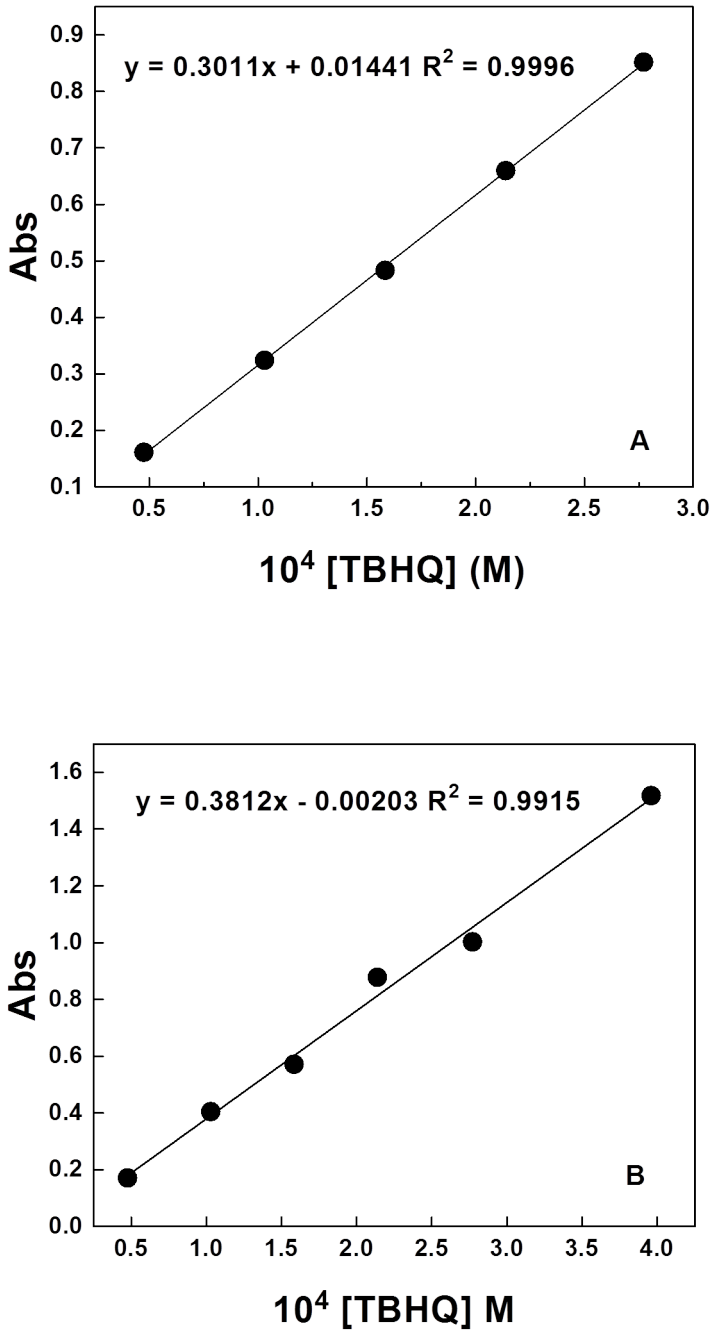

Figure 2.10: Calibration curves for TBHQ in water (A) and MCT (B).

Table 2.4: Values of k_{obs} for the reaction between 16-ArN_2^+ and TBHQ in CTAB (pH = 1.54, 0.0316 M HBr) and SDS (pH = 5.71, 0.01 M acetate buffer) emulsions of 1:1 MCT to water volume ratio in the absence of added salt at 27 °C.

Φ_I (CTAB)	10^2 k_{obs} (s^{-1})	Φ_I (SDS)	10^2 k_{obs} (s^{-1})
0.00531	1.441	0.00401	0.842
0.00694	1.313	0.00503	0.813
0.01052	0.838	0.00532	0.696
0.01511	0.647	0.00694	0.707
0.01961	0.506	0.00809	0.566
0.02504	0.411	0.01051	0.561
0.03041	0.368	0.01508	0.570
0.03500	0.266	0.01965	0.511
0.04034	0.237	0.0304	0.564
		0.0358	0.656
		0.0403	0.657
		0.0450	0.718

Table 2.5: Values of k_{obs} in CTAB and SDS emulsions at different salt concentrations.

CTAB, Φ_I = 0.01961		SDS, Φ_I = 0.01965	
[NaBr] (M)	10^2 k_{obs} (s^{-1})	[NaBr] (M)	10^2 k_{obs} (s^{-1})
0	0.506	0	0.511
0.0104	0.331	0.0103	0.638
0.0525	0.168	0.0526	0.733
0.105	0.0849	0.105	0.783

Chapter 3

Effect of droplet size on antioxidant reactivity in a nonionic emulsion

$C_{12}E_6$/hexadecane/water emulsions of constant composition, but different droplet sizes, were prepared by three mixing methods from low to high intensity, magnetic stirring, sonication, and high-pressure homogenization. Observed rate constant, k_{obs}, for the reaction of 16-ArN_2^+ with TBHQ at 25 °C and hydration numbers of $C_{12}E_6$ at 25 °C, 30 °C, and 40 °C were measured in all three emulsions. Their size distributions were measured by laser diffraction before and after each reaction. The high-pressure homogenized emulsion gave a narrow, nearly Gaussian distribution of sizes, 0.06-0.2 μm (small droplet), and wider distribution ranges were obtained for emulsions prepared by sonication, 0.1-1.5 μm (intermediate droplet), and magnetic stirring, 3-25 μm (large droplet). The values of k_{obs} are 1.4×10^{-2}, 0.8×10^{-2}, and 0.7×10^{-2} s^{-1}, respectively, and the variation from large to small droplets is greater than from large to intermediate droplets, correlating with the hydration number measurements at 25 °C: 2.3, 2.8, and 3.0 for small, intermediate, and large droplets, respectively. The decrease of hydration number from large (micron) to small (nano) droplets indicates that the interfacial region of $C_{12}E_6$ emulsions becomes "drier", and this change may be accompanied by dehydration and redistribution of $C_{12}E_6$ between the interfacial and oil region. These results are consistent with the pseudophase model assumption that rate constants for reactions in emulsions are insensitive to changes in droplet size and that the polarity of the interfacial region is insensitive to droplet size.

3.1 Hypothesis

We hypothesize that the medium properties of the interfacial region are essentially constant regardless of the droplet size of the emulsions and droplet size doesn't affect the kinetics of chemical reactions taking place in the interfacial region, or oil or aqueous regions of the emulsions. In the pseudophase model, aqueous emulsions are divided into three distinct regions: the oil droplet interior, the interfacial region created by surfactant molecules, and the continuous aqueous phase. As discussed in Chapter 1 (Section 1.2 and 1.3), component molecules in surfactant aggregates are constantly exchanging between aggregates and bulk solution. Their transfer rates are near diffusion control limit and are orders of magnitude faster than rates of most thermal reactions studied in association colloids and emulsions. Therefore, the totality of the three regions are continuous from the perspective of reactants, i.e., reactant distributions between the oil, interfacial and aqueous regions in emulsions are in dynamic equilibrium, and their relative concentrations in each region are assumed to depend on the medium or solvent properties of each region but not on the sizes or shapes of the droplets.

3.2 Introduction

3.2.1 Background

The mechanism for lipid oxidation in emulsions is different from bulk lipids due to the organization of the lipid molecules within the system and their interactions with other components at the oil-water interface. A number of factors can potentially affect the oxidative stability of oil-in-water emulsions, including fatty acid composition, aqueous phase pH and composition, type and concentration of antioxidants, droplet characteristics such as droplet size and concentration, interfacial properties such as charge, thickness, rheology, and permeability, etc.[148] A number of studies have been carried out to investigate the effect of droplet size on lipid oxidation in oil-in-water emulsions.

When keeping the emulsion compositions the same and varying the droplet size by modification of energy of emulsification, researchers have found out that emulsion droplet size has minimal impact on lipid oxidation. Lethuaut et al. found that in protein-stabilized sunflower oil emulsions with large (27.5 μm, volume mean diameter), medium (1.9 μm), and small (500 nm) droplet sizes the rates of oxygen consumption and the formation of primary oxidation products (conjugated dienes, CD) were only slightly higher when the droplet size was smaller.[149] Imai et al. analyzed the oxidation of methyl linoleate in decaglyceryl monolaurate or monostearate stabilized oil-in-water emulsions having droplets of means diameters ranging from 17 nm to 8.0 μm.[150] The oxidation rate constants were observed to be independent of the size of the oil droplt. Osborn and Akoh[151] and Paraskevopoulou et al.[152] both found that droplet size did not affect the rate of lipid oxidation in oil-in-water emulsions by measuring peroxide values over time. Kiokias et al.[153] and Dimakou et al.[154] measured the formation of conjugated dienes (CD) after a certain time of oxidation in sunflower oil emulsions stabilized by protein or Tween 20 and their results showed no dependence of changes for CD on droplet size from several hundred nanometers to several microns.

When emulsion droplet size is not the only variable, i.e., other parameters are also varied with droplet size such as surfactant type and concentration, lipid composition, it is difficult to reveal the presence of a correlation between droplet size and lipid oxdiation and the results are confusing. Hu et al.[155] reported that the formation of lipid hydroperoxides and headspace hexanal was slower in 0.5% casein stabilized corn oil emulsions having larger droplet size than in 0.5% whey protein isolate and soy protein isolate stabilized emulsions having smaller droplet size. Let et al.[156] observed lower peroxide values in smaller droplets of fish oil enriched milk emulsions, however, the emulsions of different droplet sizes were prepared with or without the additon of rapeseed oil or sodium caseinate.

To demonstrate the assumption of the pseudophase model that kinetics of chemical reactions in emulsions are not affected by droplet size, we followed the kinetics of the reaction

between 16-ArN_2^+ and TBHQ in $C_{12}E_6$ nonionic emulsions having mean droplet diameters from 100 nm to 8 μm while maintaining the emulsion compositions and reaction conditions constant. The polarity of the interfacial region in the emulsions of different droplet sizes was measured as hydration number of $C_{12}E_6$ by the chemical trapping method.

3.2.2 Estimation of hydration numbers of C_mE_n nonionic emulsions by chemical trapping

Two-component systems of water and C_mE_n (polyethylene glycol monoalkyl ethers) nonionic surfactants form a vareity of aggregate structures and phases that depend on the extent of hydration of its ethylene oxide, EO, chains.[157, 158] Below their cloud points, i.e., the lower critical solution temperature[159], nonionic surfactants form spherical and spheroidal micelles in dilute solutions and lamellar and hexagonal liquid crystal and cubic phases in more concentrated solutions. Above their cloud points nonionic surfactants form opaque suspensions that eventually phase separate. Estimating the amount of water "bound" to EO chains of aggregates of nonionic surfactants is crucial for understanding their structural and phase transitions.[160, 161]

A number of methods, e.g., light scattering, small angle neutron scattering, water (D_2O) self-diffusion by NMR and dielectric relaxation have been used to measure the amount of water associated with surfactant aggregates.[57] All these methods monitor a change in a bulk property of the system and they may sense only water hydrating the EO groups or all water trapped within the aggregate or all water that diffuses with but is "outside" of the aggregate. Our chemical trapping method based on the dediazoniation chemistry of an aggregate-bound arenediazonium ion, 4-*n*-hexadecyl-2,6-dimethylbenzenediazonium (16-2,6-ArN_2^+) (See Section 1.4.2), provides a novel way to "see" the compositions of the interfacial layer of nonionic surfactant between the oil and aqueous regions. Hydration numbers are estimated from dediazoniation product yield ratios and the selectivity of the dediazoniation reaction toward water and the terminal OH groups of C_mE_n. Comparisons of

hydration numbers obtained by methods sensitive to the collective properties of the system with our aggregate-bound probe method should provide a clearer picture of the hydration of nonionic emulsions.

Hydration numbers of C_mE_n nonionic emulsions are defined as the number of water molecules per ethylene oxide group in the interfacial layer, Equation 3.1:

$$\text{hydration number} = \frac{N_{\mathrm{W}}}{nN_{\mathrm{ROH}}} \tag{3.1}$$

where N_{W} is the moles of water in the interfacial region and N_{ROH} is the moles of terminal OH group of a C_mE_n nonionic surfactant with a polyethylene oxide chain of length n in the interfacial region, $n = 6$ for $C_{12}E_6$. The molar ratio $N_{\mathrm{W}}/N_{\mathrm{ROH}}$ is determined from the dediazoniation product yields by using Equation 3.2:

$$\frac{N_{\mathrm{W}}}{N_{\mathrm{ROH}}} = S_{\mathrm{W}}^{\mathrm{ROH}} \frac{\%16-2,6-\mathrm{ArOH}}{\%16-2,6-\mathrm{ArOE_6C_{12}}} \tag{3.2}$$

where $S_{\mathrm{W}}^{\mathrm{ROH}}$ is the selectivity of the dediazoniation reaction of 16-2,6-$\mathrm{ArN_2^+}$ toward the terminal OH group of $C_{12}E_6$ compared to water in the interfacial region of emulsions and %16-2,6-ArOH and %16-2,6-$\mathrm{ArOE_6C_{12}}$ are, respectively, measured product yields from reaction with water and $C_{12}E_6$, Figure 3.1

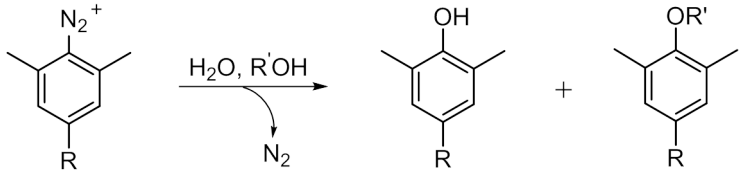

R = $C_{16}H_{33}$ or CH_3, R' = $C_{12}H_{25}(OCH_2CH_2)_6$, $H(OCH_2CH_2)_6$, $H(OCH_2CH_2)_4$

Figure 3.1: Dediazoniation reaction in $C_{12}E_6$ emulsions and in aqueous solutions of tetraethylene and hexaethylene glycols.

$S_{\mathrm{W}}^{\mathrm{ROH}}$ is estimated by assuming that it is equal to $S_{\mathrm{W}}^{\mathrm{EOH}}$, the selectivity of the water-soluble short chain analogue, 1-2,6-$\mathrm{ArN_2^+}$, toward water and the terminal OH groups in aqueous solutions of tetraethylene, E_4, and hexaethylene, E_6, glycols, Equation 3.3:

$$S_{\mathrm{W}}^{\mathrm{EOH}} = \frac{\%1-2,6-\mathrm{ArOH}}{\%1-2,6-\mathrm{ArOE}} \frac{N_{\mathrm{W}}}{2N_{\mathrm{E}}} \tag{3.3}$$

where %1-2,6-ArOH and %1-2,6-ArOE are the product yields from dediazoniation of 1-2,6-ArN_2^+ with water and glycols, for E_4/water, E_6/water, and the mixtures of E_4 and E_6/water; N_W is the moles of water and N_E is the moles of E_4 or E_6. The factor 2 corrects for the two terminal OH groups on each glycol molecule. Figure 3.2 shows a plot of product yield ratios as a function of N_W/N_E molar ratios of water and E_4, water and E_6, and aqueous mixtures of E_4 and E_6 at 18 and 40 °C. The product yield ratios are directly proportional to N_W/N_E, indicating that the selectivity of 1-2,6-ArN_2^+ toward water and terminal OH groups of glycols is independent of solution composition and temperature. The average value of S_W^{EOH} calculated from the slopes in Figure 3.2 using Equation 3.3 is 0.6. Based on this value the hydration numbers of $C_{12}E_6$ micelles with increasing $C_{12}E_6$ concentration and temperature and the hydration numbers of $C_{12}E_5$/octane/water macroemulsions as a function of increasing temperature and added NaCl were estimated, and they are in good agreement with the estimates made from water self-diffusion measurements.[57, 59]

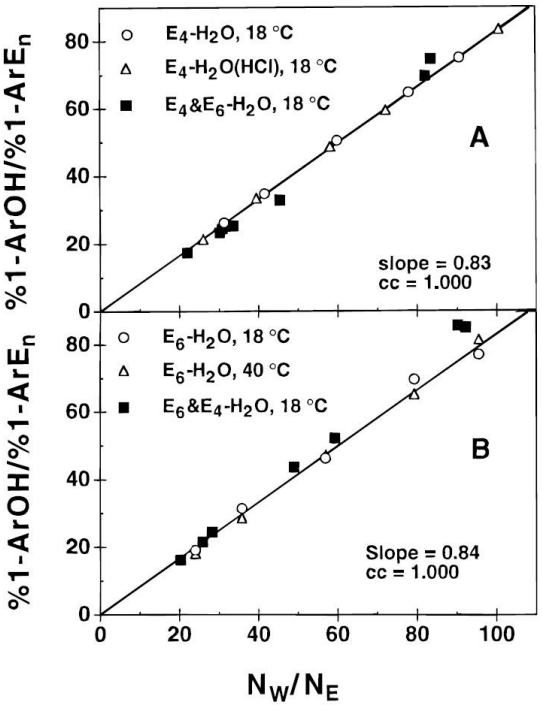

Figure 3.2: The %1-ArOH/%1-ArE_n product yield ratios from dediazoniation of 1-2,6-ArN_2^+ in aqueous E_6 (n = 6) and E_4 (n = 4) solutions and their mixtures with increasing molar ratio of water to oligoethylene oxide, N_W/N_E, at two temperatures and with added HCl (0.01 M).[57]

3.2.3 Nanoemulsions

The droplet size distributions of the emulsions we study expand from micron to nano scale. In this section, the properties of nanoemulsions compared to macroemulsions and microemulsions, and the preparation and droplet size characterization of nanoemulsions were briefly introduced.

Definition

Nanoemulsions are being increasingly utilized in the food industry to protect and deliver lipophilic functional components, such as fatty acids and oil-soluble flavors, vitamins, and nutraceuticals because they have a number of potential advantages over conventional emulsions for particular applications due to their small droplet sizes, e.g., higher optical clarity, improved stability and increased bioavailability.[162]

A conventional emulsion, also known as macroemulsion, usually has droplets with mean radii between 100 nm and 100 μm. It is thermodynamically unstable which means the free energy of the emulsion itself is higher than that of the separated oil and water phases. As a result, conventional emulsions break down over time. Conventional emulsions are optically opaque because the dimensions of their droplets are similar to the wavelength of light, therefore, they scatter light strongly (provided there is a significant refractive index contrast between the oil and water phases). A nanoemulsion is essentially conventional emulsion with very small droplets, i.e., mean radii between 10 to 100 nm.[163] Nanoemulsions are optically transparent or only slight turbid because the droplet size is much smaller than the wavelength of light so that light scattering is weak. The very small droplet size enhances nanoemulsion stability to droplet aggregation and gravitationaly separation than conventional emulsions.[163] However, like conventional emulsions, these systems are still two phases and thermodynamically unstable , therefore, will break down eventually. In contrast, a microemulsion is a thermodynamically stable system that contains droplets with

mean radii between 2 to 100 nm. Note that a microemulsion is only thermodynamically stable under certain conditions (e.g., composition and temperature). The turbidity of microemulsions is similar to nanoemulsions given their similar droplet sizes. The characteristics of macroemulsions, nanoemulsions and microemulsions are summarized in Table 3.1.[164]

Table 3.1: Comparison of thermodynamic stability and physicochemical properties of different types of emulsions prepared from oil, water and emulsifier.

System	Droplet Radius	Thermodynamic Stability	Surface-to-Mass Ratio (m^2/g droplets)	Optical Properties
Macroemulsion	100 nm-100 μm	Unstable	0.07-70	Turbid/Opaque
Nanoemulsion	10-100 nm	Unstable	70-330	Clear/Turbid
Microemulsion	2-100 nm	Stable	330-1300	Clear/Turbid

Formation

Nanoemulsions can be prepared by a variety of methods that are categorized as either higher-energy or low- energy depending on the underlying principle.[163, 165]

High-energy methods The most commonly used methods to produce nanoemulsions because they can be used with a wide variety of different oil and emulsifier types. High-energy methods utilize mechanical devices called "homogenizers" that are capable of generating extremely intensive disruptive forces to produce tiny droplets. In general, two opposing processes occurring within the homogenizer govern the droplet size-droplet disruption and coalescence.[166] To break down the droplets, the disruptive forces generated by the homogenizer must exceed the restoring forces holding the droplets into spherical shape.[167] The restoring forces increases with increasing interfacial tension (γ) and decreasing droplet radius (r), given by the Laplace Pressure: $\Delta P = \gamma/2r$. Therefore, the smaller the droplet radii become, the more difficult to break them up further.

Three types of mechanical devices are typically used to produce nanoemulsions including high pressure valve homogenizers, micrfluidizers, and ultrasonic devices, Figure 3.3. **High**

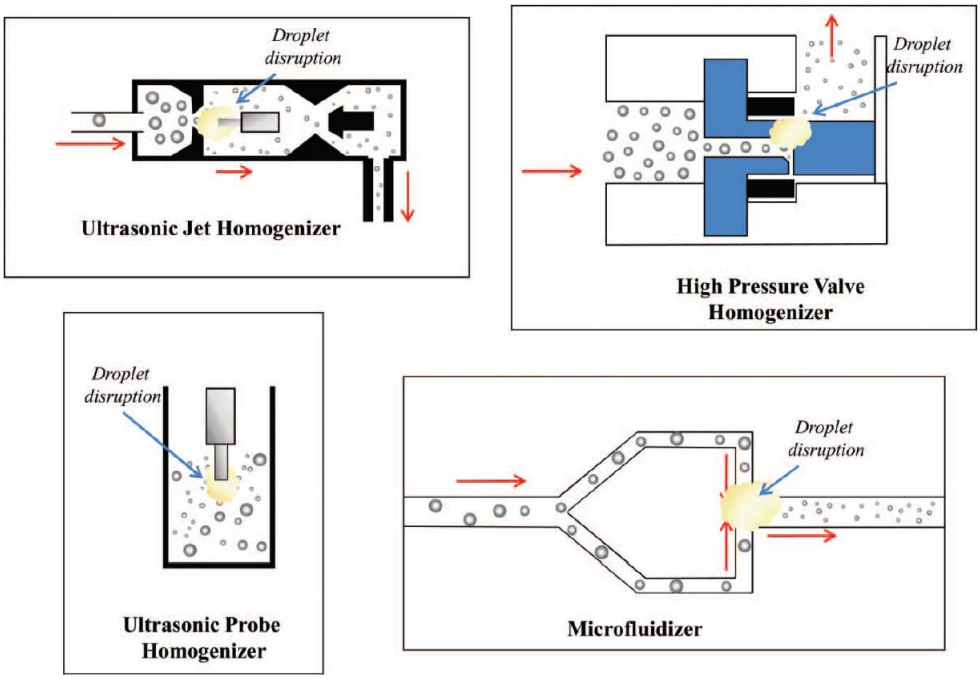

Figure 3.3: Cartoons showing the principles of various mechanical devices to prepare nanoemulsions using high-energy approaches: high pressure valve homogenizer, microfluidizer, ultrasonic jet homogenizer and ultrasonic probe homogenizer.[162]

pressure valve homogenizers are effective at reducing the droplet sizes of coarse emulsions. The coarse emulsions are pumped into a chamber and then forced through a narrow valve at the end of the chamber where it experiences a combination of intense disruptive forces including elongational flow, eddies and stress fluctuation that break down larger droplets into smaller ones. The droplet size produced by high pressure valve homogenizers usually decreases as the nubmer of passes and/or the homogenization pressure increases. **Microfuidizers** also use high pressures to force a pre-mixed emulsion through a narrow orifice to promote droplet disruption. Specifically, emulsion flow is divided into two streams through a channel, each stream passes through a separate fine channel, and then the two streams meet in an interaction chamber. When the two rapidly-moving streams of emulsions collide with each other, intense disruptive forces are generated within the interaction chamber. **Ultrasonic** homogenizers employ cavitation effects.[168] The sonicator probe generates intense mechanical vibrations within the liquid mixtures being homogenized that lead to the

formation, growth, and collapse of small bubbles in the liquids, i.e., cavitation. The collapse of the micro-bubbles formed by cavitation create intense disruptive forces in the immediate vicinity of the sonicator probe that result in droplet disruption.

Low-energy methods These approaches rely on the spontaneous formation of tiny oil droplets in oil-water-emulsifier mixed systems when either their composition or their environment is altered.[163, 169, 170] Generally there are two methods for making nanoemulsions based on the low-energy approach: spontaneous emulsification (Figure 3.4) and phase-inversion methods including phase-inversion temperature, phase-inversion composition, and emulsions-inversion point methods (mechanisms not shown).[165, 170, 171]

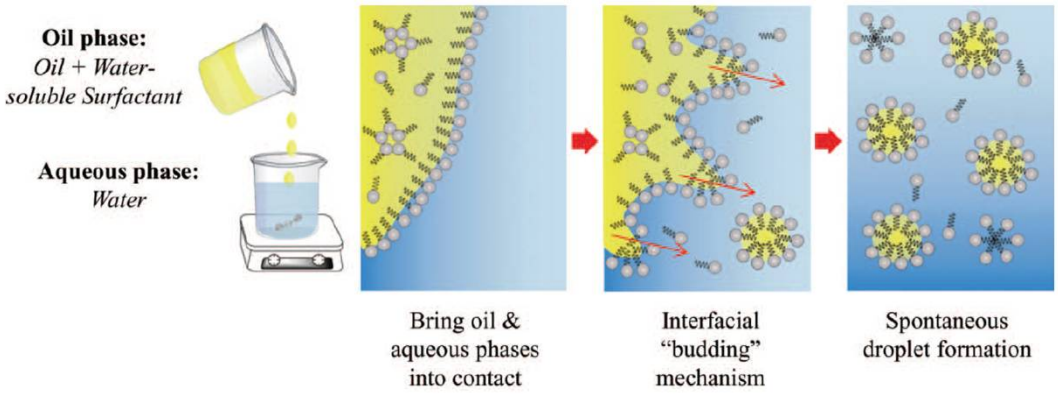

Figure 3.4: Cartoons showing proposed mechanism for spontaneous emulsification: when an oil phase containing a water-soluble surfactant is mixed with an aqueous phase, the water-soluble surfactant moves from the oil phase to the aqueous phase, leading to interfacial turbulence and spontaneous oil droplet formation.[162]

Low-energy approaches are more effective at producing small droplets than high-energy approaches, but they only work with limited types of oils and surfactants and they often require relatively high concentrations of surfactants.

In the thesis work, $C_{12}E_6$ nonionic nanoemulsions were prepared using high pressure valve homogenizer.

Droplet size characterization-Laser diffraction vs dynamic light scattering

Both laser diffraction and dynamic light scattering (DLS) are popular techniques for droplet size measurement in emulsions. The central idea of laser diffraction is that a droplet will scatter the laser beam at an angle determined by that droplet's size.[172] Smaller droplets scatter at larger angles than bigger droplets. A series of photodetectors placed at different angles measure the diffraction pattern of a collection of droplets defined by intensity and angle, which can be transformed into a droplet size distribution result. DLS measures the Brownian motion of droplets in a liquid and relates it to the size of the droplets.[173] An important feature of Brownian motion for DLS is that small droplets move quickly and large droplets move more slowly. When moving droplets are illuminated by a laser, the scattering intensity fluctuates. If large droplets are being measured, then, as they are moving slowly, the intensity of the scattered light will also fluctuate slowly. Similarly, the intensity of the scattered light for small droplets will fluctuate quickly. Size distributions can be calculated from the correlation functions for large and small droplets. The two techniques also have different detection limits. Laser diffraction is capable of measuring down to 10 nm and up to 3000 μm. The size range for DLS is usually from 1 nm to 6 μm, and both the lower and upper limits depend on the concentration and condition of the sample, as well as environmental factors.

3.3 Results

3.3.1 Droplet sizes

$C_{12}E_6$/hexadecane/water emulsions of 1:4 oil to water volume ratio and 3 vol% surfactant were prepared by using three different levels of shear intensity including high pressure homogenization (high), sonication (moderate), and magnetic stirring (low). Their droplet size distributions were obtained by laser diffraction instead of DLS because the values of the droplet sizes for macroemulsions including the emulsions prepared by magnetic stirring and

sonication measured by laser diffraction were larger than measured by DLS. Given that the upper detection limit of DLS is several micron meters, compared to several thousand micron meters for laser diffraction, and it is sample and concentration dependent, we believe that the results from laser diffraction are the accurate one, Figure 3.5. The high pressure ho-

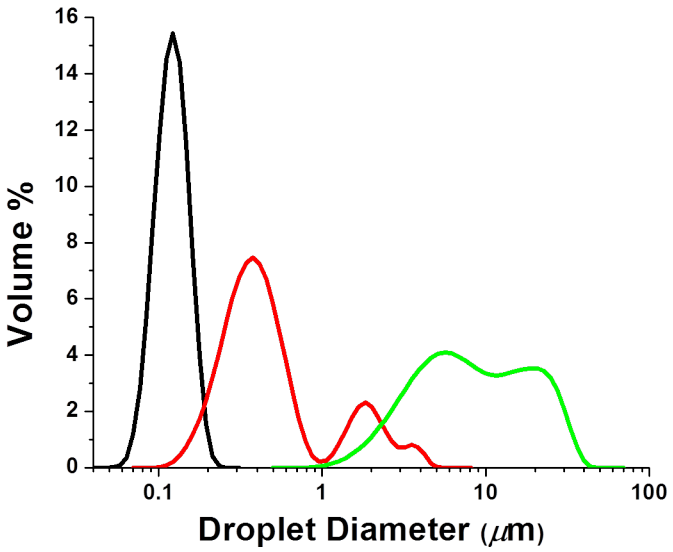

Figure 3.5: Laser diffraction generated droplet size distributions for $C_{12}E_6$/hexadecane/water emulsions (1:4 oil to water volume ratio, 3 vol% surfactant) produced by high pressure homogenization for small droplets (black), sonication for intermediate droplets (red), and magnetic stirring for large droplets (green) at 25 °C. The mean droplet diameters are 0.122 (black), 0.369 (red), and 8.643 (green) μm, respectively.

mogenized emulsion gave a narrow, nearly Gaussian distribution of sizes, 0.06-0.2 μm (small droplets), but wider distribution ranges were obtained for emulsions prepared by sonication, 0.1-1.5 μm (intermediate droplets), and magnetic stirring, 3-25 μm (large droplets). The nanoemulsion exhibited higher optical clarity with a bluish rim as compared with the other two sets of droplet sizes.

Figure 3.6 shows the droplet size distributions of all the emulsions before and after the dediazoniation reactions at three temperatures, 25 °C (A), 30 °C (B), and 40 °C (C). For the emulsions produced by high pressure homogenization and sonication, the droplet size distribution stay in the same range before and after reaction. The sizes of the coarse

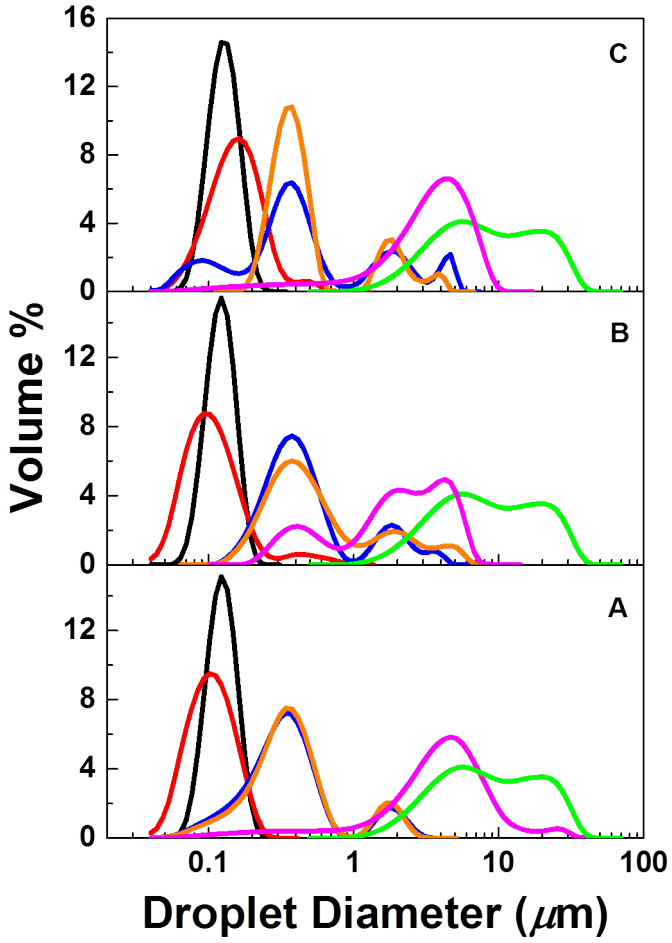

Figure 3.6: Droplet size disbributions for $C_{12}E_6$/hexadecane/water emulsions produced by high pressure homogenization (black, before; red, after), sonication (blue, before; orange, after), and magnetic stirring (green, before; magenta, after) before and after the dediazoniation reactions at T = 25 °C (A), 30 °C (B), and 40 °C (C).

emulsions prepared by magnetic stirring are smaller at the end of the reaction, probably due to the constant stirring throughout the reaction, but they are still in micron meter range and generally larger than the sonicated emulsion droplets. When the temperature increases from 25 °C to 40 °C, the variation of the droplet size distributions of the high pressure homogenized and sonicated emulsions before and after reaction becomes slightly greater.

3.3.2 k_{obs} as a function of droplet size

The observed first-order rate constant, k_{obs}, for the reaction of 16-ArN_2^+ with TBHQ in $C_{12}E_6$/hexadecane/water emulsions of constant composition (1:4 oil to water volume ratio, 3 vol.% surfactant), but different droplet sizes, were obtained by the azo dye derivatization method. The values of k_{obs} are 1.4×10^{-2}, 0.8×10^{-2}, and 0.7×10^{-2} s^{-1}, in high pressure homogenized, sonicated, and stirred emulsions, respectively, and the maximum variation is only a factor of 2 while the mean droplet diameter changed by a factor of 70 from 0.122 (high pressure homogenization) to 8.643 (magnetic stirring) μm, Figure 3.5.

3.3.3 Characterization of dediazoniation reaction products and calculation of hydration numbers

Chemical trapping experiments were carried out in $C_{12}E_6$/hexadecane/water emulsions prepared by high pressure homogenization, sonication, and magnetic stirring at 25 °C, 30 °C, and 40 °C. Three products were identified and quantified by HPLC: 4-*n*-hexadecyl-2,6-dimethylphenol, 16-2,6-ArOH, dodecylhexaethylene glycol 4-*n*-hexadecyl-2,6-dimethylphenyl ether, 16-2,6-ArE_6C_{12}, and *n*-hexadecyl-3,5-dimethylbenzene, 16-2,6-ArH. The first two products are formed by dediazoniation of 16-2,6-ArN_2^+. 16-2,6-ArH (and the unidentified oxidized product) are produced by a redox reaction between 16-2,6-ArN_2^+ and 16-2,6-ArOH, Figure 3.7.[60] HPLC peak areas, measured percent yields, and calibration curves of the

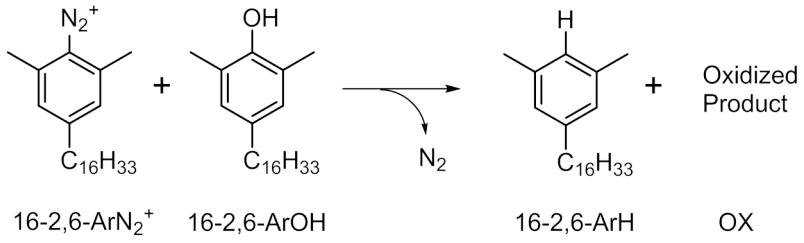

Figure 3.7: Reduction of 16-2,6-ArN_2^+ by 16-2,6-ArOH

three products are given in the Appendix (Table 3.4). Table 3.2 lists normalized product yields (average of three injections) of 16-2,6-ArOH and 16-2,6-ArE_6C_{12} from dediazoniation

of 16-2,6-ArN_2^+ in the emulsions of different droplet sizes with increasing temperature. The

Table 3.2: Normalized product yields of 16-2,6-ArOH and 16-2,6-ArE_6C_{12} from dediazoniation of 16-2,6-ArN_2^+ and hydration numbers calculated from the normalized product yields of 16-2,6-ArOH and 16-2,6-ArE_6C_{12} in $C_{12}E_6$/hexadecane/water emulsions (1:4 oil to water volume ratio, 3 vol% surfactant) of different droplet sizes at various temperatures.

T (°C)	Droplet	Normalized yield		Hydration number
		%16-2,6-ArOH	%16-2,6-ArE_6C_{12}	
25	Large	96.81	3.19	3.0
	Intermediate	96.55	3.45	2.8
	Small	95.81	4.19	2.3
30	Large	96.51	3.49	2.8
	Intermediate	96.40	3.60	2.7
	Small	95.68	4.32	2.2
40	Large	96.42	3.58	2.7
	Intermediate	96.20	3.80	2.5
	Small	95.60	4.40	2.2

consumption of 16-2,6-ArOH for the formation of 16-2,6-ArH has been corrected to obtain normalized yields of %16-2,6-ArOH and %16-2,6-ArE_6C_{12} (See Table 3.4). The values in Table 3.2 show that the yields of 16-2,6-ArE_6C_{12} increase with a concomitant decrease in the yields of 16-2,6-ArOH as the droplet size decreases at constant temperature, and also increase with temperature. The hydration numbers of $C_{12}E_6$ emulsions of different droplet sizes at three different temperatures calculated from the percent yields of 16-2,6-ArOH and 16-2,6-ArE_6C_{12} by using Equations 3.1 and 3.2 and by setting $S_W^{ROH} = S_W^{EOH} = 0.6$ are also shown in Table 3.2. At constant temperature, the hydration number decreases with droplet size. From large to intermediate droplets, the hydration number decreases by only 2.9-7.6%, however, from large to small droplets, it decreases by 19.3-24.4%. For the droplets of the same size, the hydration number slightly decreases with temperature.

3.4 Discussion

3.4.1 Hydration number of nonionic micelles and emulsions and temperature effects on hydration number

The chemical trapping results in macroemulsions show that the hydration number of $C_{12}E_5$ emulsions (1:1 oil to water volume ratio and 1.5 vol% surfactant) at 20 °C is 2.5, compared to a 70% larger value of 4.2 of $C_{12}E_6$ micelles (0.01 M) at the same temperature[57, 59]. This indicates that the interfacial region in oil-in-water $C_{12}E_5$ macroemulsions is considerably less hydrated than that in aqueous micelles. The lower hydration number indicates that the macroemulsions have lower curvature than the aqueous micelles, which contributes to their thermodynamic instability.[59]

Dehydration of the interfacial region with increasing temperature has been observed by chemical trapping in $C_{12}E_6$ micelles and $C_{12}E_5$ emulsions in our group[57, 59] as well as by molecular dynamics simulations[174]. The decrease in the hydration number is greater in the micelles (from 4.2 at 20 °C to 2.9 at 60 °C through the cloud point at 50 °C) than in the macroemulsions (from 2.5 at 20 °C to 2.2 at 45 °C through the balanced point at 32.7 °C, balanced point is at which the spontaneous curvature of the surfactant aggregate is about zero and is the transition between the oil-in-water to water-in-oil emulsion[175]). The decrease in the hydration number with temperature shows no marked transition at the balanced point, consistent with the oriented wedge theory that the stabilities of macroemulsions depend on monolayer bending elasticity and not on abrupt changes in intermolecular forces.[176] The results in Table 3.2 for $C_{12}E_6$ macroemulsions show similar trends as $C_{12}E_5$ macroemulsions: the hydration number decreases from 3.0 to 2.7 in magnetic stirred emulsions and from 2.8 to 2.5 in sonicated emulsions from 25 to 40 °C, again, consistent with the oriented wedge theory. However in nanoemulsions, the hydration number stays almost the same within the temperature range: 2.3 at 25 °C, 2.2 at 30 °C, and 2.2 at 40 °C, indicating that nanoemulsions have better stability over temperature than macroemulsions.

3.4.2 Possible explanation for the decrease of hydration number of $C_{12}E_6$ emulsions with the decrease of droplet size

Both fluid, opaque emulsions and optically transparent microemulsions are composed of oil, interfacial, and water regions of very similar bulk and microscopic properties. The primary difference is that microemulsions are thermodynamically stable and emulsions are kinetically stable two-phase systems. Strey et al. have reported that there is a non-negligible monomeric solubility of nonionic surfactant, polyoxyethylene alkyl ethers (C_mE_n), in the oil phase of H_2O-*n*-alkane-C_mE_n type microemulsions.[177] Similarly, there could be a certain amount of $C_{12}E_6$ dissolved in the oil pool of $C_{12}E_6$/hexadecane/H_2O emulsions because the components of fluid emulsions are in dynamic equilibrium just as they are in homogeneous microemulsions. During the breakdown of the large droplets into smaller ones, surfactant monomers might redistribute between the interfacial and oil region, resulting in more $C_{12}E_6$ molecules covering the droplets. By using the monomeric solubility of $C_{12}E_5$ in tetradecane, $\gamma_{\mathrm{mon,b}}$ (mass fraction), in $C_{12}E_5$/tetradecane/H_2O microemulsions of 1:1 oil to water volume ratio determined by Strey, $\gamma_{\mathrm{mon,b}} = 0.019$, we estimated that in our system, $C_{12}E_6$/hexadecane/H_2O emulsions of 1:4 oil to water volume ratio and 3 vol% surfactant, the mass fraction of $C_{12}E_6$ dissolved in the oil and the molar ratio of $C_{12}E_6$ in the interfacial region over the hexadecane in the oil region, which are, 10% and 1/10, respectively.

3.4.3 Change of k_{obs} with decreasing droplet size

In terms of the pseudophase kinetic model, the distributions of all components between the oil, interfacial, and aqueous regions in a fluid emulsion are in dynamic equilibrium, i.e., their concentrations in each region remain constant because component diffusion is extremely fast. The distribution of components is assumed to depend on the medium properties of each region but not on the size or shape of the droplets in the emulsion. Because component molecules and ions diffuse orders of magnitude faster than rates of most thermal reactions, we assume that the values of the observed rate constant, k_{obs}, for the reaction

between 16-ArN_2^+ and TBHQ in $C_{12}E_6$/hexadecane/H_2O emulsions are independent on droplet size. This assumption holds in conventional emulsions with mean radii larger than 100 nm, Section 3.2.2. When the droplet size gets down to nanoscale (mean radii $<$ 100 nm), the assumption doesn't hold apparently. However, this may not be necessarily the case because besides the change of the droplet size, the hydration number also changes. In essence, the interfacial region is a mixed solvent composed of water, polyoxyethylene groups, and hydrocarbon. The decreasing hydration number, i.e, the decreasing number of water molecules per ethylene oxide group, from micron to nano scale indicates that the medium properties of the interfacial region change, it becomes "drier", which may affect k_{I} or $P_{\mathrm{O}}^{\mathrm{I}}$ and $P_{\mathrm{W}}^{\mathrm{I}}$ or both in Equation 3.4:

$$k_{\mathrm{obs}} = k_2[\mathrm{TBHQ_T}] = \frac{[\mathrm{TBHQ_T}]k_{\mathrm{I}}P_{\mathrm{O}}^{\mathrm{I}}P_{\mathrm{W}}^{\mathrm{I}}}{\Phi_{\mathrm{O}}P_{\mathrm{W}}^{\mathrm{I}} + \Phi_{\mathrm{I}}P_{\mathrm{O}}^{\mathrm{I}}P_{\mathrm{W}}^{\mathrm{I}} + \Phi_{\mathrm{W}}P_{\mathrm{O}}^{\mathrm{I}}} \tag{3.4}$$

Note that k_{obs} hardly changes from large ($k_{\mathrm{obs}} = 0.7 \times 10^{-2}$ s^{-1}) to intermediate ($k_{\mathrm{obs}} = 0.8 \times 10^{-2}$ s^{-1}) droplets in conventional emulsions, and it increases by a factor of 2 from large to small ($k_{\mathrm{obs}} = 1.4 \times 10^{-2}$ s^{-1}) droplets, i.e., from conventional to nano emulsions. This is consistent with the results that the hydration number decreases to a greater extent from large to small droplets than from large to intermediate droplets, Table 3.2.

3.5 Conclusions/Future work

Large (3-25 μm), intermediate (0.1-1.5 μm), and small (0.06-0.2 μm) droplets of $C_{12}E_6$/hexadecane/water emulsions of 1:4 oil to water volume and 3 vol% surfactant concentration were prepared by magnetic stirring, sonication, and high pressure homogenization, respectively. Observed rate constant, k_{obs}, for the reaction of 16-ArN_2^+ with TBHQ at 25 °C and hydration numbers of $C_{12}E_6$ at 25 °C, 30 °C, and 40 °C were measured for the three emulsion droplet size distributions. Laser diffraction results show no significant change of droplet size distributions before and after the reaction for all three emulsions. The values of k_{obs} are 0.7×10^{-2} (large droplet), 0.8×10^{-2} (intermediate droplet), and 1.4×10^{-2}

(small droplet) s^{-1}. The variation in k_{obs} from large to small droplets is greater than that from large to intermediate droplets, which correlates with the hydration number results at 25 °C: 3.0 for large droplet, 2.8 for intermediate droplet, and 2.3 for small droplet. The decrease of hydration number from micron to nano scale indicates that the interfacial region of $C_{12}E_6$ emulsions becomes "drier", and this maybe caused by the redistribution of $C_{12}E_6$ between the interfacial and oil region. A decrease in interfacial hydration could change the polarity of the interfacial region and thereby the second-order interfacial rate constant, k_I, or the partition constants P^I_O and P^I_W that affect k_{obs}. Overall, these results support the assumption of pseudophase kinetic model that rate constants for reactions in emulsions of different sizes are insensitive to changes in droplet size in emulsions of constant composition and that the medium properties of the interfacial region are insensitive to droplet size.

To further demonstrate that the above pseudophase model assumption holds in all types of emulsions, kinetics experiments for the reaction of 16-ArN_2^+ with an antioxidant should be carried out in cationic (e.g., CTAB), anionic (e.g., SDS), and zwitterionic (e.g., SB3-14 (*N*-tetradecyl-*N*,*N*-dimethylammonio-1-propanesulfonate)) emulsions of different droplet sizes.

3.6 Experimental

3.6.1 Materials

Hexaethylene glycol monododecyl ether, $C_{12}E_6$ (TCI, >97%), hexadecane and diethyl ether, Et_2O (Aldrich, anhydrous), HCl standard solution (Aldrich, 0.973 N), N-(1-Naphthyl)ethylenediamine dihydrochloride, NED (Aldrich, >98%), and *tert*-butanol (*t*-BuOH), *iso*-propanol (*i*-PrOH), hexane, ethyl acetate, methanol and acetonitrile (Aldrich, HPLC grade), and silica (Aldrich, 70-230 mesh) were used as received. Tetraethylene glycol, E_4 (Aldrich, 99%), was vacuum distilled and *tert*-butylhydroquinone, TBHQ (Aldrich, 97%), was recrystallized from MeOH before use. 4-*n*-Hexadecyl-2,6-dimethylbenzenediazonium tetrafluoroborate

(16-2,6-ArN_2BF_4) and 4-*n*-hexadecylbenzenediazonium tetrafluoroborate (16-ArN_2BF_4) were prepared earlier in our lab. All water used in preparation of solutions was distilled, passed over activated carbon and deionizing resin, and redistilled.

3.6.2 Emulsion preparation

$C_{12}E_6$/hexadecane/H_2O emulsions of 1:4 oil to water volume ratio were prepared in an erlenmeyer flask by dissolving a 0.931 g of surfactant in 6 mL of hexadecane followed by addition of 24 mL of aqueous solution to the surfactant/oil mixture. The volume fraction of $C_{12}E_6$ (density $\approx$ 1 g/mL) in the emulsion is 3%. The aqueous phase is distilled water for chemical trapping experiments and 3 mM HCl for kinetic experiments, respectively. Emulsion droplet sizes were varied by using different mixing methods. Coarse emulsions containing large droplets were prepared by magnetic stirring for 2 h. Intermediate droplets were prepared by sonication of large droplets by using an open bath sonicator (FS20H, Fisher Scientific) for 25 min. Nanoemulsions were prepared by homogenizing sonicated emulsions by using the EmulsiFlex-C3 high-pressure homogenizer (Avestin Inc., Ottawa, Canada) for 3 min at 600 bar.

3.6.3 Droplet size distribution measurements

All emulsion droplet size distributions were obtained by using a Beckman-Coulter LS-13 320 Laser Diffraction apparatus (Beckman-Coulter, Inc. Brea, CA, USA). Samples were run for combined obscuration (the amount of light scatter from the presence of droplets within a laser beam) and polarization intensity differential scattering (PIDS, it illuminates the droplets sequentially with vertically and horizontally polarized light from three different visible wavelengths and the differential scattering patterns produced are measured 36 times, thus providing the primary size information for droplets in the 0.04 μm to 0.4 μm range and enhances the resolution of the droplet size distributions up to 0.8 μm) analysis. A refractive index of 1.434 was used for hexadecane. The unit was triple-rinsed between

samples. Droplet sizes were reported as the volume-weighted mean diameter, D (4,3) = $\sum n_i d_i^4 / \sum n_i d_i^3$, where n_i is the number of droplets with diameter d_i.[172] Droplet size distributions were described by three values, the D10, D50, and D90. The D50, the median, is defined as the diamter where half of the population lies below this value. Simarly, 90 percent of the distribution lies below the D90, and 10 percent of the population lies below the D10. Droplet sizes were measured before and after reactions to check for droplet growth.

3.6.4 Dediazoniation reaction and product yields

Dediazoniation was initiated by injecting freshly prepared 10 μL of a 0.04 M 16-2,6-ArN_2BF_4 stock solution in ice cold MeCN into a thermally equilibrated 10-mL volumetric flask containing 2 mL of an already prepared emulsion. Coarse emulsions prepared as described above were stirred continuously with a magnetic stirrer throughout the time course of the reaction to prevent phase separation. Emulsions prepared by sonication and high pressure homogenization did not need to be stirred during the reaction. The reactions ran for at least 6 half-lives (>97%) at all temperatures (6 $t_{1/2} \approx 48$ h at 25 °C, 10 $t_{1/2} \approx 8$ h at 40 °C).

After dediazoniation was complete, t-BuOH was added to the mark of the 10-mL volumetric flask, diluting all the components by a factor of 5. All final solutions were transparent and homogeneous. Dediazoniation products of 16-2,6-ArN_2BF_4 were separated by HPLC (Perkin-Elmer Series 200) using a mobile phase of 64% MeOH/36% i-PrOH with flow rate of 0.4 mL/min. Typical retention times in minutes are: 16-2,6-ArOH, 13.6; 16-2,6-ArH, 25.9; 16-2,6-ArE_6C_{12}, 31.6. Absorbances were monitered at 220 nm. Product concentrations were obtained from their HPLC peak areas by using calibration curves determined with standard solutions. 16-2,6-ArE_6C_{12} was not synthesized independently, the concentration of which was obtained by using the calibration curve for 16-2,6-ArE_4.[57]

3.6.5 Synthesis of tetraethylene glycol 4-hexadecyl-2,6-dimethylphenyl mono ether, 16-2,6-ArE$_4$

Freshly distilled E_4 (5 mL) and 0.15 g of 16-2,6-ArN_2BF_4 (0.15 g) were placed together in a 10-mL round bottom flask, covered, and stirred overnight at 40 °C. The mixture was extraced with Et_2O (3×5 mL), and the combined ether extracts were washed with water (3×10 mL), dried over $MgSO_4$, and rotary evaporated to give a pale yellow solid. HPLC showed several peaks for the product. The product mixture was then passed through a silica column with the eluent being the mixture of 1:1 (v/v) hexane to ethyl acetate to remove byproducts, and only a single peak appeared in the HPLC chromatogram after the column chromatography (retention time = 13.4 min). The mass of the final product is 0.152 g (86%). ^{1}H NMR ($CDCl_3$) δ (ppm): 0.88 (3 H, t, RCH_3), 1.26 (26 H, br s, $(CH_2)_{13}$), 1.56 (2 H, br, CH_2), 2.25 (6 H, s, *o*-ArCH_3), 2.47 (2 H, t, *p*-ArCH_2), 3.63-3.93 (16 H, m, Ar-$(OCH_2CH_2)_4$), 6.80 (2 H, s, ArH).

3.6.6 Kinetics

Values of the observed rate constant, k_{obs} s^{-1}, for the reaction of 16-ArN_2BF_4 and TBHQ in the emulsions of the same compositions but different droplet sizes were determined by trapping unreacted 16-ArN_2^+ with the coupling reagent NED as a function of time. The reaction was initiated by adding an aliquot of 16-ArN_2BF_4 stock solution in MeCN to the emulsion containing TBHQ stock solution in MeOH. The final concentration of TBHQ is 10 times larger than that of 16-ArN_2BF_4 so that the reaction follows first order kinetics. During the reaction, aliquots of the reaction mixture were withdrawn at specific time intervals and added immediately to NED ethanol solution to initiate the azo dye formation. The resulting solution is homogeneous and transparent permitting direct spectrometric measurement of the azo dye's absorbance by UV-Vis, which is proportional to the concentration of unreacted 16-ArN_2^+. Figure 3.8 shows the plots of the good first order kinetics that were obtained in the emulsions of three sets of droplet size distributions.

3.7 Appendix

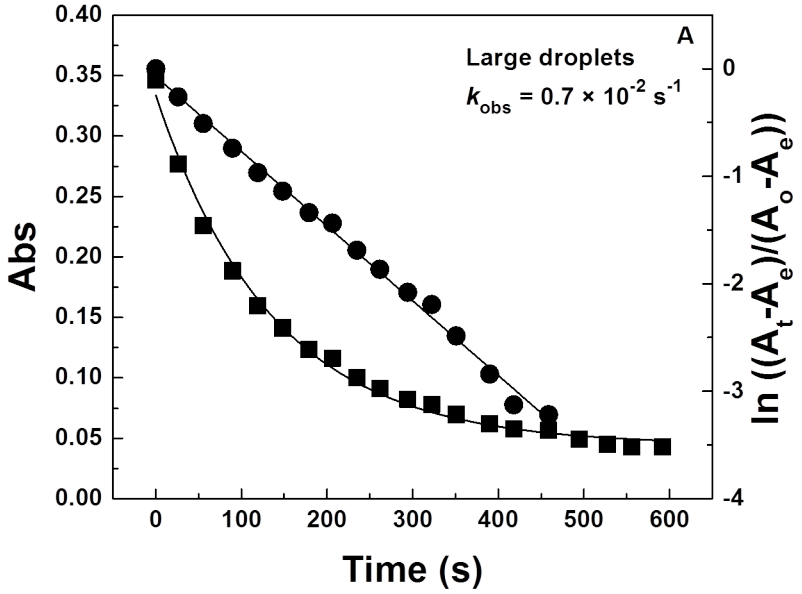
A
Large droplets
k_{obs} = 0.7 × 10^{-2} s^{-1}
Abs
ln ((A$_t$-A$_e$)/(A$_o$-A$_e$))
Time (s)
0.00
0.05
0.10
0.15
0.20
0.25
0.30
0.35
0.40
0
100
200
300
400
500
600
-4
-3
-2
-1
0

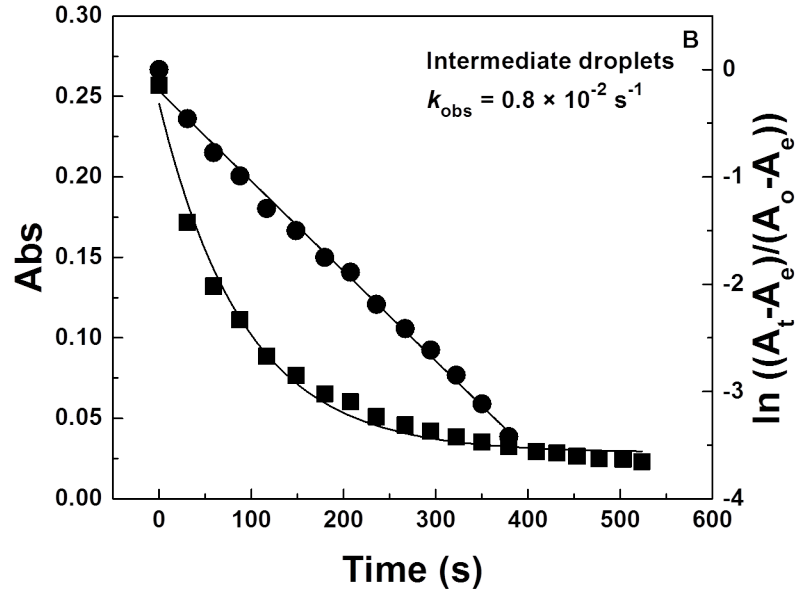
B
Intermediate droplets
k_{obs} = 0.8 × 10^{-2} s^{-1}
Abs
ln ((A$_t$-A$_e$)/(A$_o$-A$_e$))
Time (s)
0.00
0.05
0.10
0.15
0.20
0.25
0.30
0
100
200
300
400
500
600
-4
-3
-2
-1
0

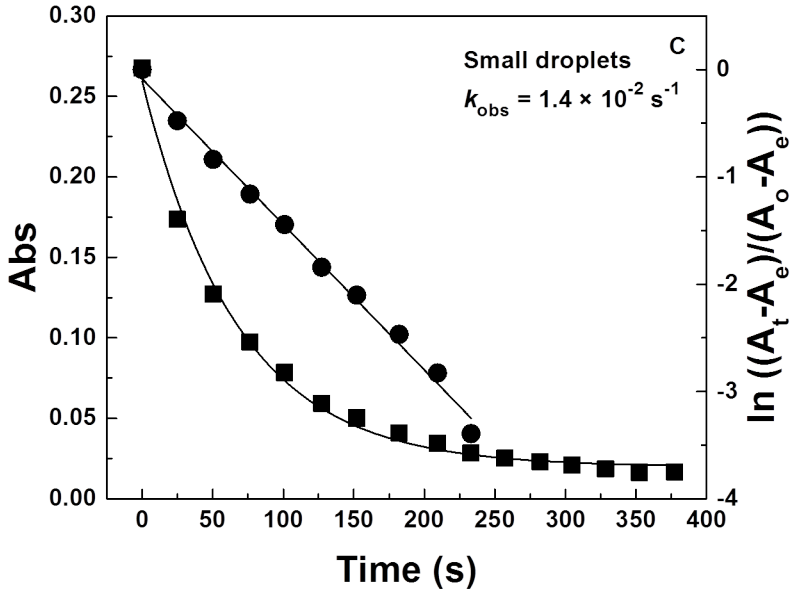

Figure 3.8: Typical azo dye absorbance versus time plot (■) and $\ln((A_t - A_e)/(A_o - A_e))$ versus time plot (●) for the reaction of 16-ArN_2^+ with TBHQ in $C_{12}E_6$/hexadecane/H_2O emulsions (pH = 2.54, 3 mM HCl) of different droplet size distributions (A: large, B: intermediate, C: small). [16-ArN_2^+] = 3.24×10^{-4} M, [TBHQ] = 3.24×10^{-3} M, T = 25 °C. In all runs, R^2 is at least 0.994 for 4-5 half-lives.

Table 3.3: The mean, median (D50), D10, and D90 droplet diameters generated by laser diffraction of $C_{12}E_6$/hexadecane/H_2O emulsions prepared by high pressure homogenization, sonication, and magnetic stirring before and after the dediazoniation reaction at three different temperatures.

T (°C)	Preparation method	Time measured	Mean (μm)	Median (μm)	D10 (μm)	D90 (μm)
25	High pressure homogenization	Before reaction	0.128	0.128	0.094	0.174
		After reaction	0.108	0.108	0.067	0.173
	Sonication	Before reaction	0.369	0.350	0.153	1.414
		After reaction	0.388	0.364	0.166	1.499
	Magnetic stirring	Before reaction	8.643	8.486	3.029	25.23
		After reaction	3.569	4.250	1.031	9.378
30	High pressure homogenization	Before reaction	0.125	0.126	0.093	0.170
		After reaction	0.115	0.108	0.066	0.201
	Sonication	Before reaction	0.521	0.430	0.236	1.989
		After reaction	0.634	0.493	0.245	2.625
	Magnetic stirring	Before reaction	8.643	8.486	3.029	25.23
		After reaction	1.836	2.223	0.416	5.126
40	High pressure homogenization	Before reaction	0.135	0.133	0.096	0.180
		After reaction	0.161	0.161	0.093	0.268
	Sonication	Before reaction	0.480	0.402	0.103	2.567
		After reaction	0.532	0.407	0.273	2.035
	Magnetic stirring	Before reaction	8.643	8.486	3.029	25.23
		After reaction	2.943	3.694	0.934	6.794

Table 3.4: HPLC peak areas, observed yields, and normalized yields for dediazoniation reaction of about 4×10^{-5} M 16-2,6-ArN_2^+ in $C_{12}E_6$/hexadecane/H_2O emulsions of different droplet sizes at 25 °C.

T = 25 °C	Peak area[a] (10^{-6} μV•s)			Observed yield[b] (%)				Normalized yield[c] (%)	
	16-2,6-ArOH	16-2,6-ArE_6C_{12}	16-2,6-ArH	16-2,6-ArOH	16-2,6-ArE_6C_{12}	16-2,6-ArH	Total	16-2,6-ArOH	16-2,6-ArE_6C_{12}
Large droplets	3.198	0.1128	0.0462	81.69	2.71	1.20	86.80	96.83	3.17
	3.239	0.1143	0.0440	82.73	2.76	1.12	87.73	96.81	3.19
	3.248	0.1168	0.0449	82.96	2.80	1.15	88.06	96.78	3.22
Intermediate	3.618	0.1469	0.0349	80.40	3.01	0.78	84.97	96.42	3.58
droplets	4.090	0.1597	0.0382	90.89	3.24	0.87	95.87	96.59	3.41
	3.990	0.1527	0.0357	88.71	3.11	0.80	93.42	96.64	3.36
Small droplets	2.918	0.1356	0.0699	75.40	3.25	1.83	82.31	95.93	4.04
	2.742	0.1354	0.0648	70.85	3.24	1.68	77.45	95.72	4.28
	2.771	0.1350	0.0637	71.60	3.24	1.65	78.14	95.76	4.24

Table 3.5: HPLC peak areas, observed yields, and normalized yields for dediazoniation reaction of about 4×10^{-5} M 16-2,6-ArN_2^+ in $C_{12}E_6$/hexadecane/H_2O emulsions of different droplet sizes at 30 °C.

T = 30 °C	Peak area[a] (10^{-6} μV•s)			Observed yield[b] (%)				Normalized yield (%)	
	16-2,6-ArOH	16-2,6-ArE_6C_{12}	16-2,6-ArH	16-2,6-ArOH	16-2,6-ArE_6C_{12}	16-2,6-ArH	Total	16-2,6-ArOH	16-2,6-ArE_6C_{12}
Large droplets	3.357	0.1336	0.0401	85.20	3.15	1.02	90.39	96.48	3.52
	3.342	0.1327	0.0457	84.82	3.13	1.17	90.29	96.49	3.51
	3.328	0.1293	0.0460	84.47	3.06	1.17	89.87	96.55	3.45
Intermediate	3.349	0.1355	0.0289	82.29	3.09	0.71	86.80	96.41	3.59
droplets	3.256	0.1344	0.0340	80.00	3.06	0.84	84.74	96.35	3.65
	3.061	0.1223	0.0360	75.21	2.81	0.88	79.78	96.44	3.56
Small droplets	2.929	0.1486	0.0898	71.97	3.36	2.24	79.81	95.67	4.33
	2.947	0.1526	0.0913	72.41	3.44	2.26	80.37	95.60	4.40
	2.938	0.1459	0.0973	72.19	3.30	2.41	80.31	95.76	4.24

Table 3.6: HPLC peak areas, observed yields, and normalized yields for dediazoniation reaction of about 4×10^{-5} M 16-2,6-ArN_2^+ in $C_{12}E_6$/hexadecane/H_2O emulsions of different droplet sizes at 40 °C.

T = 40 °C	Peak area[a] (10^{-6} μV•s)			Observed yield[b] (%)				Normalized yield (%)	
	16-2,6-ArOH	16-2,6-ArE_6C_{12}	16-2,6-ArH	16-2,6-ArOH	16-2,6-ArE_6C_{12}	16-2,6-ArH	Total	16-2,6-ArOH	16-2,6-ArE_6C_{12}
Large droplets	3.262	0.1295	0.0596	84.29	3.11	1.55	90.50	96.50	3.50
	3.306	0.1385	0.0676	85.43	3.31	1.76	92.26	96.34	3.66
	3.334	0.1365	0.0670	86.15	3.27	1.76	92.94	96.41	3.59
Intermedite	3.334	0.1420	0.0305	86.60	3.41	0.81	91.63	96.25	3.75
droplets	3.322	0.1410	0.0308	86.29	3.38	0.81	91.29	96.26	3.74
	3.325	0.1488	0.0278	86.36	3.55	0.73	91.37	96.08	3.92
Small droplets	3.029	0.1566	0.0501	78.68	3.72	1.32	85.04	95.56	4.44
	3.001	0.1533	0.0464	77.95	3.65	1.22	84.04	95.59	4.41
	3.015	0.1513	0.0509	78.31	3.61	1.32	84.56	95.66	4.34

a. The injection volume of each sample is 100 μL. b. HPLC calibration curves: [16-2,6-ArOH] = 10^{-11} μV•s (6 pts, $R^2 = 0.9998$)[69], [16-2,6-ArE_6C_{12}] = 0.8435×10^{-11} μV•s + 1.13×10^{-7} (the calibration curve for 16-2,6-ArE_4, 5 pts, $R^2 = 0.9993$), [16-2,6-ArH] = 1.01×10^{-11} μV•s (6 pts, $R^2 = 1.0000$)[69]. %Yield 16-ArX = 100[16-ArX]/[16-ArN_2^+], X = OH, E_6C_{12}, H. %Total = %16-2,6-ArOH + %16-2,6-ArE_6C_{12} + 2(%16-2,6-ArH). c. Normalized %Yield 16-2,6-ArOH = (%16-2,6-ArOH + %16-ArH)/(%16-2,6-ArOH + %16-2,6-ArH + %16-2,6-ArE_6C_{12}), Normalized %Yield 16-2,6-ArE_6C_{12} = 1 - Normalized %Yield 16-2,6-ArOH

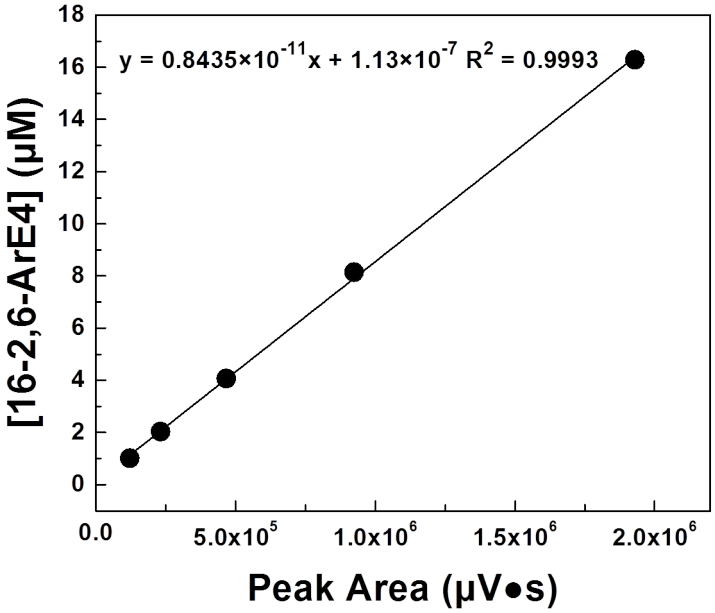

Figure 3.9: Calibration curve for 16-2,6-ArE_4

Chapter 4

Antioxidant chain length effect on its reactivity in vesicles

Recently, a nonlinear relationship between the efficiency and hydrophobicity of AO in oil-in-water emulsions has been observed and summarized as the "cutoff effect": as the hydrophobicity of a homologous series of AOs increases, their efficiency increase and reach maxima at intermediate chain lengths and then decrease at longer chain lengths. However, our kinetics experiments for the reaction of 16-ArN_2^+ with a homologous series of gallate esters in DDAB vesicular solutions show a different trend: the AO efficiency of gallate esters characterized by the observed first-order rate constant, k_{obs} ($k_I(AO_I)$), increases from methyl to propyl gallates then remains almost constant for propyl, octyl, dodecyl, hexadecyl, and stearyl gallates. This result supports the pseudophase model assumption that rate of reaction between 16-ArN_2^+ and an AO in surfactant aggregates depends on the AO concentration within the interfacial region and should aid in establishing a clearer understanding between AO efficiency and its polarity in aggregated systems.

4.1 Background

The polar paradox hypothesis has been used to characterize the activities of antioxidants (AOs) in aggregated systems in relation to their polarity since it was proposed three decades ago. However, contradictory results have been reported in recent years, and they were reviewed by Shahidi and Zhong recently.[107] The polar paradox hypothesis predicts a linear relationship between the polarity and efficacy of AO in emulsions, i.e., as the hydrophobicity of a series of homologous AOs increases, their efficacy in emulsions would increase because a larger fraction of the AO would be associated with the emulsion droplets. However, recent

work shows an unexpected nonlinear activity for lipophilic alkyl esters of phenolic AOs in emulsions, i.e., AO activity increases with the alkyl chain length and reaches a maximum at intermediate chain lengths, after which further increase in AO chain length results in a significant decrease in activity.[178, 179, 180, 181, 182] This nonlinear phenomena is referred to as the "cutoff effect" because it suggests a "collapse" in AO efficiency at longer chain lengths and it appears to be a general characteristic of AO hydrophobicity because it has been observed with different AOs including chlorogenates, rosmarinates, hydroxytyrosols, and gallate esters, for example, Figure 4.1. Similar phenomena have been observed in cell culture studies for a range of biological activities such as anesthetic, antimicrobial, and cytotoxic properties, which go through maxima with increasing AO hydrophobicity.[107]

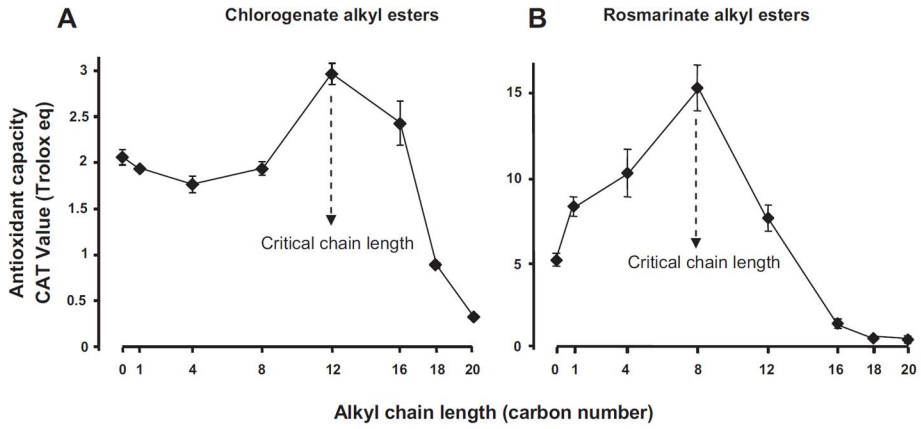

Figure 4.1: Antioxidant capacity of chlorogenate (A)[178] and rosmarinate (B)[180] esters in response to alkyl chain length in stripped oil-in-water emulsions.

Three hypotheses have been proposed to account for the cutoff effect: (a) the ability of AO to move toward the oxidation sites is decreased with increasing AO chain length; (b) increased solubility of more hydrophobic AO in the hydrocarbon region drives the AO away from the interface where oxidation primarily occurs; (c) long-chain AOs self-aggregate possibly into micelles in the aqueous phase rather than orient themselves at the oil/water interface.[183] However, no convincing evidence was found to support these hypotheses due to the lack of proper methods for monitoring reactions at the interface and determining AO

distributions within the emulsion.

Very recently, Losada-Barreiro et al. determined the distributions of gallic acid (GA) and propyl, otcyl, and lauryl gallates (PG, OG, and LG, respectively) in stripped corn oil and olive oil emulsions by using the chemical kinetic method based on the pseudophase model and compared their distributions with their AO efficiencies measured by using the Schaal oven test. The results show that at any given volume faction of emulsifier, the percentage of AO in the interfacial region follows the order PG > GA > OG > LG, matching the AO efficiency order, Figure 4.2.[184] Similar results were obtained for caffeic acid and its

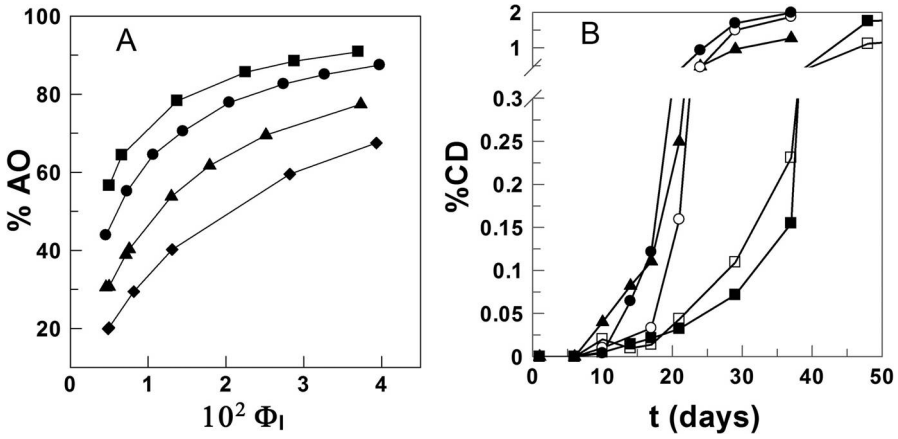

Figure 4.2: (A) Percentage of AO in the interfacial region of a 3:7 olive oil/Tween 20/acidic water (pH 3.7) emulsion at 25 °C. (■) PG, (●) GA, (▲) OG, and (♦) LG. (B) Oxidative stability of 3:7 olive oil emulsions determined by the time required for the formation of 1% conjugated dienes (%CD). (▲) Control, (●) LG, (○) OG, (■) PG, and (□) GA. [AO] ≈ 3.3×10^{-4} M, T = 45 °C.

alkyl esters in olive oil emulsions using the chemical kinetic method by Costa et al.. Figure 4.3 shows that AO efficiencies, partition constants for distributions of AOs between the oil and interfacial region, $P_{\mathrm{O}}^{\mathrm{I}}$, and the percentage of the AOs in the interfacial region all reach maxima at OG.[185] These results provide clear evidence that an AO's efficiency correlates with its fraction in the interfacial region of an emulsion. The similarities of the distribution and efficiency profiles for gallic acid, caffeic acid, and their esters are a consequence of the properties of emulsions at dynamic equilibrium as described by the pseudophase kinetic model. Therefore, the chemical kinetic method provides a natural

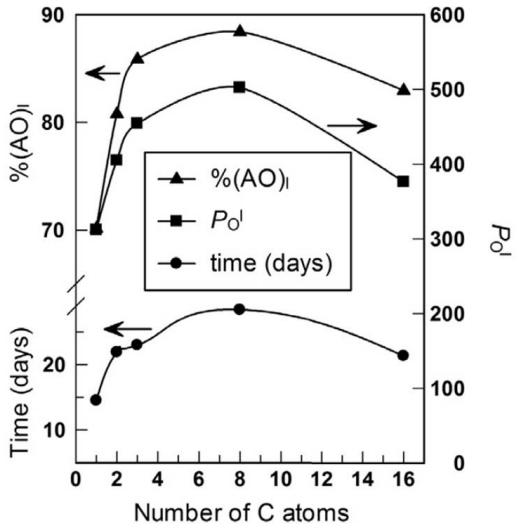

Figure 4.3: Time required to reach 1% conjugated dienes and values of $P_{\mathrm{O}}^{\mathrm{I}}$ and $\%\mathrm{AO_I}$ as a function of the number of C atoms in the alkyl chain of caffeic acid esters.

explanation for the cutoff effect, a maximum followed by a decrease in AO efficiency with increasing AO hydrophobicity.

4.2 Hypothesis

Based on the results from Losada-Barreiro et al.[184] and Costa et al.[185], Figure 4.2 and 4.3, we hypothesized that the AO efficiency of a homologous series of gallate esters characterized by the observed rate constant, k_{obs}, for the reaction of 16-$\mathrm{ArN_2^+}$ with gallate esters would plateau as the alkyl chain length increases in vesicles.

4.3 Justification

The critical packing parameter (p) of surfactant in vesicle structure is between 1/2 and 1, Figure 4.4.[186] Thus, the volume of the hydrocarbon region of vesicles, i.e., the total volume of surfactant tails, is roughly 50% of the total aggregate volume. Assume the total aggregate volume is equal to the total volume of surfactant molecules in the vesicular solution. In 15 mL of a 10 mM DDAB (didodecyldimethylammonium bromide, density $\approx$ 1) vesicular solution, the total volume of DDAB molecules is about 0.07 mL, and the

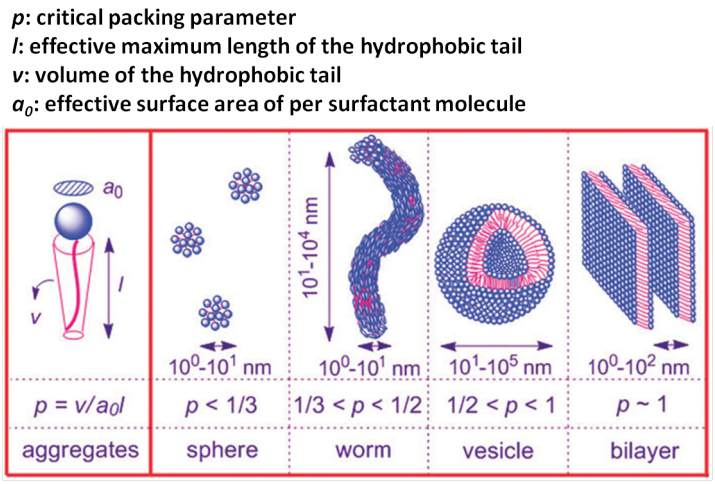

Figure 4.4: Relationship between the packing parameter p and the aggregate morphologies

total volume of the hydrocarbon region is approximately 0.035 mL. However, in 15 mL of a CTAB emulsion of 1:1 volume ratio of oil:water, the volume of the oil pool is 7.5 mL, that is about 200 times the volume of the hydrocarbon region of the 10 mM DDAB vesicular solution. In addition, in vesicular solutions, the totality of vesicle aggregates are treated as a whole because the relative volume of the interfacial region versus the volume of the hydrocarbon region is constant and is proportional to the volume ratio of surfactant head group to hydrocarbon tail. However, in oil-in-water emulsions, the relative volume of the interfacial region versus the volume of the hydrocarbon core changes with the volume of added oil. Therefore, we postulate that even strongly hydrophobic AOs are unable to fully partition into the hydrocarbon region of vesicles but orient at the headgroup-water interface.

Very recently, Marquardt et al. determined, by means of small-angle neutron diffraction, that not only is α-tocopherol's hydroxyl group located at the lipid-water interface but its tail also resides far from the center of 1-palmitoyl-2-oleoyl-*sn*-glycero-3-phosphocholine (POPC) bilayers, Figure 4.5. In addition, they demonstrated that α-tocopherol's hydroxyl group is always above the lipid backbone in bilayers with different headgroup, backbone, and tail compositions.[187, 188] Their results corroborated our postulation that hydrophobic long-chain AOs are located at the headgroup-water interface of bilayer vesicles.

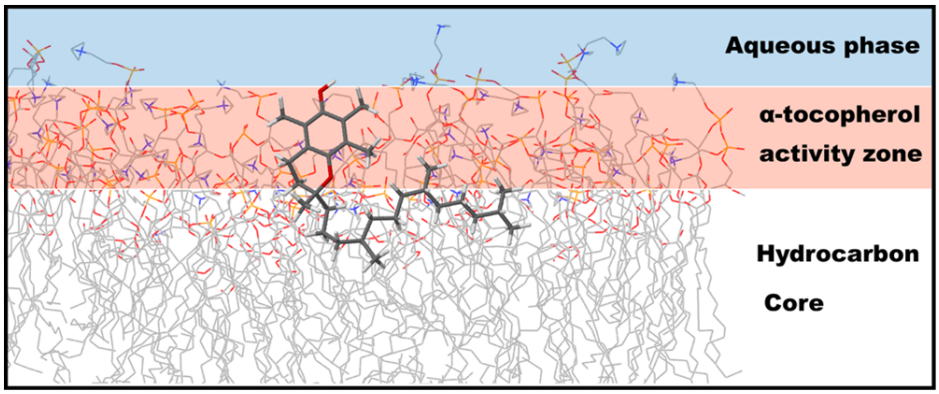

Figure 4.5: Schematic of the α-tocopherol location in a POPC membrane as determined by neutron diffraction[187]

In the pseudophase model, the rate at which the AO reacts with 16-ArN_2^+ in the interfacial region depends on the volume of the interfacial region and the fraction of AO in the region, i.e, the AO concentration in moles per liter of interfacial volume:

$$\text{rate} = k_{\text{obs}}[16 - \text{ArN}_2^+{}_{\text{T}}] = k_{\text{I}}(16 - \text{ArN}_2^+{}_{\text{I}})(\text{AO}_{\text{I}})\Phi_{\text{I}} \tag{4.1}$$

Because the diffusivities of AOs are orders of magnitude faster than their rate of reaction with 16-ArN_2^+ and because the stoichiometric AO concentration is in large excess, the concentration of the AO in the interfacial region remains constant throughout the time course of the reaction and is equal for all the AOs when completely bound at the same stoichiometric AO concentration. As a result, the rate constant, k_{obs}, for the reaction of 16-ArN_2^+ and gallate esters with increasing chain length is expected to level off once all the esters are fully associated with the vesicles:

$$k_{\text{obs}} = k_{\text{I}}(\text{AO}_{\text{I}}) = \text{constant} \tag{4.2}$$

4.4 Results and discussion

4.4.1 Vesicle preparation and characterization by dynamic light scattering

Spontaneous formation of vesicles from totally synthetic amphiphiles, didodecyldimethylammonium bromide (DDAB), was first reported by Kunitake and Okahata in 1977.[189]

Clear vesicular solutions (10 mM) of DDAB were prepared by dispersing DDAB in water followed by sonication. Vesicle size distributions measured by dynamic light scattering (DLS) are shown in Figure 4.6. The average diameter (z average) of three repetitive measurements

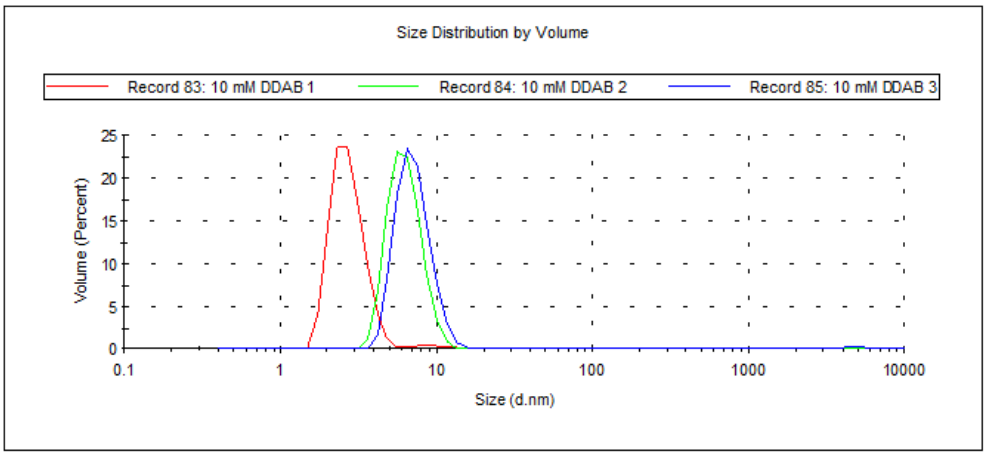

Figure 4.6: DLS generated size distributions for 10 mM DDAB vesicular solution. Color coded curves represent three repetitive runs with z average diameter being 77 (red), 77 (green), and 95 (blue) nm.

is 83 nm, close to the value of 50 nm measured by electron microscopy.[189]

Because DDAB is monovalent and cationic, the same as that of CTAB, the pH of the vesicular solution needs to be adjusted so that the reaction between 16-ArN_2^+ and AOs can be followed at a reasonable rate as discussed in Chapter 2 (Section 2.2.2). Menger et al. reported that injection of 100 μL of 0.1 M NaBr into 200 μL of 1 mM DDAB vesicles causes the DDAB to precipitate into a solid mass.[190] We observed a dramatic increase in solution turbidity when 2.5 μL of 1 M HBr was added into 1 mL of 10 mM DDAB vesicular solution. However, addition of HCl of the same concentration as HBr to 10 mM DDAB vesicular solution produced only a slight increase in solution turbidity (final pH = 2.65). Fontana et al. observed that addition of NaCl with concentratons ranging between 5 and 15 mM to a 2.5 mM DDAB vesicular solution, the turbidity of the system increases, which they attributed to a reduction in the electrostatic repulsion between the headgroups of DDAB by chloride ion, facilicating the growth of DDAB vesicles.[191] An increase in size of DDAB vesicles on addition of HCl was seen by us, Figure 4.7. Therefore, HCl is the suitable acid

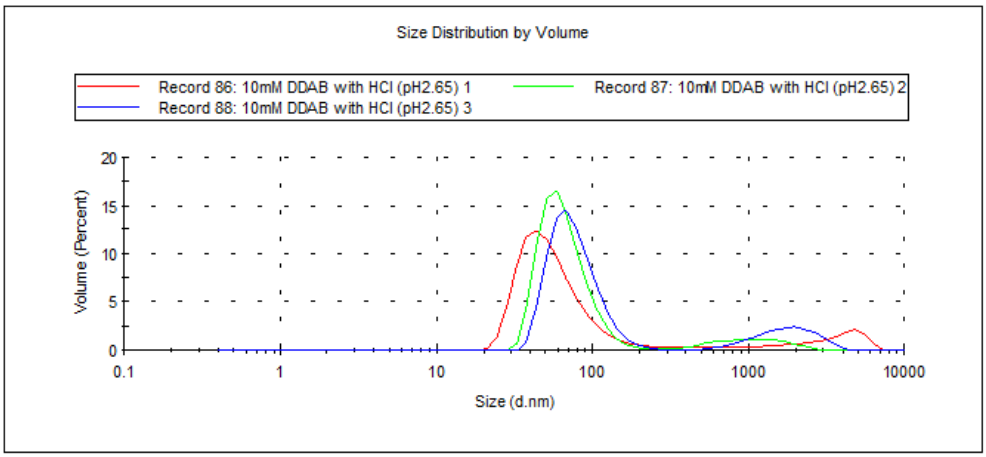

Figure 4.7: Size distributions for 10 mM DDAB vesicular solution in the presence of HCl (pH = 2.65). Color coded curves represent three repetitive runs with z average diameter being 117 (red), 115 (green), and 117 (blue) nm.

for the system to control the pH and follow the reactions by UV-Vis spectrophotometry.

4.4.2 Kinetics for the reaction of 16-ArN$_2^+$ with a homologous series of gallate esters in DDAB vesicular solution

The reaction between 16-ArN$_2^+$ and a homologous series of gallate esters including methyl gallate (MG), propyl gallate (PG), octyl gallate (OG), dodecyl gallate (DG), hexadecyl gallate (HG), and stearyl gallate (SG) in 10 mM DDAB vesicular solution in the presence of HCl (pH 2.65) at 27 °C was monitored by UV-Vis spectroscopy. The concentration of the AOs is 5 times that of 16-ArN$_2^+$ so that the reaction follows first-order kinetics. The UV spectra of 16-ArN$_2^+$ and all the gallate esters overlapped between 320 nm to 220 nm showing a λ_{max} around 275 nm, Figure 4.8. The absorbance change was followed at 283 nm instead of 275 nm because the scattering of light due to the solution turbidity caused slight fluctuation in UV absorbance, that was the greatest at λ_{max}. The decrease of absorbance at 283 nm with time indicates the depletion of 16-ArN$_2^+$ as the reaction proceeds because the AO concentration almost stays constant throughout the time course of the reaction. Kinetics experiments were carried out for all the AOs in two batches of DDAB vesicular solutions (experiment for HG was repeated in the same batch of DDAB solution because

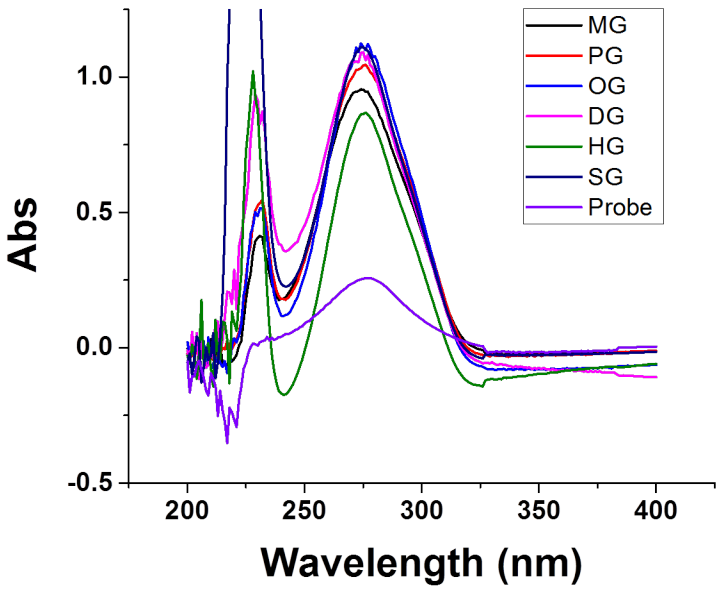

Figure 4.8: UV spectra of all the gallate esters (1.22×10^{-4} M) and the probe (2.4×10^{-5} M) in 10 mM DDAB vesicular solution with added HCl (pH 2.65).

the reagent was purchased after the first set of experiments was finished). Kinetic plots for the first set of kinetics experiments are shown in Figure 4.9 (See Figure in Appendix for the second set of kinetic plots). The correlation coefficients of the linear fitting for two AOs with the most (DG) and least (SG) absorbance fluctuation are 0.993 and 0.999, respectively. DLS measurements were performed on the vesicular solution at the end of each reaction and the results show no significant change in size distribution indicating the vesicles are stable throughout the time course of the reaction (See Figure 4.11 in Appendix).

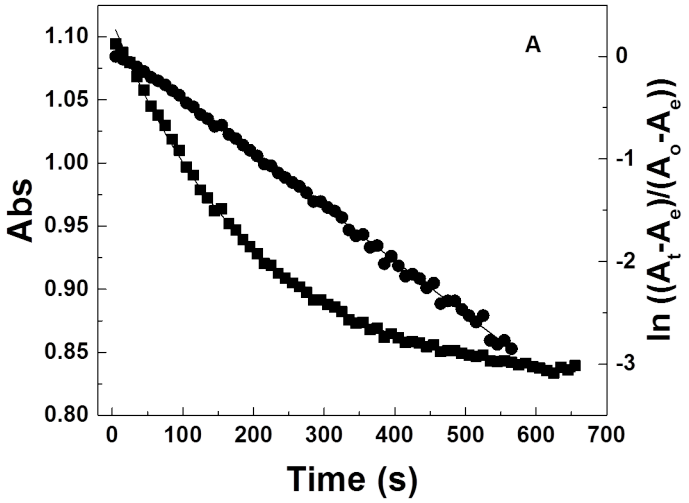
A
Abs
Time (s)
ln ((A_t-A_e)/(A_o-A_e))
1.10
1.05
1.00
0.95
0.90
0.85
0.80
0
100
200
300
400
500
600
700
0
-1
-2
-3

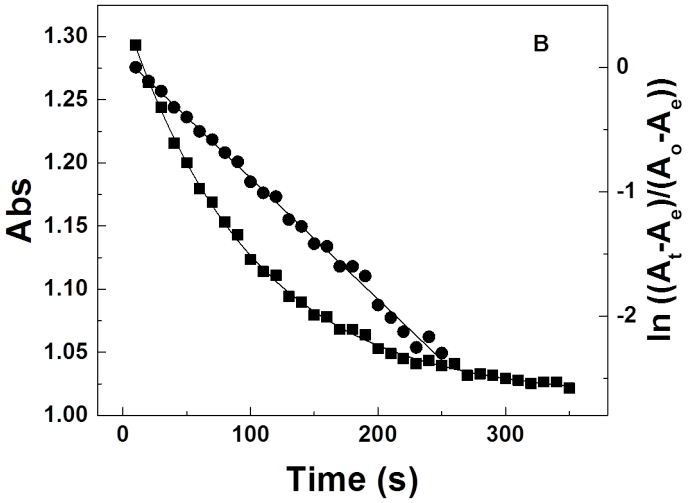
B
Abs
Time (s)
ln ((A_t-A_e)/(A_o-A_e))
1.30
1.25
1.20
1.15
1.10
1.05
1.00
0
100
200
300
0
-1
-2

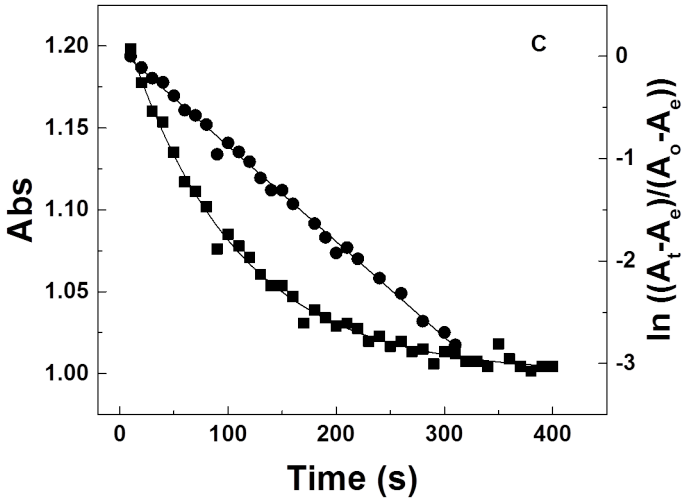
C
Abs
Time (s)
ln ((A_t-A_e)/(A_o-A_e))
1.20
1.15
1.10
1.05
1.00
0
100
200
300
400
0
-1
-2
-3

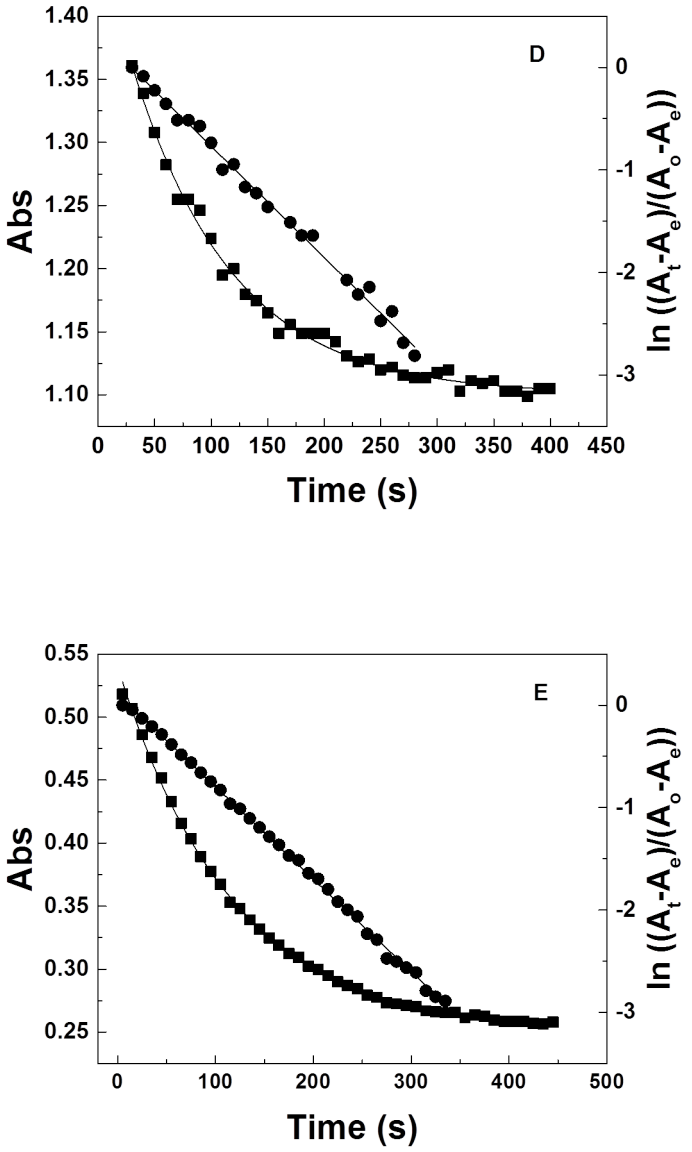

Figure 4.9: Absorbance at 283 nm versus time plot (■) and $\ln((A_t - A_e)/(A_o - A_e))$ versus time plot (●) for the reaction of 16-ArN_2^+ with MG (A), PG (B), OG (C), DG (D), and SG (E) in the first batch of 10 mM DDAB vesicular solution in the presence of HCl (pH 2.65). [16-ArN_2^+] = 2.4×10^{-5} M, [AO] = 1.22×10^{-4} M, T = 27 °C. In all runs, R^2 is at least 0.993 for 4-5 half-lives.

The observed first-order rate constant, k_{obs}, as a function of the alkyl chain length of gallate esters is shown in Figure 4.10. Although the values of the two sets of data obtained in two different batches of DDAB vesicular solutions differ by 20-30% (reason for the variation is unclear, note that data is reproducible in the same batch of vesicular solution), they

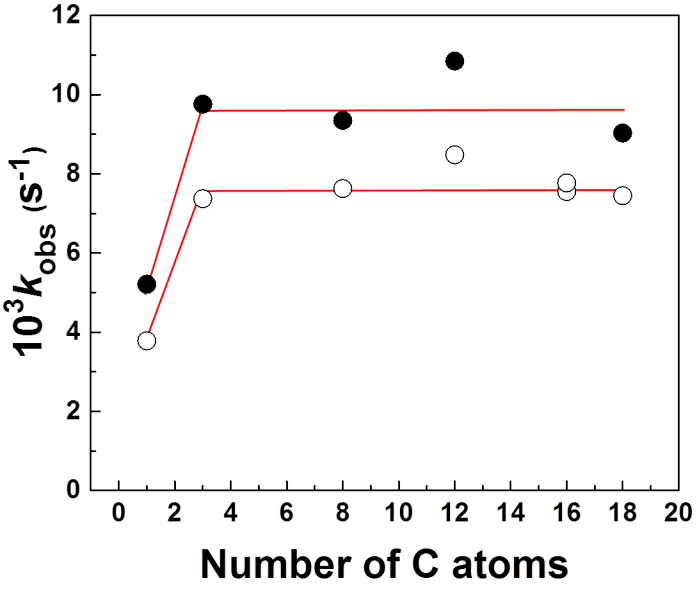

Figure 4.10: The observed first-order rate constant, k_{obs}, for the reaction between 16-ArN_2^+ and a homologous series of gallate esters in DDAB vesicular solution as a function of the number of C atoms in the alkyl chain of gallate esters. Solid and open circles represent two sets of data obtained in two different batches of DDAB solutions (measurement of k_{obs} for HG was repeated in the same batch of DDAB solution). Lines are drawn to aid the eye.

show the same trend: k_{obs} increases from MG to PG almost by a factor of 2 then levels off from PG to SG with slight fluctuations. This result is different from the "cutoff effect" in oil-in-water emulsions summarized that AO activity shows a maximum at intermediate chain lengths followed by a decrease in their activity. In oil-in-water emulsions, as the AO hydrophobicity increases, a substantial fraction of the long-chain AOs partition into the oil region, evidenced by the partition constant between the interfacial and oil region, P_{O}^{I} ((AO_I)/(AO_O) ratio), measured by the chemical kinetic method: $P_{\text{O}}^{\text{I}} = 242$, 29.8, 19.4 for PG, OG, and LG in corn oil emulsions, respectively.[184] Because lipid oxidation primarily occurs in the proximity of the emulsion droplet interface, a decrease in the fraction of AO in the interfacial region lowers the AO efficiency. In vesicles, the long-chain AOs can only orient at the interface due to the very small hydrocarbon region of vesicles and this assumption was supported by the α-tocopherol location at the lipid-water interface of phospholipid bilayers determined by using small-angle neutron diffraction[187], thus, the concentration

of all the gallate esters in the interfacial region should be the same except MG having a substantial solubility in the aqueous phase (1.06 g/100 g water at 25 °C [192]). Because the reaction between 16-ArN_2^+ and AOs takes place only in the interfacial region, and $k_{obs} = k_I(AO_I)$ in which k_I reflects the polarity of the interfacial region and is independent of the AO distributions, k_{obs} plateaus once all the gallate esters are bound with vesicles as shown in Figure 4.10.

4.5 Conclusions

The observed first-order rate constant, k_{obs}, for the reaction of a chemical probe, 16-ArN_2^+, with a homologous series of gallate esters in 10 mM DDAB vesicular solution with added HCl (pH 2.65) were measured by UV-Vis spectroscopy. Two sets of k_{obs} versus the number of C atoms in the alkyl chain of gallate esters data were obtained in two different batches of DDAB solutions. Although the two sets of values for k_{obs} differ by 20-30% (probably caused by the different batches of DDAB solutions), they show the same trends that k_{obs} initially increases from C1 to C3 then levels off from C3 to C18 with slight fluctuations. This result is consistent with the pseudophase model assumption that the rate at which 16-ArN_2^+ reacts with the AO in aggregated systems depends on the AO concentration in moles per liter of interfacial volume. Because the volume of the hydrocarbon region of vesicles are very small, and because the ratio of the interfacial volume to the hydrocarbon volume is constant, long-chain gallate esters cannot partition into the hydrocarbon region but only orient at the interface. Therefore, the AO concentration in the interfacial region is equal for all the gallate esters that are fully associated with the vesicles at constant stoichiometric AO concentration. As a result, k_{obs} is smaller for hydrophilic methyl gallate and increases and remains almost constant for hydrophobic propyl, octyl, dodecyl, hexadecyl, and stearyl gallates. Our result differs from the "cutoff effect" that AO's efficiency reaches a maximum at an intermediate alkyl chain length and decreases at longer chain length and it should aid in establishing a clearer understanding between the AO efficiency and its distributions

within aggregated systems.

4.6 Future work

The discrepancy in Figure 4.10 is not fully understood. We suspected that it was caused by the two different batches of DDAB solution. Kinetics experiments for all the gallate esters will be carried out and repeated in the same batch of DDAB vesicular solution to test our thought. To further demonstrate our assumption that k_{obs} plateaus once the AOs are completely bound with the vesicles, gallate esters with 20 carbon atoms in the alkyl chain will be used for kinetics experiments.

We also propose to investigate the relationship between k_{obs} and AO chain length in micelles. Micellar solutions usually contain two components: water and surfactant, like vesicular solutions. Micellar and vesicular solutions are similar except that the surfactant is generally twin-tailed and forms closed bilayers that contain a water pool in vesicular solutions. Both the inside and outside interfacial regions of vesicles are like micellar surfaces. The core regions of both vesicles and micelles are composed of the hydrocarbon tails of surfactant, which take up approximately 50% each of the total aggregate volume, and they both have a constant relative volume of the interfacial region versus the volume of the hydrocarbon region that is proportional to the volume ratio of surfactant head group to hydrocarbon tail. In kinetics and partitioning experiments, the totality of both vesicles and micelles is treated as a single "phase" in which reactants are either bound or free.[97] Therefore, we expect that similar results for the reaction of 16-ArN_2^+ with a homologous series of gallate esters would be observed in micellar solutions as in vesicular solutions.

4.7 Experimental

4.7.1 Materials

Methyl gallate (>98%), propyl gallate (>98%), octyl gallate (>98%), dodecyl gallate (>98%), hexadecyl gallate (>95%), and stearyl gallate (>97%) were purchased from TCI America and used as received. HPLC-grade methanol and acetonitrile and inorganic reagents were purchased from Sigma Aldrich. Didodecyldimethylammonium bromide (>98%, Alfa Aesar) was recrystallized from acetone:ethyl ether (50:50 v/v) mixture. 4-*n*-Hexadecylbenzenediazonium tetrafluoroborate (16-ArN_2BF_4) was prepared earlier in our lab. All water used in preparation of solutions was distilled, passed over activated carbon and deionizing resin, and redistilled.

4.7.2 Vesicle preparation and size measurement

Transparent DDAB vesicular solution (10 mM) was obtained by sonication (FS20H Fisher Scientific, water-bath type) for 2 h at 50 °C. 2.5 μL of 1 M HCl was added into 1 mL solution to give a final pH of 2.65 and the solution turbidity increased slightly. Dynamic light scattering (DLS) analysis was carried out on a Zetasizer nanoseries ZS90 (Malvern instruments) in triplicate. The results include volume-based distributions and the intensity-weighted mean diameter (often called the "z average"). Measurements were performed on vesicular solutions in the absence and presence of HCl and after the reactions of 16-ArN_2^+ with gallate esters with various chain lengths for stability evaluation purpose. All the solutions were filtered through 0.22 μm syringe filters before measurement.

4.7.3 Determining k_{obs} by UV-Vis

An aliquot of freshly prepared 10 mM stock solution of DDAB with added HCl (pH 2.65) was transferred from the volumetric flask to the cuvette. The same amount of the solution

was transferred to another cuvette and used as control solution to cancel out the background absorbance caused by scattering of light by the solution turbidity from the vesicles. Both cuvettes were placed in thermostated UV-Vis spectrometer compartments after the temperature was constant at 27 °C. The UV spectra of all the gallate esters (MG, PG, OG, DG, HG, and SG) and the probe, 16-ArN_2BF_4, in vesicular solution were recorded between 400 to 200 nm. They overlapped between 320 to 200 nm and both showed a λ_{max} around 275 nm. Fluctuation in absorbance at λ_{max} was observed for most of the gallate esters.

Aliquots of freshly prepared stock solutions of 0.081 M gallate ester in methanol and 0.024 M 16-ArN_2BF_4 in acetonitrile were added sequentially to the reaction cuvette via syringe to initiate the reaction. The final concentrations of gallate ester and 16-ArN_2BF_4 were 1.22×10^{-4} and 2.4×10^{-5} M respectively. Loss of 16-ArN_2BF_4 was followed by the decrease in absorbance at 283 nm, slightly off the λ_{max} to mitigate the absorbance fluctuation. Absorbance versus time plots were obtained and the values of the observed first-order rate constant, k_{obs}, for the reaction between 16-ArN_2BF_4 and a homologous series of gallate esters were calculated from the slopes of $\ln((A_t - A_e)/(A_0 - A_e))$ versus time plots.

4.8 Appendix

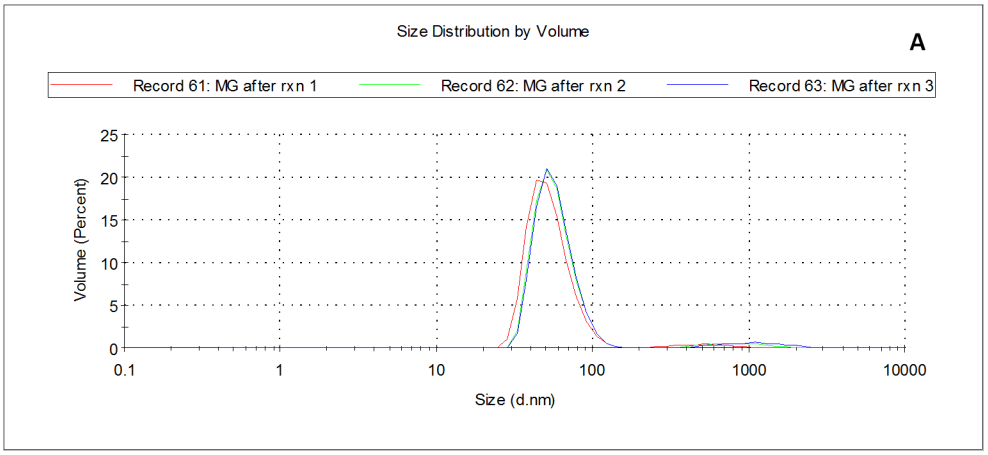

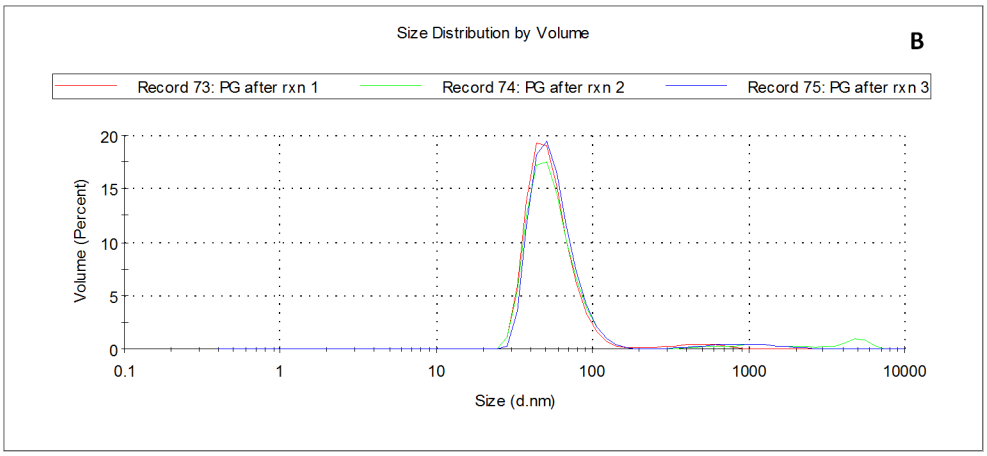
Size Distribution by Volume
B
Record 73: PG after rxn 1
Record 74: PG after rxn 2
Record 75: PG after rxn 3
Volume (Percent)
0
5
10
15
20
0.1
1
10
100
1000
10000
Size (d.nm)

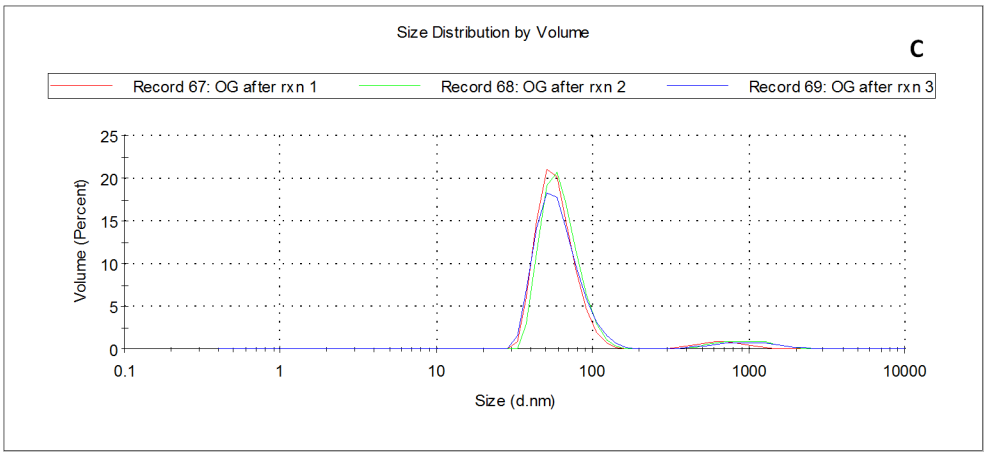
Size Distribution by Volume
C
Record 67: OG after rxn 1
Record 68: OG after rxn 2
Record 69: OG after rxn 3
Volume (Percent)
0
5
10
15
20
25
0.1
1
10
100
1000
10000
Size (d.nm)

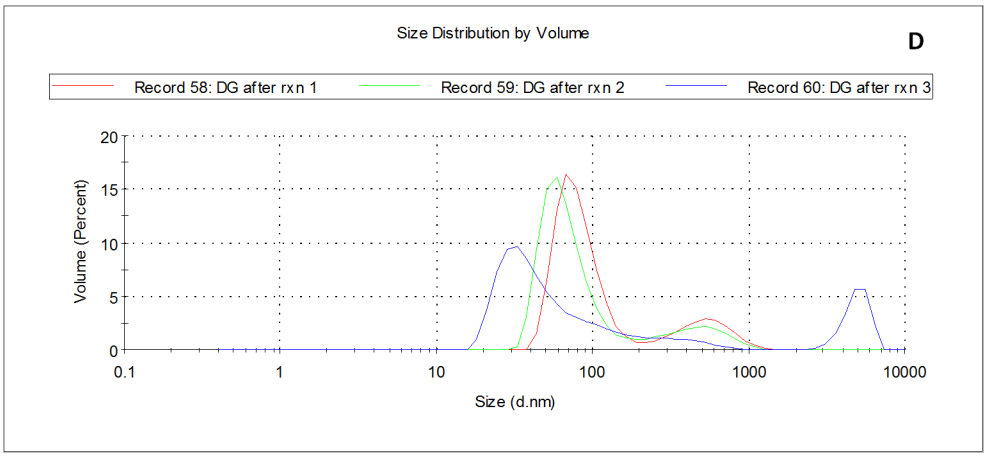
Size Distribution by Volume
D
Record 58: DG after rxn 1
Record 59: DG after rxn 2
Record 60: DG after rxn 3
Volume (Percent)
0
5
10
15
20
0.1
1
10
100
1000
10000
Size (d.nm)

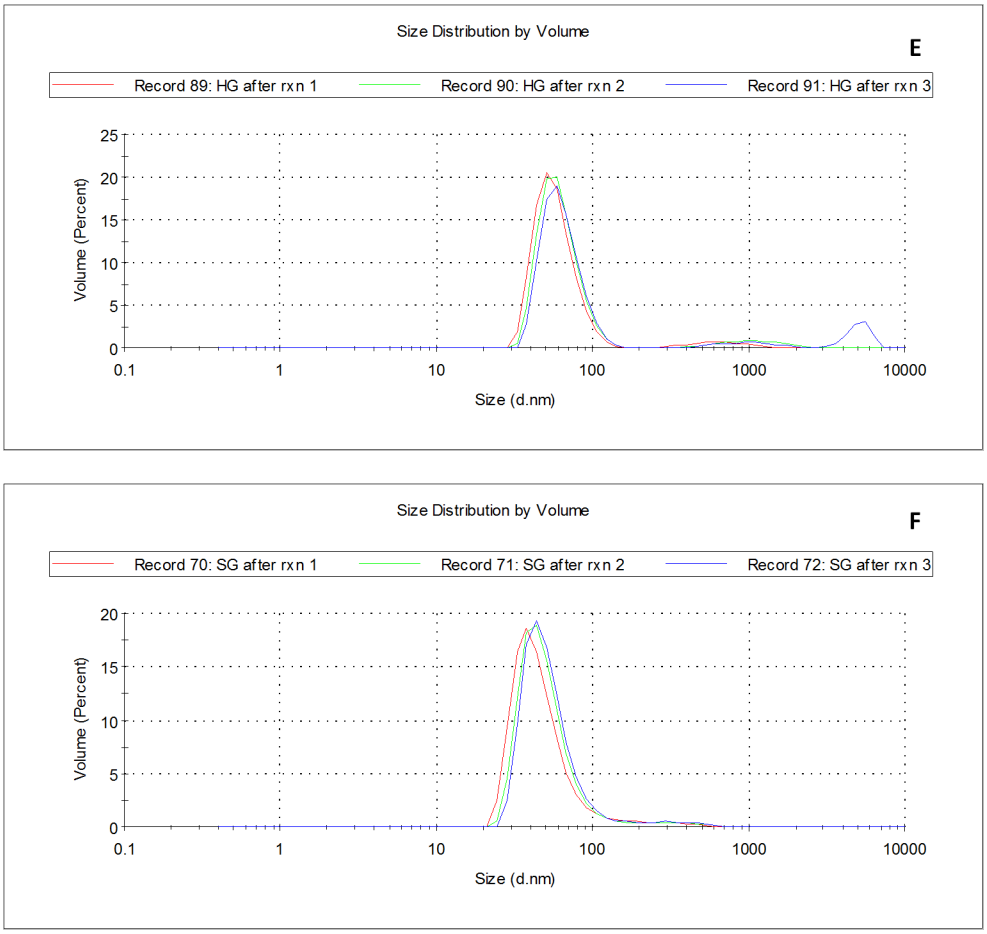

Figure 4.11: Size distributions obtained by DLS for 10 mM DDAB vesicular solutions with added HCl (pH 2.65) after the reactions of 16-ArN_2^+ with MG (A), PG (B), OG (C), DG (D), HG (E), and SG (F).

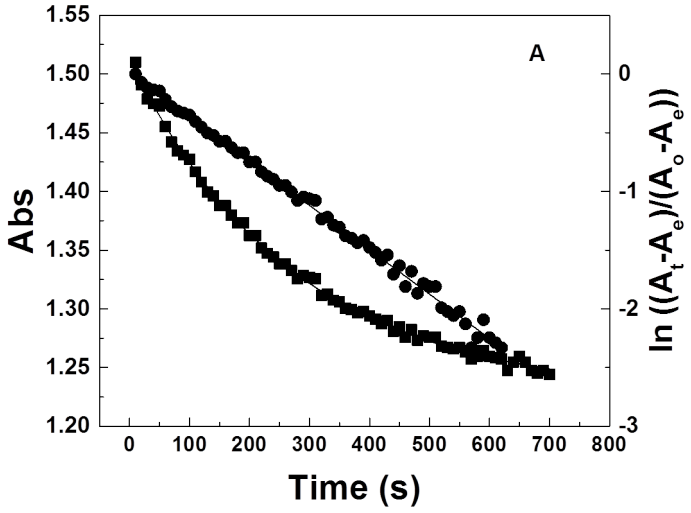

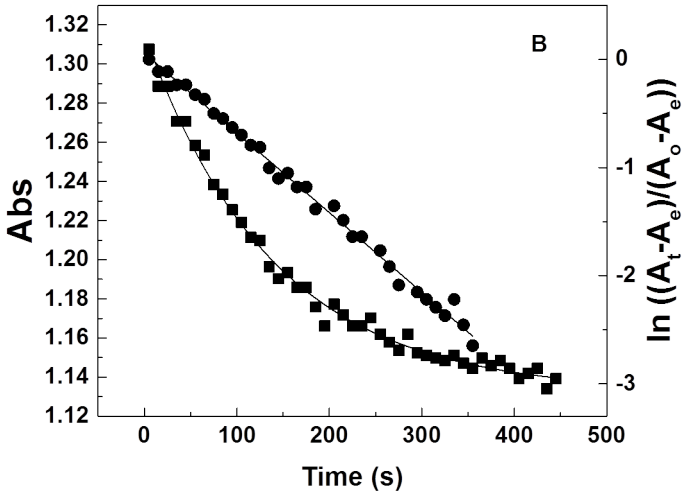
B
Abs
Time (s)
ln ((A_t-A_e)/(A_o-A_e))
1.32
1.30
1.28
1.26
1.24
1.22
1.20
1.18
1.16
1.14
1.12
0
100
200
300
400
500
0
-1
-2
-3

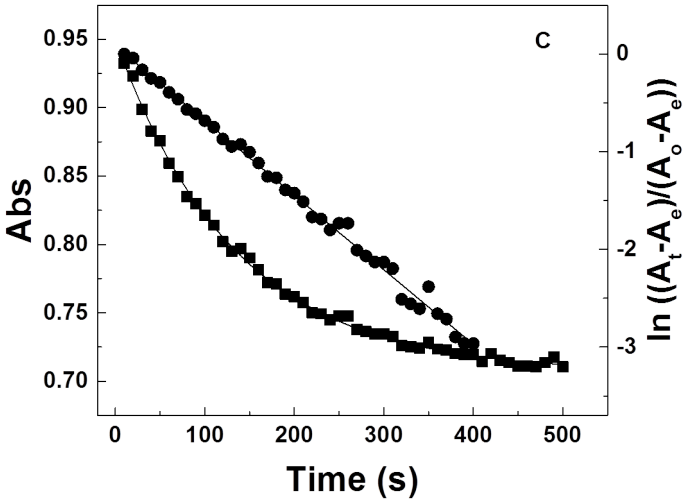
C
Abs
Time (s)
ln ((A_t-A_e)/(A_o-A_e))
0.95
0.90
0.85
0.80
0.75
0.70
0
100
200
300
400
500
0
-1
-2
-3

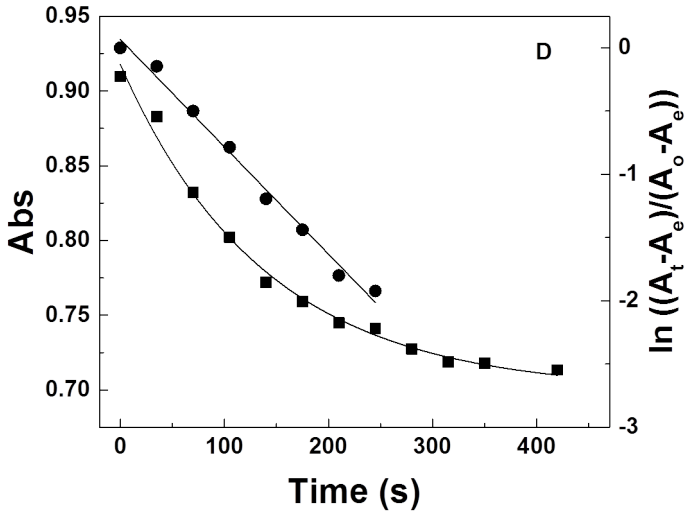
D
Abs
Time (s)
ln ((A_t-A_e)/(A_o-A_e))
0.95
0.90
0.85
0.80
0.75
0.70
0
100
200
300
400
0
-1
-2
-3

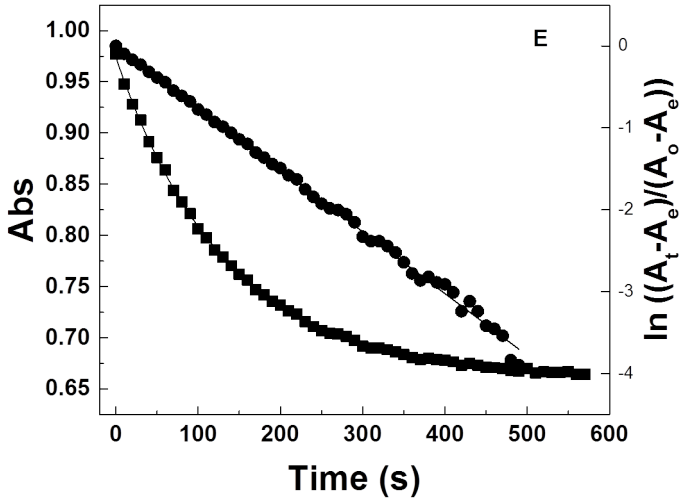
E
Abs
Time (s)
ln ((A_t-A_e)/(A_o-A_e))
1.00
0.95
0.90
0.85
0.80
0.75
0.70
0.65
0
100
200
300
400
500
600
0
-1
-2
-3
-4

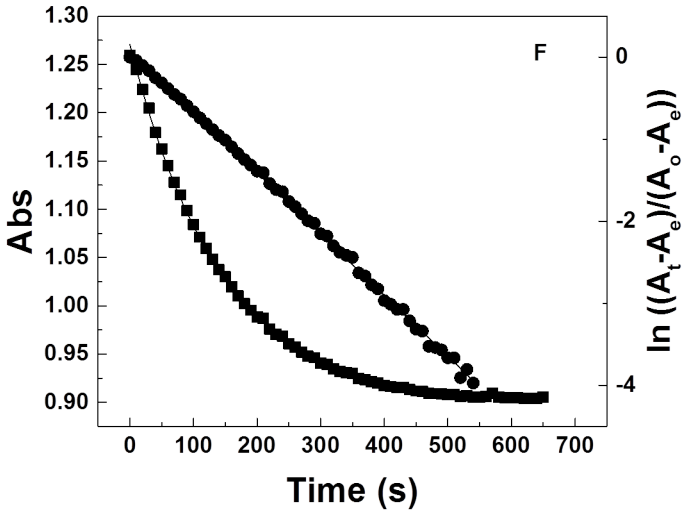

Figure 4.12: Absorbance at 283 nm versus time plot (■) and $\ln((A_t - A_e)/(A_o - A_e))$ versus time plot (●) for the reaction of 16-ArN_2^+ with MG (A), PG (B), OG (C), DG (D), HG (E), and SG (F) in the second batch of 10 mM DDAB vesicular solution in the presence of HCl (pH 2.65). [16-ArN_2^+] = 2.4×10^{-5} M, [AO] = 1.22×10^{-4} M, T = 27 °C. In all runs, R^2 is at least 0.99 for 3-5 half-lives.

Table 4.1: Two data sets of k_{obs} as a function of number of C atoms in the alkyl chain of gallate esters at 27 °C.

	First set	Second set
Number of C atoms	$10^3 k_{obs}$ (s^{-1})	$10^3 k_{obs}$ (s^{-1})
1	5.21	3.78
3	9.76	7.37
8	9.35	7.63
12	10.85	8.48
16		7.55
		7.77
18	9.03	7.45

References

[1] K. Holmberg, B. Jönsson, B. Kronberg, and B. Lindman, *Surfactants and polymers in aqueous solution.* John Wiley & Sons, 2002.

[2] J. Zhang, *Estimating interfacial Urea and Antioxidant Concentrations.* PhD thesis, Rutgers University, 2003.

[3] L. S. Romsted, *Surfactant Science and Technology: Retrospects and Prospects.* CRC Press, 2013.

[4] L. S. Romsted, "Do amphiphile aggregate morphologies and interfacial compositions depend primarily on interfacial hydration and ion-specific interactions? the evidence from chemical trapping," *Langmuir*, vol. 23, no. 2, pp. 414–424, 2007.

[5] S. Tascioglu, "Micellar solutions as reaction media," *Tetrahedron*, vol. 52, no. 34, pp. 11113–11152, 1996.

[6] T. Imae, R. Kamiya, and S. Ikeda, "Formation of spherical and rod-like micelles of cetyltrimethylammonium bromide in aqueous nabr solutions," *Journal of colloid and interface science*, vol. 108, no. 1, pp. 215–225, 1985.

[7] T. Imae and S. Ikeda, "Sphere-rod transition of micelles of tetradecyltrimethylammonium halides in aqueous sodium halide solutions and flexibility and entanglement of long rodlike micelles," *The Journal of Physical Chemistry*, vol. 90, no. 21, pp. 5216–5223, 1986.

[8] T. Imae and S. Ikeda, "Characteristics of rodlike micelles of cetyltrimethylammonium chloride in aqueous nacl solutions: Their flexibility and the scaling laws in dilute and semidilute regimes," *Colloid and Polymer Science*, vol. 265, no. 12, pp. 1090–1098, 1987.

[9] V. Soldi, J. Keiper, L. S. Romsted, I. M. Cuccovia, and H. Chaimovich, "Arenediazonium salts: New probes of the interfacial compositions of association colloids. 6. relationships between interfacial counterion and water concentrations and surfactant headgroup size, sphere-to-rod transitions, and chemical reactivity in cationic micelles," *Langmuir*, vol. 16, no. 1, pp. 59–71, 2000.

[10] J. H. Fendler, "Reactivity control in membrane mimetic systems," *Pure and Applied Chemistry*, vol. 54, no. 10, pp. 1809–1817, 1982.

[11] E. W. Kaler, A. K. Murthy, B. E. Rodriguez, and J. Zasadzinski, "Spontaneous vesicle formation in aqueous mixtures of single-tailed surfactants," *Science*, vol. 245, no. 4924, pp. 1371–1374, 1989.

[12] L. L. Brasher and E. W. Kaler, "A small-angle neutron scattering (sans) contrast variation investigation of aggregate composition in catanionic surfactant mixtures," *Langmuir*, vol. 12, no. 26, pp. 6270–6276, 1996.

[13] M. T. Yatcilla, K. L. Herrington, L. L. Brasher, E. W. Kaler, S. Chiruvolu, and J. A. Zasadzinski, "Phase behavior of aqueous mixtures of cetyltrimethylammonium bromide (ctab) and sodium octyl sulfate (sos)," *The Journal of Physical Chemistry*, vol. 100, no. 14, pp. 5874–5879, 1996.

[14] Y. Xia, I. Goldmints, P. W. Johnson, T. A. Hatton, and A. Bose, "Temporal evolution

of microstructures in aqueous ctab/sos and ctab/hdbs solutions," *Langmuir*, vol. 18, no. 10, pp. 3822–3828, 2002.

[15] U. Olsson, K. Nakamura, H. Kunieda, and R. Strey, "Normal and reverse vesicles with nonionic surfactant: solvent diffusion and permeability," *Langmuir*, vol. 12, no. 12, pp. 3045–3054, 1996.

[16] M. Zackrisson Oskolkova, E. Norrman, and U. Olsson, "Study of the micelle-to-vesicle transition and smallest possible vesicle size by temperature-jumps," *Journal of colloid and interface science*, vol. 396, pp. 173–177, 2013.

[17] R. Zana, *Dynamics of surfactant self-assemblies: micelles, microemulsions, vesicles and lyotropic phases*. CRC press, 2005.

[18] E. Aniansson and S. N. Wall, "Kinetics of step-wise micelle association," *The Journal of Physical Chemistry*, vol. 78, no. 10, pp. 1024–1030, 1974.

[19] I. V. Berezin, K. Martinek, and A. Yatsimirskii, "Physicochemical foundations of micellar catalysis," *Russian Chemical Reviews*, vol. 42, no. 10, p. 787, 1973.

[20] C. A. Bunton, F. Nome, F. H. Quina, and L. S. Romsted, "Ion binding and reactivity at charged aqueous interfaces," *Accounts of chemical research*, vol. 24, no. 12, pp. 357–364, 1991.

[21] J. Fendler, *Catalysis in micellar and macromoleular systems*. Elsevier, 2012.

[22] V. K. Balakrishnan, X. Han, G. W. VanLoon, J. M. Dust, J. Toullec, and E. Buncel, "Acceleration of nucleophilic attack on an organophosphorothioate neurotoxin, fenitrothion, by reactive counterion cationic micelles. regioselectivity as a probe of

substrate orientation within the micelle," *Langmuir*, vol. 20, no. 16, pp. 6586–6593, 2004.

[23] J. Sjöblom, R. Lindberg, and S. E. Friberg, "Microemulsionsphase equilibria characterization, structures, applications and chemical reactions," *Advances in colloid and interface science*, vol. 65, pp. 125–287, 1996.

[24] M.-J. Schwuger, K. Stickdorn, and R. Schomaecker, "Microemulsions in technical processes," *Chemical reviews*, vol. 95, no. 4, pp. 849–864, 1995.

[25] L. García-Río, J. Leis, and J. Mejuto, "Pseudophase approach to reactivity in microemulsions: quantitative explanation of the kinetics of the nitrosation of amines by alkyl nitrites in aot/isooctane/water microemulsions," *The Journal of Physical Chemistry*, vol. 100, no. 26, pp. 10981–10988, 1996.

[26] K. Holmberg, "Organic reactions in microemulsions," *Current opinion in colloid & interface science*, vol. 8, no. 2, pp. 187–196, 2003.

[27] H. Chaimovich and I. Cuccovia, "Quantitative analysis of reagent distribution and reaction rates in vesicles," in *Amphiphiles at Interfaces*, pp. 67–77, Springer, 1997.

[28] P. L. Luisi, P. Walde, and T. Oberholzer, "Lipid vesicles as possible intermediates in the origin of life," *Current opinion in colloid & interface science*, vol. 4, no. 1, pp. 33–39, 1999.

[29] P. Walde, H. Umakoshi, P. Stano, and F. Mavelli, "Emergent properties arising from the assembly of amphiphiles. artificial vesicle membranes as reaction promoters and regulators," *Chemical Communications*, vol. 50, no. 71, pp. 10177–10197, 2014.

[30] L. M. Goncalves, T. G. Kobayakawa, D. Zanette, H. Chaimovich, and I. M. Cuccovia, "Effects of micelles and vesicles on the oximolysis of p-nitrophenyl diphenyl phosphate: A model system for surfactant-based skin-defensive formulations against organophosphates," *Journal of pharmaceutical sciences*, vol. 98, no. 3, pp. 1040–1052, 2009.

[31] D. M. Davies, N. D. Gillitt, and P. M. Paradis, "Catalysis and inhibition of the iodide reduction of peracids by surfactants: partitioning of reactants, product and transition state between aqueous and micellar pseudophases," *Journal of the Chemical Society, Perkin Transactions 2*, no. 4, pp. 659–666, 1996.

[32] D. Zanette, Â. A. Ruzza, S. J. Froehner, and E. Minatti, "Polymer-surfactant interactions demonstrated by a kinetic probe: degree of ionization," *Colloids and Surfaces A: Physicochemical and Engineering Aspects*, vol. 108, no. 1, pp. 91–100, 1996.

[33] V. R. Correia, I. M. Cuccovia, M. Stelmo, and H. Chaimovich, "Electrostatic micellar effects on the rate of spontaneous decomposition of m-nitrophenyl 9-fluorenecarboxylate," *Journal of the American Chemical Society*, vol. 114, no. 6, pp. 2144–2146, 1992.

[34] C. A. Bunton, "The dependence of micellar rate effects upon reaction mechanism," *Advances in colloid and interface science*, vol. 123, pp. 333–343, 2006.

[35] F. Menger and M. Ladika, "Origin of rate accelerations in an enzyme model: The p-nitrophenyl ester syndrome," *Journal of the American Chemical Society*, vol. 109, no. 10, pp. 3145–3146, 1987.

[36] C. A. Bunton and J. R. Moffatt, "Micellar reactions of hydrophilic ions: a coulombic

model," *The Journal of Physical Chemistry*, vol. 89, no. 20, pp. 4166–4169, 1985.

[37] L. S. Romsted, *Rate enhancements in micellar systems.* PhD thesis, Indiana University, 1975.

[38] L. S. Romsted, C. A. Bunton, and J. Yao, "Micellar catalysis, a useful misnomer," *Current opinion in colloid & interface science*, vol. 2, no. 6, pp. 622–628, 1997.

[39] C. A. Bunton, "Reactivity in aqueous association colloids. descriptive utility of the pseudophase model," *Journal of molecular liquids*, vol. 72, no. 1, pp. 231–249, 1997.

[40] C. A. Bunton, E. J. Fendler, G. Sepulveda, and K.-U. Yang, "Micellar-catalyzed hydrolysis of nitrophenyl phosphates," *Journal of the American Chemical Society*, vol. 90, no. 20, pp. 5512–5518, 1968.

[41] H. Al-Lohedan, C. A. Bunton, and M. M. Mhala, "Micellar effects upon spontaneous hydrolyses and their relation to mechanism," *Journal of the American Chemical Society*, vol. 104, no. 24, pp. 6654–6660, 1982.

[42] L. S. Romsted, "A general kinetic theory of rate enhancements for reactions between organic substrates and hydrophilic ions in micellar systems," in *Micellization, solubilization, and microemulsions*, pp. 509–530, Springer, 1977.

[43] C. A. Bunton, L. S. Romsted, and C. Thamavit, "The pseudophase model of micellar catalysis. addition of cyanide ion to n-alkylpyridinium ions," *Journal of the American Chemical Society*, vol. 102, no. 11, pp. 3900–3903, 1980.

[44] L. S. Romsted, "Quantitative treatment of benzimidazole deprotonation equilibria in aqueous micellar solutions of cetyltrimethylammonium ion (ctax, x-= cl-, br-,

and no3-) surfactants. 1. variable surfactant concentration," *The Journal of Physical Chemistry*, vol. 89, no. 23, pp. 5107–5113, 1985.

[45] L. S. Romsted, "Quantitative treatment of benzimidazole deprotonation equilibria in aqueous micellar solutions of cetyltrimethylammonium ion (ctax, x-= cl-, br-, and no3-) surfactants. 2. effect of added salt," *The Journal of Physical Chemistry*, vol. 89, no. 23, pp. 5113–5118, 1985.

[46] J. H. Fendler and W. L. Hinze, "Reactivity control in micelles and surfactant vesicles. kinetics and mechanism of base-catalyzed hydrolysis of 5, 5'-dithiobis (2-nitrobenzoic acid) in water, hexadecyltrimethylammonium bromide micelles, and dioctadecyldimethylammonium chloride surfactant vesicles," *Journal of the American Chemical Society*, vol. 103, no. 18, pp. 5439–5447, 1981.

[47] F. H. Quina and H. Chaimovich, "Ion exchange in micellar solutions. 1. conceptual framework for ion exchange in micellar solutions," *Journal of Physical Chemistry*, vol. 83, no. 14, pp. 1844–1850, 1979.

[48] H. Chaimovich, J. B. Bonilha, M. J. Politi, and F. H. Quina, "Ion exchange in micellar solutions. 2. binding of hydroxide ion to positive micelles," *Journal of Physical Chemistry*, vol. 83, no. 14, pp. 1851–1854, 1979.

[49] V. I. Martín, M. del Mar Graciani, A. Rodríguez, and M. L. Moyá, "Kinetic studies in micellar solutions of novel bromide mono-and dimeric surfactants with phenyl and cyclohexyl rings in the head group," *Colloids and Surfaces A: Physicochemical and Engineering Aspects*, vol. 409, pp. 52–60, 2012.

[50] I. M. Cuccovia, F. H. Quina, and H. Chaimovich, "A remarkable enhancement of the

rate of ester thiolysis by synthetic amphiphile vesicles," *Tetrahedron*, vol. 38, no. 7, pp. 917–920, 1982.

[51] O. A. El Seoud and A. M. Chinelatto, "Acid-base indicator equilibria in aerosol-ot reversed micelles in heptane. the use of buffers," *Journal of colloid and interface science*, vol. 95, no. 1, pp. 163–171, 1983.

[52] R. d. R. Pereira, D. Zanette, and F. Nome, "Application of the pseudophase ion-exchange model to kinetics in microemulsions of anionic detergents," *Journal of Physical Chemistry*, vol. 94, no. 1, pp. 356–361, 1990.

[53] R. A. Mackay, "Reactions in microemulsions. the ion-exchange model," *The Journal of Physical Chemistry*, vol. 86, no. 24, pp. 4756–4758, 1982.

[54] M. N. Khan and M. H. R. Azri, "Effects of [nabr] on the rate of intramolecular general base-assisted hydrolysis of n-(2-hydroxyphenyl) phthalimide in the presence of cationic micelles: kinetic evidence for the probable micellar structural transition," *The Journal of Physical Chemistry B*, vol. 114, no. 24, pp. 8089–8099, 2010.

[55] A. Chaudhuri, J. A. Loughlin, L. S. Romsted, and J. Yao, "Arenediazonium salts: New probes of the interfacial compositions of association colloids. 1. basic approach, methods, and illustrative applications," *Journal of the American Chemical Society*, vol. 115, no. 18, pp. 8351–8361, 1993.

[56] A. Chaudhuri, L. S. Romsted, and J. Yao, "Arenediazonium salts: new probes of the interfacial compositions of association colloids. 2. binding constants of butanol and hexanol in aqueous three-component cetyltrimethylammonium bromide microemulsions," *Journal of the American Chemical Society*, vol. 115, no. 18, pp. 8362–8367,

1993.

[57] L. S. Romsted and J. Yao, "Arenediazonium salts: New probes of the interfacial compositions of association colloids. 4. estimation of the hydration numbers of aqueous hexaethylene glycol monododecyl ether, c12e6, micelles by chemical trapping," *Langmuir*, vol. 12, no. 10, pp. 2425–2432, 1996.

[58] L. S. Romsted and J. Yao, "New probes of the interfacial compositions of association colloids. 5. determination of hydration numbers and radial distributions of terminal hydroxyl groups in mixed nonionic cmen micelles by chemical trapping," *Langmuir*, vol. 15, no. 2, pp. 326–336, 1999.

[59] J. Yao and L. S. Romsted, "Arenediazonium salts: New probes of the compositions of association colloids. 7. average hydration numbers and cl-concentrations in the surfactant film of nonionic c12e5/octane/water macroemulsions: Temperature and nacl concentration effects," *Langmuir*, vol. 16, no. 23, pp. 8771–8779, 2000.

[60] Y. Geng, L. S. Romsted, and F. Menger, "Specific ion pairing and interfacial hydration as controlling factors in gemini micelle morphology. chemical trapping studies," *Journal of the American Chemical Society*, vol. 128, no. 2, pp. 492–501, 2006.

[61] Y. Geng, L. S. Romsted, S. Froehner, D. Zanette, L. J. Magid, I. M. Cuccovia, and H. Chaimovich, "Origin of the sphere-to-rod transition in cationic micelles with aromatic counterions: specific ion hydration in the interfacial region matters," *Langmuir*, vol. 21, no. 2, pp. 562–568, 2005.

[62] L. S. Romsted, J. Zhang, and L. Zhuang, "Mechanism of reaction of an arenediazonium ion in aqueous solutions of acetamide, n-methylacetamide, and n, n-dimethylacetamide. a potential method for chemically tagging peptide bonds at aggregate interfaces," *Journal of the American Chemical Society*, vol. 120, no. 39, pp. 10046–10054, 1998.

[63] L. S. Romsted and J. Zhang, "Kinetic method for determining antioxidant distributions in model food emulsions: distribution constants of t-butylhydroquinone in mixtures of octane, water, and a nonionic emulsifier," *Journal of agricultural and food chemistry*, vol. 50, no. 11, pp. 3328–3336, 2002.

[64] L. S. Romsted and J. Zhang, "Determining antioxidant distributions in model food emulsions: development of a new kinetic method based on the pseudophase model in micelles and opaque emulsions," in *Trends in Colloid and Interface Science XVI*, pp. 182–187, Springer, 2004.

[65] K. Gunaseelan, L. S. Romsted, E. González-Romero, and C. Bravo-Díaz, "Determining partition constants of polar organic molecules between the oil/interfacial and water/interfacial regions in emulsions: a combined electrochemical and spectrometric method," *Langmuir*, vol. 20, no. 8, pp. 3047–3055, 2004.

[66] V. Sánchez-Paz, M. J. Pastoriza-Gallego, S. Losada-Barreiro, C. Bravo-Díaz, K. Gunaseelan, and L. S. Romsted, "Quantitative determination of α-tocopherol distribution in a tributyrin/brij 30/water model food emulsion," *Journal of colloid and interface science*, vol. 320, no. 1, pp. 1–8, 2008.

[67] Q. Gu, C. Bravo-Díaz, and L. S. Romsted, "Using the pseudophase kinetic model to interpret chemical reactivity in ionic emulsions: Determining antioxidant partition

constants and interfacial rate constants," *Journal of colloid and interface science*, vol. 400, pp. 41–48, 2013.

[68] X. Gao, C. Bravo-Díaz, and L. S. Romsted, "Interpreting ion-specific effects on the reduction of an arenediazonium ion by t-butylhydroquinone (tbhq) using the pseudophase kinetic model in emulsions prepared with a zwitterionic sulfobetaine surfactant," *Langmuir*, vol. 29, no. 16, pp. 4928–4933, 2013.

[69] Y. Zhang, L. S. Romsted, L. Zhuang, and S. de Jong, "Simultaneous determination of interfacial molarities of amide bonds, carboxylate groups, and water by chemical trapping in micelles of amphiphiles containing peptide bond models," *Langmuir*, vol. 29, no. 2, pp. 534–544, 2012.

[70] H. Zollinger, "Reactivity and stability of arenediazonium ions," *Accounts of Chemical Research*, vol. 6, no. 10, pp. 335–341, 1973.

[71] A. Hegarty, "Kinetics and mechanisms of reactions involving diazonium and diazo groups," *Diazonium and Diazo Groups: Volume 2 (1978)*, pp. 511–591, 1978.

[72] C. G. Swain, J. E. Sheats, and K. G. Harbison, "Evidence for phenyl cation as an intermediated in reactions of benzenediazonium salts in solution," *Journal of the American Chemical Society*, vol. 97, no. 4, pp. 783–790, 1975.

[73] I. M. Cuccovia, M. A. da Silva, H. M. Ferraz, J. R. Pliego Jr, J. M. Riveros, and H. Chaimovich, "Revisiting the reactions of nucleophiles with arenediazonium ions: dediazoniation of arenediazonium salts in aqueous and micellar solutions containing alkyl sulfates and alkanesulfonates and an ab initio analysis of the reaction pathway," *Journal of the Chemical Society, Perkin Transactions 2*, no. 9, pp. 1896–1907, 2000.

[74] J. Scaiano and N. Kim-Thuan, "Diazonium salts in photochemistry iii: Attempts to characterize aryl cations," *Journal of photochemistry*, vol. 23, no. 2, pp. 269–276, 1983.

[75] S. M. Gasper, C. Devadoss, and G. B. Schuster, "Photolysis of substituted benzenediazonium salts: spin-selective reactivity of aryl cations," *Journal of the American Chemical Society*, vol. 117, no. 19, pp. 5206–5211, 1995.

[76] E. S. Lewis and W. H. Hinds, "The bimolecular displacement of nitrogen from p-nitrobenzenediazonium ion1," *Journal of the American Chemical Society*, vol. 74, no. 2, pp. 304–308, 1952.

[77] E. S. Lewis, L. D. Hartung, and B. M. McKay, "Reaction of diazonium salts with nucleophiles. xiii. identity of the rate-and product-determining steps," *Journal of the American Chemical Society*, vol. 91, no. 2, pp. 419–425, 1969.

[78] P. Burri and H. Zollinger, "Dediazoniations of arene diazonium ions in homogeneous solution. part iii: Heterolytic arylations in 2, 2, 2-trifluoroethanol-an sn1-or an sn2-reaction?," *Helvetica Chimica Acta*, vol. 56, no. 7, pp. 2204–2216, 1973.

[79] L. S. Romsted, "Interfacial compositions of surfactant assemblies by chemical trapping with arenediazonium ions: method and applications," *Reactions and Synthesis in Surfactant Systems*, p. 265, 2001.

[80] M. C. Garcia-Meijide, C. Bravo-Diaz, and L. Romsted, "A new method for monitoring dediazoniation reactions: Simultaneous monitoring of concentration and rates

of product formation and loss of starting material for the dediazoniation of p-methylbenzenediazonium tetrafluoroborate," *International journal of chemical kinetics*, vol. 30, no. 1, pp. 31–39, 1998.

[81] R. Pazo-Llorente, M. J. Sarabia-Rodriguez, C. Bravo-Diaz, and E. Gonzalez-Romero, "Hydroxy-and chloro-dediazoniation of 2-and 3-methylbenzenediazonium tetrafluoroborate in aqueous solution," *International journal of chemical kinetics*, vol. 31, no. 1, pp. 73–82, 1999.

[82] R. ODA, L. S. Romsted, and et al., "Manuscript in preparation," 2015.

[83] L. S. Romsted, J. Zhang, I. M. Cuccovia, M. J. Politi, and H. Chaimovich, "Concentration of urea in interfacial regions of aqueous cationic, anionic, and zwitterionic micelles determined by chemical trapping," *Langmuir*, vol. 19, no. 22, pp. 9179–9190, 2003.

[84] Y. Geng and L. S. Romsted, "Ion pair formation in water. association constants of bolaform, bisquaternary ammonium, electrolytes by chemical trapping," *The Journal of Physical Chemistry B*, vol. 109, no. 49, pp. 23629–23637, 2005.

[85] I. M. Cuccovia, I. N. da Silva, H. Chaimovich, and L. S. Romsted, "New method for estimating the degree of ionization and counterion selectivity of cetyltrimethylammonium halide micelles: chemical trapping of free counterions by a water soluble arenediazonium ion," *Langmuir*, vol. 13, no. 4, pp. 647–652, 1997.

[86] P. K. Das, G. V. Srilakshmi, and A. Chaudhuri, "Experimental probing of water and counterion concentrations inside a reversed micelle water-pool: An overlooked parameter in micellar enzymology?," *Langmuir*, vol. 15, no. 4, pp. 981–987, 1999.

[87] O. G. Berg, J. Rogers, B.-Z. Yu, J. Yao, L. S. Romsted, and M. K. Jain, "Thermodynamic and kinetic basis of interfacial activation: resolution of binding and allosteric effects on pancreatic phospholipase a2 at zwitterionic interfaces," *Biochemistry*, vol. 36, no. 47, pp. 14512–14530, 1997.

[88] I. M. Cuccovia, L. S. Romsted, and H. Chaimovich, "Determination of halide concentrations at the interface of zwitterionic micelles by chemical trapping: influence of the orientation of the dipole and the nature of the cation," *Journal of colloid and interface science*, vol. 220, no. 1, pp. 96–102, 1999.

[89] G. Savelli, R. Germani, and L. Brinchi, "Reactivity control by aqueous amphiphilic self-assembling systems," in *Reactions and Synthesis in Surfactant Systems*, vol. 100, p. 175, CRC Press, 2001.

[90] K. J. Reszka and C. F. Chignell, "Epr and spin-trapping investigation of free radicals from the reaction of 4-methoxybenzenediazonium tetrafluoroborate with melanin and melanin precursors," *Journal of the American Chemical Society*, vol. 115, no. 17, pp. 7752–7760, 1993.

[91] M. P. Doyle, J. K. Guy, K. C. Brown, S. N. Mahapatro, C. M. VanZyl, and J. R. Pladziewicz, "Outer-sphere one-electron reductions of arenediazonium salts," *Journal of the American Chemical Society*, vol. 109, no. 5, pp. 1536–1540, 1987.

[92] C. Ruchardt, E. Merz, B. Freudenberg, M. J. Opgenorth, C. C. Tan, and R. Werner, "Free radical reactions of aromatic diazonium salts," *Chem. Soc. Spec. Publ.*, no. 24, pp. 51–70, 1970.

[93] K. C. Brown and M. P. Doyle, "Reduction of arenediazonium salts by hydroquinone.

kinetics and mechanism for the electron-transfer step," *The Journal of Organic Chemistry*, vol. 53, no. 14, pp. 3255–3261, 1988.

[94] J. Jirkovskỳ, A. Fojtík, and H. G. O. Becker, "Photoinduced decomposition of aryldiazonium salts," *Collection of Czechoslovak Chemical Communications*, vol. 46, no. 7, pp. 1560–1565, 1981.

[95] L. S. Romsted in *Supramolecular Chemistry from Molecules to Nanomaterials*, vol. 1, p. 181, John Wiley & Sons, 2012.

[96] C. A. Bunton and L. Romsted, "Organic reactivity in microemulsions," in *Handbook of Microemulsion Science and Technology*, pp. 457–482, Marcel Dekker: New York, 1999.

[97] C. Bravo-Diaz, L. S. Romsted, C. Liu, S. Losada-Barreiro, M. J. Pastoriza-Gallego, X. Gao, Q. Gu, G. Krisnan, V. Sánchez-Paz, Y. Zhang, *et al.*, "To model chemical reactivity in heterogeneous emulsions: Think homogeneous microemulsions," *Langmuir*, 2015.

[98] C. D Bravo-Díaz, "Diazohydroxides, diazoethers and related species," in *Patai's Chemistry of Functional Groups: The Chemistry of Hydroxylamines, Oximes, and Hydroxamic Acids*, vol. 2, p. 853, Wiley Online Library, 2011.

[99] U. Costas-Costas, C. Bravo-Diaz, and E. Gonzalez-Romero, "Sodium dodecyl sulfate micellar effects on the reaction between arenediazonium ions and ascorbic acid derivatives," *Langmuir*, vol. 19, no. 13, pp. 5197–5203, 2003.

[100] M. J. Pastoriza-Gallego, A. Fernández-Alonso, S. Losada-Barreiro, V. Sánchez-Paz, and C. Bravo-Díaz, "Kinetics and mechanism of the reaction between 4-hexadecylbenzenediazonium ions and vitamin c in emulsions: further evidence of the formation of diazo ether intermediates in the course of the reaction," *Journal of Physical Organic Chemistry*, vol. 21, no. 7-8, pp. 524–530, 2008.

[101] L. S. Romsted and C. Bravo-Díaz, "Modeling chemical reactivity in emulsions," *Current Opinion in Colloid & Interface Science*, vol. 18, no. 1, pp. 3–14, 2013.

[102] C. Bravo-Díaz and E. González-Romero, "Polarographic detection of arenediazonium ions. optimization of the method and application for investigating dediazoniation mechanisms," *Electroanalysis*, vol. 15, no. 4, pp. 303–311, 2003.

[103] F. Shahidi and Y. Zhong, "Lipid oxidation and improving the oxidative stability," *Chemical Society Reviews*, vol. 39, no. 11, pp. 4067–4079, 2010.

[104] D. McClements and E. Decker, "Lipid oxidation in oil-in-water emulsions: Impact of molecular environment on chemical reactions in heterogeneous food systems," *Journal of Food Science*, vol. 65, no. 8, pp. 1270–1282, 2000.

[105] C. Berton, M.-H. Ropers, M. Viau, and C. Genot, "Contribution of the interfacial layer to the protection of emulsified lipids against oxidation," *Journal of agricultural and food chemistry*, vol. 59, no. 9, pp. 5052–5061, 2011.

[106] A. Heins, D. B. McPhail, T. Sokolowski, H. Stöckmann, and K. Schwarz, "The location of phenolic antioxidants and radicals at interfaces determines their activity," *Lipids*, vol. 42, no. 6, pp. 573–582, 2007.

[107] F. Shahidi and Y. Zhong, "Revisiting the polar paradox theory: a critical overview,"

Journal of agricultural and food chemistry, vol. 59, no. 8, pp. 3499–3504, 2011.

[108] H. Yuji, J. Weiss, P. Villeneuve, L. J. López Giraldo, M.-C. Figueroa-Espinoza, and E. A. Decker, "Ability of surface-active antioxidants to inhibit lipid oxidation in oil-in-water emulsion," *Journal of agricultural and food chemistry*, vol. 55, no. 26, pp. 11052–11056, 2007.

[109] E. N. Frankel and A. S. Meyer, "The problems of using one-dimensional methods to evaluate multifunctional food and biological antioxidants," *Journal of the Science of Food and Agriculture*, vol. 80, no. 13, pp. 1925–1941, 2000.

[110] L. Castle and M. J. Perkins, "Inhibition kinetics of chain-breaking phenolic antioxidants in sds micelles. evidence that intermicellar diffusion rates may be rate-limiting for hydrophobic inhibitors such as. alpha.-tocopherol," *Journal of the American Chemical Society*, vol. 108, no. 20, pp. 6381–6382, 1986.

[111] D. Daniels and H. Martin, "Antioxidants in oats: Mono-esters of caffeic and ferulic acids," *Journal of the Science of Food and Agriculture*, vol. 18, no. 12, pp. 589–595, 1967.

[112] W. Cort, "Hemoglobin peroxidation test screens antioxidants," *Food technology*, 1974.

[113] J. W. Scott, W. M. Cort, H. Harley, D. R. Parrish, and G. Saucy, "6-hydroxychroman-2-carboxylic acids: Novel antioxidants," *Journal of the American Oil Chemists Society*, vol. 51, no. 5, pp. 200–203, 1974.

[114] S. Dziedzic and B. Hudson, "Phosphatidyl ethanolamine as a synergist for primary antioxidants in edible oils," *Journal of the American Oil Chemists Society*, vol. 61, no. 6, pp. 1042–1045, 1984.

[115] W. L. Porter, E. D. Black, and A. M. Drolet, "Use of polyamide oxidative fluorescence test on lipid emulsions: contrast in relative effectiveness of antioxidants in bulk versus dispersed systems," *Journal of Agricultural and Food Chemistry*, vol. 37, no. 3, pp. 615–624, 1989.

[116] W. L. Porter, "Recent trends in food applications of antioxidants," in *Autoxidation in food and biological systems*, pp. 295–365, Springer, 1980.

[117] E. N. Frankel, S.-W. Huang, J. Kanner, and J. B. German, "Interfacial phenomena in the evaluation of antioxidants: bulk oils vs emulsions," *Journal of Agricultural and Food Chemistry*, vol. 42, no. 5, pp. 1054–1059, 1994.

[118] R. Mateos, M. Trujillo, G. Pereira-Caro, A. Madrona, A. Cert, and J. L. Espartero, "New lipophilic tyrosyl esters. comparative antioxidant evaluation with hydroxytyrosyl esters," *Journal of agricultural and food chemistry*, vol. 56, no. 22, pp. 10960–10966, 2008.

[119] G. Pereira-Caro, A. Madrona, L. Bravo, J. L. Espartero, F. Alcudia, A. Cert, and R. Mateos, "Antioxidant activity evaluation of alkyl hydroxytyrosyl ethers, a new class of hydroxytyrosol derivatives," *Food chemistry*, vol. 115, no. 1, pp. 86–91, 2009.

[120] S.-W. Huang, A. Hopia, K. Schwarz, E. N. Frankel, and J. B. German, "Antioxidant activity of α-tocopherol and trolox in different lipid substrates: bulk oils vs oil-in-water emulsions," *Journal of Agricultural and Food Chemistry*, vol. 44, no. 2, pp. 444–452, 1996.

[121] S.-W. Huang and E. N. Frankel, "Antioxidant activity of tea catechins in different lipid systems," *Journal of Agricultural and Food Chemistry*, vol. 45, no. 8, pp. 3033–3038,

1997.

[122] M.-E. Cuvelier, V. Bondet, and C. Berset, "Behavior of phenolic antioxidants in a partitioned medium: structureactivity relationship," *Journal of the American Oil Chemists' Society*, vol. 77, no. 8, pp. 819–824, 2000.

[123] J. Chalas, C. Claise, M. Edeas, C. Messaoudi, L. Vergnes, A. Abella, and A. Lindenbaum, "Effect of ethyl esterification of phenolic acids on low-density lipoprotein oxidation," *Biomedicine & pharmacotherapy*, vol. 55, no. 1, pp. 54–60, 2001.

[124] W. Chaiyasit, R. J. Elias, D. J. McClements, and E. A. Decker, "Role of physical structures in bulk oils on lipid oxidation," *Critical Reviews in Food Science and Nutrition*, vol. 47, no. 3, pp. 299–317, 2007.

[125] S.-W. Huang, E. N. Frankel, R. Aeschbach, and J. B. German, "Partition of selected antioxidants in corn oil-water model systems," *Journal of Agricultural and Food Chemistry*, vol. 45, no. 6, pp. 1991–1994, 1997.

[126] S. S. Pekkarinen, H. Stöckmann, K. Schwarz, I. M. Heinonen, and A. I. Hopia, "Antioxidant activity and partitioning of phenolic acids in bulk and emulsified methyl linoleate," *Journal of Agricultural and Food Chemistry*, vol. 47, no. 8, pp. 3036–3043, 1999.

[127] C. Jacobsen, K. Schwarz, H. Stöckmann, A. S. Meyer, and J. Adler-Nissen, "Partitioning of selected antioxidants in mayonnaise," *Journal of agricultural and food chemistry*, vol. 47, no. 9, pp. 3601–3610, 1999.

[128] K. Schwarz, S.-W. Huang, J. B. German, B. Tiersch, J. Hartmann, and E. N. Frankel, "Activities of antioxidants are affected by colloidal properties of oil-in-water and

water-in-oil emulsions and bulk oils," *Journal of agricultural and food chemistry*, vol. 48, no. 10, pp. 4874–4882, 2000.

[129] H. Stöckmann, K. Schwarz, and T. Huynh-Ba, "The influence of various emulsifiers on the partitioning and antioxidant activity of hydroxybenzoic acids and their derivatives in oil-in-water emulsions," *Journal of the American Oil Chemists' Society*, vol. 77, no. 5, pp. 535–542, 2000.

[130] H. Stöckmann and K. Schwarz, "Partitioning of low molecular weight compounds in oil-in-water emulsions," *Langmuir*, vol. 15, no. 19, pp. 6142–6149, 1999.

[131] D. J. McClements, *Food emulsions: principles, practices, and techniques*. CRC press, 2004.

[132] W. A. Pryor, J. A. Cornicelli, L. J. Devall, B. Tait, B. Trivedi, D. Witiak, and M. Wu, "A rapid screening test to determine the antioxidant potencies of natural and synthetic antioxidants," *The Journal of Organic Chemistry*, vol. 58, no. 13, pp. 3521–3532, 1993.

[133] L. R. C. Barclay and M. R. Vinqvist, "Membrane peroxidation: inhibiting effects of water-soluble antioxidants on phospholipids of different charge types," *Free Radical Biology and Medicine*, vol. 16, no. 6, pp. 779–788, 1994.

[134] K. Schwarz, E. Frankel, and J. German, "Partition behaviour of antioxidative phenolic compounds in heterophasic systems," *Lipid/Fett*, vol. 98, no. 3, pp. 115–121, 1996.

[135] M. N. Khan, *Micellar catalysis*, vol. 133. CRC Press, 2006.

[136] L. S. R. Rutgers, "Interfacial compositions of surfactant assemblies by chemical trapping with arenediazonium ions: method and applications," *Reactions and Synthesis in Surfactant Systems*, p. 265, 2001.

[137] C. A. Bunton, M. M. Mhala, and J. R. Moffatt, "Reactions of anionic nucleophiles in anionic micelles: a quantitative treatment," *The Journal of Physical Chemistry*, vol. 93, no. 23, pp. 7851–7856, 1989.

[138] Z.-M. He, J. A. Loughlin, and L. S. Romsted, "Micelle effects on reactivity in concentrated salt solutions: Two new approaches to interpreting counterion effects on the acid catalyzed hydrolysis of a hydrophobic ketal in aqueous solutions of cationic micelles," *Bol. Soc. Chil. Quim*, vol. 35, no. 1, pp. 43–53, 1990.

[139] K. Gunaseelan, L. S. Romsted, M.-J. P. Gallego, E. González-Romero, and C. Bravo-Díaz, "Determining α-tocopherol distributions between the oil, water, and interfacial regions of macroemulsions: Novel applications of electroanalytical chemistry and the pseudophase kinetic model," *Advances in colloid and interface science*, vol. 123, pp. 303–311, 2006.

[140] J. D. Morgan, D. H. Napper, G. G. Warr, and S. K. Nicol, "Measurement of the selective adsorption of ions at air/surfactant solution interfaces," *Langmuir*, vol. 10, no. 3, pp. 797–801, 1994.

[141] L. Romsted, K. Mittal, and B. Lindman, *Surfactants in Solution*, vol. 2. Plenum, New York, 1984.

[142] Y. Marcus and A. S. Kertes, *Ion exchange and solvent extraction of metal complexes*. John Wiley & Sons, 1969.

[143] W. Jencks and J. Regenstein, "Ionization constants of acids and bases," *Handbook of biochemistry and molecular biology*, vol. 1, pp. 305–352, 1976.

[144] C. A. Bunton and C. P. Cowell, "The binding of phenols and phenoxide ions to cationic

micelles," *Journal of colloid and interface science*, vol. 122, no. 1, pp. 154–162, 1988.

[145] P. Saveyn, E. Cocquyt, D. Sinnaeve, J. C. Martins, D. Topgaard, and P. Van der Meeren, "Nmr study of the sorption behavior of benzyl alcohol derivatives into sonicated and extruded dioctadecyldimethylammonium chloride (dodac) dispersions: the relevance of membrane fluidity," *Langmuir*, vol. 24, no. 7, pp. 3082–3089, 2008.

[146] A. Heins, T. Sokolowski, H. Stöckmann, and K. Schwarz, "Investigating the location of propyl gallate at surfaces and its chemical microenvironment by 1h nmr," *Lipids*, vol. 42, no. 6, pp. 561–572, 2007.

[147] M. Bonnaud, J. Weiss, and D. J. McClements, "Interaction of a food-grade cationic surfactant (lauric arginate) with food-grade biopolymers (pectin, carrageenan, xanthan, alginate, dextran, and chitosan)," *Journal of agricultural and food chemistry*, vol. 58, no. 17, pp. 9770–9777, 2010.

[148] T. Waraho, D. J. McClements, and E. A. Decker, "Mechanisms of lipid oxidation in food dispersions," *Trends in food science & technology*, vol. 22, no. 1, pp. 3–13, 2011.

[149] L. Lethuaut, F. Métro, and C. Genot, "Effect of droplet size on lipid oxidation rates of oil-in-water emulsions stabilized by protein," *Journal of the American Oil Chemists' Society*, vol. 79, no. 5, pp. 425–430, 2002.

[150] H. Imai, T. Maeda, M. Shima, and S. Adachi, "Oxidation of methyl linoleate in oil-in-water micro-and nanoemulsion systems," *Journal of the American Oil Chemists' Society*, vol. 85, no. 9, pp. 809–815, 2008.

[151] H. T. Osborn and C. C. Akoh, "Effect of emulsifier type, droplet size, and oil concentration on lipid oxidation in structured lipid-based oil-in-water emulsions," *Food*

Chemistry, vol. 84, no. 3, pp. 451–456, 2004.

[152] D. Paraskevopoulou, D. Boskou, and A. Paraskevopoulou, "Oxidative stability of olive oil–lemon juice salad dressings stabilized with polysaccharides," *Food Chemistry*, vol. 101, no. 3, pp. 1197–1204, 2007.

[153] S. Kiokias, C. Dimakou, and V. Oreopoulou, "Effect of heat treatment and droplet size on the oxidative stability of whey protein emulsions," *Food Chemistry*, vol. 105, no. 1, pp. 94–100, 2007.

[154] C. P. Dimakou, S. N. Kiokias, I. V. Tsaprouni, and V. Oreopoulou, "Effect of processing and storage parameters on the oxidative deterioration of oil-in-water emulsions," *Food Biophysics*, vol. 2, no. 1, pp. 38–45, 2007.

[155] M. Hu, D. J. McClements, and E. A. Decker, "Lipid oxidation in corn oil-in-water emulsions stabilized by casein, whey protein isolate, and soy protein isolate," *Journal of Agricultural and Food Chemistry*, vol. 51, no. 6, pp. 1696–1700, 2003.

[156] M. B. Let, C. Jacobsen, and A. S. Meyer, "Lipid oxidation in milk, yoghurt, and salad dressing enriched with neat fish oil or pre-emulsified fish oil," *Journal of agricultural and food chemistry*, vol. 55, no. 19, pp. 7802–7809, 2007.

[157] P.-G. Nilsson, H. Wennerstrom, and B. Lindman, "Non-ionic micelles-size, shape, hydration and intermicellar interactions from self-diffusion studies," *Chemica Scripta*, vol. 25, no. 1, pp. 67–72, 1985.

[158] B. Lindman, A. Carlsson, G. Karlström, and M. Malmsten, "Nonionic polyhers and surfactants-some anomalies in temperature dependence and in interactions with ionic

surfactants," *Advances in Colloid and interface Science*, vol. 32, no. 2, pp. 183–203, 1990.

[159] W. Brown, R. Johnsen, P. Stilbs, and B. Lindman, "Size and shape of nonionic amphiphile (c12e6) micelles in dilute aqueous solutions as derived from quasielastic and intensity light scattering, sedimentation, and pulsed-field-gradient nuclear magnetic resonance self-diffusion data," *The Journal of Physical Chemistry*, vol. 87, no. 22, pp. 4548–4553, 1983.

[160] P. G. Nilsson, H. Wennerstroem, and B. Lindman, "Structure of micellar solutions of nonionic surfactants. nuclear magnetic resonance self-diffusion and proton relaxation studies of poly (ethylene oxide) alkyl ethers," *The Journal of Physical Chemistry*, vol. 87, no. 8, pp. 1377–1385, 1983.

[161] S. S. Funari, M. C. Holmes, and G. J. Tiddy, "Intermediate lyotropic liquid crystal phases in the c16eo6/water system," *The Journal of Physical Chemistry*, vol. 98, no. 11, pp. 3015–3023, 1994.

[162] D. J. McClements and J. Rao, "Food-grade nanoemulsions: formulation, fabrication, properties, performance, biological fate, and potential toxicity," *Critical reviews in food science and nutrition*, vol. 51, no. 4, pp. 285–330, 2011.

[163] T. Tadros, P. Izquierdo, J. Esquena, and C. Solans, "Formation and stability of nanoemulsions," *Advances in colloid and interface science*, vol. 108, pp. 303–318, 2004.

[164] T. G. Mason, J. Wilking, K. Meleson, C. Chang, and S. Graves, "Nanoemulsions: formation, structure, and physical properties," *Journal of Physics: Condensed Matter*, vol. 18, no. 41, p. R635, 2006.

[165] N. Anton and T. F. Vandamme, "The universality of low-energy nano-emulsification," *International Journal of Pharmaceutics*, vol. 377, no. 1, pp. 142–147, 2009.

[166] S. M. Jafari, E. Assadpoor, Y. He, and B. Bhandari, "Re-coalescence of emulsion droplets during high-energy emulsification," *Food hydrocolloids*, vol. 22, no. 7, pp. 1191–1202, 2008.

[167] P. Walstra, "Principles of emulsion formation," *Chemical Engineering Science*, vol. 48, no. 2, pp. 333–349, 1993.

[168] S. Kentish, T. Wooster, M. Ashokkumar, S. Balachandran, R. Mawson, and L. Simons, "The use of ultrasonics for nanoemulsion preparation," *Innovative Food Science & Emerging Technologies*, vol. 9, no. 2, pp. 170–175, 2008.

[169] K. Bouchemal, S. Briançon, E. Perrier, and H. Fessi, "Nano-emulsion formulation using spontaneous emulsification: solvent, oil and surfactant optimisation," *International Journal of Pharmaceutics*, vol. 280, no. 1, pp. 241–251, 2004.

[170] N. Anton, J.-P. Benoit, and P. Saulnier, "Design and production of nanoparticles formulated from nano-emulsion templatesa review," *Journal of Controlled Release*, vol. 128, no. 3, pp. 185–199, 2008.

[171] P. Fernandez, V. André, J. Rieger, and A. Kühnle, "Nano-emulsion formation by emulsion phase inversion," *Colloids and Surfaces A: Physicochemical and Engineering Aspects*, vol. 251, no. 1, pp. 53–58, 2004.

[172] B. Coulter, "Ls 13 320 laser diffraction particle size analyzer instrument manual," *Beckman Coulter Inc*, vol. 11800, 2003.

[173] M. Instruments, "Zetasizer nano series user manual," *Worcestershire: Malvern Instruments Ltd*, 2004.

[174] F. Sterpone, G. Briganti, S. Melchionna, and C. Pierleoni, "Pressure-induced core packing and interfacial dehydration in nonionic c12e6 micelle in aqueous solution," *Langmuir*, vol. 24, no. 12, pp. 6067–6071, 2008.

[175] A. Kabalnov and J. Weers, "Macroemulsion stability within the winsor iii region: theory versus experiment," *Langmuir*, vol. 12, no. 8, pp. 1931–1935, 1996.

[176] A. Kabalnov and H. Wennerström, "Macroemulsion stability: the oriented wedge theory revisited," *Langmuir*, vol. 12, no. 2, pp. 276–292, 1996.

[177] S. Burauer, T. Sachert, T. Sottmann, and R. Strey, "On microemulsion phase behavior and the monomeric solubility of surfactant," *Physical Chemistry Chemical Physics*, vol. 1, no. 18, pp. 4299–4306, 1999.

[178] M. Laguerre, L. J. López Giraldo, J. Lecomte, M. C. Figueroa-Espinoza, B. Baréa, J. Weiss, E. A. Decker, and P. Villeneuve, "Chain length affects antioxidant properties of chlorogenate esters in emulsion: the cutoff theory behind the polar paradox," *Journal of Agricultural and Food Chemistry*, vol. 57, no. 23, pp. 11335–11342, 2009.

[179] A. Panya, M. Laguerre, J. Lecomte, P. Villeneuve, J. Weiss, D. J. McClements, and E. A. Decker, "Effects of chitosan and rosmarinate esters on the physical and oxidative stability of liposomes," *Journal of Agricultural and Food Chemistry*, vol. 58, no. 9, pp. 5679–5684, 2010.

[180] M. Laguerre, L. J. López Giraldo, J. Lecomte, M. C. Figueroa-Espinoza, B. Baréa, J. Weiss, E. A. Decker, and P. Villeneuve, "Relationship between hydrophobicity and

antioxidant ability of phenolipids in emulsion: a parabolic effect of the chain length of rosmarinate esters," *Journal of Agricultural and Food Chemistry*, vol. 58, no. 5, pp. 2869–2876, 2010.

[181] A. Panya, M. Laguerre, C. Bayrasy, J. Lecomte, P. Villeneuve, D. J. McClements, and E. A. Decker, "An investigation of the versatile antioxidant mechanisms of action of rosmarinate alkyl esters in oil-in-water emulsions," *Journal of Agricultural and Food Chemistry*, vol. 60, no. 10, pp. 2692–2700, 2012.

[182] I. Medina, S. Lois, D. Alcántara, R. Lucas, and J. C. Morales, "Effect of lipophilization of hydroxytyrosol on its antioxidant activity in fish oils and fish oil-in-water emulsions," *Journal of Agricultural and Food Chemistry*, vol. 57, no. 20, pp. 9773–9779, 2009.

[183] M. Laguerre, C. Bayrasy, A. Panya, J. Weiss, D. J. McClements, J. Lecomte, E. A. Decker, and P. Villeneuve, "What makes good antioxidants in lipid-based systems? the next theories beyond the polar paradox," *Critical Reviews in Food Science and Nutrition*, vol. 55, no. 2, pp. 183–201, 2015.

[184] S. Losada Barreiro, C. Bravo-Díaz, F. Paiva-Martins, and L. S. Romsted, "Maxima in antioxidant distributions and efficiencies with increasing hydrophobicity of gallic acid and its alkyl esters. the pseudophase model interpretation of the cutoff effect," *Journal of Agricultural and Food Chemistry*, vol. 61, no. 26, pp. 6533–6543, 2013.

[185] M. Costa, S. Losada-Barreiro, F. Paiva-Martins, C. Bravo-Díaz, and L. S. Romsted, "A direct correlation between the antioxidant efficiencies of caffeic acid and its alkyl esters and their concentrations in the interfacial region of olive oil emulsions. the pseudophase model interpretation of the cut-off effect," *Food Chemistry*, vol. 175, pp. 233–242, 2015.

[186] Z. Chu, C. A. Dreiss, and Y. Feng, "Smart wormlike micelles," *Chemical Society Reviews*, vol. 42, no. 17, pp. 7174–7203, 2013.

[187] D. Marquardt, N. Kucerka, J. Katsaras, and T. A. Harroun, "α-tocopherols location in membranes is not affected by their composition," *Langmuir*, vol. 31, no. 15, pp. 4464–4472, 2014.

[188] D. Marquardt, J. A. Williams, N. Kucerka, J. Atkinson, S. R. Wassall, J. Katsaras, and T. A. Harroun, "Tocopherol activity correlates with its location in a membrane: a new perspective on the antioxidant vitamin e," *Journal of the American Chemical Society*, vol. 135, no. 20, pp. 7523–7533, 2013.

[189] T. Kunitake and Y. Okahata, "A totally synthetic bilayer membrane," *Journal of the American Chemical Society*, vol. 99, no. 11, pp. 3860–3861, 1977.

[190] F. Menger and N. Balachander, "Chemically-induced aggregation, budding, and fusion in giant vesicles: direct observation by light microscopy," *Journal of the American Chemical Society*, vol. 114, no. 14, pp. 5862–5863, 1992.

[191] A. Fontana, P. De Maria, G. Siani, and B. H. Robinson, "Kinetics of breakdown of vesicles from didodecyldimethylammonium bromide induced by single chain surfactants and by osmotic stress in aqueous solution," *Colloids and Surfaces B: Biointerfaces*, vol. 32, no. 4, pp. 365–374, 2003.

[192] L.-L. Lu and X.-Y. Lu, "Solubilities of gallic acid and its esters in water," *Journal of Chemical & Engineering Data*, vol. 52, no. 1, pp. 37–39, 2007.